A Dissertation for the Degree

of Doctor of Philosophy

The role of midbrain dorsal periaqueductal gray astrocytes in mouse defensive and panic-like behaviors

방어 및 공황관련 행동에서 중뇌 수도관주위의 회색질 성상교세포의 역할

February 2023

The Graduate School of Seoul National University
College of Natural Sciences
Neuroscience Major

Ellane Eda Barcelon

이학박사학위논문

The role of midbrain dorsal periaqueductal gray astrocytes in mouse defensive and panic-like behaviors

방어 및 공황관련 행동에서 중뇌 수도관주위의 회색질 성상교세포의 역할

2023 년 2 월

서울대학교 대학원

자연과학대학 협동과정 뇌과학전공

엘 레 인

The role of midbrain dorsal periaqueductal gray astrocytes in mouse defensive and panic-like behaviors

Advisor**: Sung Joong Lee, Ph.D.**

A dissertation submitted in partial fulfillment
of the requirement for the degree of
DOCTOR OF PHILOSOPHY

November 2022

The Graduate School of Seoul National University
College of Natural Sciences
Neuroscience Major

Ellane Eda Barcelon

Confirming the Ph.D. Dissertation written by
Ellane Eda Barcelon
December 2022

Chair	최세영	(Seal)
Vice Chair	이성중	(Seal)
Examiner	이용석	(Seal)
Examiner	최석우	(Seal)
Examiner	전상범	(Seal)

Dedication

To Rev. Kwang-ok Park and Professor Emeritus Kye Joon Lee,
this is the best doctor I did not know 7 years ago that I wanted to become.
Thank you for the opportunity.

저를 믿어주셔서 감사합니다.

Acknowledgements

This work would not be possible without the help of so many people to whom I am extremely thankful.

I am immensely grateful to my advisor, Professor Sung Joong Lee for allowing me to join his laboratory and for creating this environment of learning and working with excellence. I am also deeply thankful to my mentor, Dr. Woo-hyun Cho, for being the most patient and passionate teacher and a very supportive friend as well. The last seven years in Korea and in graduate school have been a period of personal and professional development for me. I am eternally grateful to these incredible advisor and mentors for allowing me to maximize my potential as a scientist and also to my amazing lab mates for being the most supportive friends I never expect to have in Korea. They help me grow as a person, enjoy this PhD journey, and undoubtedly appreciate South Korea. I am still convinced that they are the nicest and brightest Koreans I have ever met.

I would also like to thank my dissertation panel members, Dr. Se-Young Choi, Dr. Yongseok Lee, Dr. Sukwoo Choi, and Dr. Sangbeom Jun, for their invaluable insights that helped shape this manuscript into its best version. It is an honor to have them as my thesis jury.

I would also like to acknowledge the Samsung Global Scholarship Foundation and the Leader Scientist Scholarship Committee for choosing me and supporting me financially through my challenging academic course years. Samsung Global Scholarship Foundation not only provided financial assistance, but also introduced me to a larger world of meeting other international students all over Korea as they select and nurture these talented future leaders of the world.

I am also deeply thankful to Dr. Byeong Moon Kim and Dr. Sang-Im Yoo, my advisors as president of the SNU International Student Organization and team leader in SNU International Church, for nurturing my leadership potential and acknowledging my abilities 'outside science' to serve a larger and more diverse community than I had in the Philippines. I am thankful to meet and be guided by Christian scientists and to be able to join them in serving an incredible international community in SNU.

Also, I am forever grateful to Rev. Kwang-ok Park and Professor Emeritus Kye Joon Lee, for without them I wouldn't be where I am now. They are the ones who opened the opportunity for me to study in Korea. They insist in me to be a visionary, a leader of the young generation of my country. These people invested their efforts and hope for the young generation for a brighter and godly future. I will not forget how much they believed in me. They changed my life forever and for that I am deeply grateful and honored.

I also would like to thank my family and friends back in the Philippines for their constant moral support and prayers throughout this challenging journey far from home. My family is my unlimited source of encouragement and motivation; the ones who always remind me to have fun and be grateful of what I do; my parents; Anna and Epifanio, my siblings; Rosh Ejay, Bethel, and Abie Jesse.

Above all else, to the Creator, Yahweh, my Lord and Savior, through whom and for whom all things exist, alone are all the glory and honor.

Abstract

The role of midbrain dorsal periaqueductal gray astrocytes in mouse defensive and panic-related behaviors

Ellane Eda Barcelon
Interdisciplinary Program in Neuroscience
College of Natural Sciences
The Graduate School of Seoul National University

Upon exposure to threat, survival depends on defensive behaviors, yet maladaptive defensive behavior often results in panic-like behavior. Therefore, these behaviors must be optimized in order for animals to efficiently avoid danger and maximize the chance of survival. The midbrain dorsal periaqueductal gray (dPAG) which integrates information between forebrain areas and brainstem, controls defensive behaviors and is involved in panic-related disorders as reported from both humans and rodent studies. Various forms of defensive behaviors have been used as read-out for normal fear and maladaptive anxiety. However, the underlying substrates of the dysregulation of fear and defensive responses remains mostly unexplored. Also, prior studies mainly focused on investigating neuronal activity underlying defensive responses of mice. However, increasing number of evidences showed that not only neurons but also astrocytes regulate animal behaviors particularly fear and anxiety behaviors. To this end, the role of astrocyte in dPAG in expression and regulation of defensive behaviors is still unknown. Therefore, this

study aimed to address whether dPAG astrocyte is engaged in modulating mouse defensive and panic-related behaviors and the possible mechanisms involved.

Using in vivo calcium recording, it was demonstrated that dPAG astrocytes are activated against threatening situation triggering mouse defensive behaviors. Optogenetic activation and pharmacologic ablation of astrocytes provided evidence that dPAG astrocytes and the subsequent gliotransmitter ATP release are required for the manifestation of optimal defensive behavior, thus aberrant activation of dPAG astrocytes leads to maladaptive defensive behavior. Moreover, the study suggests that dPAG astrocyte is one of the underlying neurobiological substrates of fear responses and defensive dysregulation and might be an important cue in panic-related behaviors via a distinct calcium activity increase and ATP release.

Key words: defensive behaviors, astrocyte, dorsal periaqueductal gray, threat, panic-like behaviors

Student Number: 2016-22072

Table of Contents

List of Figures

Abbreviations

AAV	Adeno-associated virus
AAVDJ	Adeno associated virus with serotype DJ
ACSF	Artificial cerebrospinal fluid
AMPA	alpha-amino-3-hydroxy-5-methyl-4-isoxazolepropionic acid
ATP	Adenosine triphosphate
CamKII	Calmodulin-dependent protein kinase II
ChR2	Channelrhodopsin
CO_2	Carbon dioxide
CPP	Conditioned place preference
dlPAG	Dorsolateral periaqueductal gray
dPAG	Dorsal periaqueductal gray
DREADD	Designer receptors exclusively activated by designer drug
DSM	Diagnostic and Statistical Manual of Mental Health Disorders
eHpHR	Enhanced halorhodopsin from *Natronomonas*
EPM	Elevated plus maze
FST	Forced swim test
GABA	Gamma-aminobutyric acid
GAD	Generalized anxiety disorder
GCaMP6f	Fast variant of genetically-encoded calcium indicator
GfaABC1D	Truncated version of the astrocyte-specific promoter GFAP
GFAP	Glial fibrially acidic protein
GLT-1	Glutamate transport-1

GPCR	G-protein coupled receptor
hM3Dq	Human M3 muscarinic receptor linked to the Gq protein
HRP	Horseradish peroxidase
hSyn	Human synapsin 1 (neuronal gene promoter)
Ins(1,4,5)P3	inositol (1,4,5)- triphosphate
L-AAA	L-alpha-aminoadipic acid
lPAG	Lateral periaqueductal gray
mPFC	Medial prefrontal cortex
mSC	Medial superior colliculus
NeuN	Neuronal nuclear protein
NMDA	N-methyl-D-aspartate
OFT	Open field test
Opto-vTrap	Optogenetic trap for reversible inhibition of vesicular release
PAG	Periaqueductal gray
PAP	Perisynaptic astrocyte processes
PBGN	Parabigeminal nucleus
PBS	Phosphate buffered saline
PTSD	Post-traumatic stress disorder
RC car	Remote control car
RTPP	Real-time place preference
S100β	S100-calcium-binding-protein beta
SC	Superior colliculus
SNRI	Serotonin-norepinephrine reuptake inhibitor
SSRI	Selective serotonin reuptake inhibitor

TCSPC	Time-correlated single-photon counting
TMT	Trimethylthiazoline; fox odor
TST	Tail suspension test
VGlut2	Vesicular glutamate transporter 2
vlPAG	Ventrolateral periaqueductal gray
vPAG	Ventral periaqueductal gray
VTA	Ventral tegmental area
5-HT	Serotonin

1. Introduction

"As soon as there was life, there was danger…The defensive survival circuits of humans and other mammals can be conceptualized as manifestations of an ancient survival function—the ability to detect danger and respond to it—that may in fact pre-date animals and their nervous systems, and perhaps may go back to the beginning of life." — Joseph E. LeDoux, 2021

1.1 Background of the Study

1.1.1. Defensive behaviors

Upon encountering danger and threatening situation, survival depends on efficient and pertinent defensive behaviors. Exposure to threatening situations such as the presence of a predator or stimuli indicating imminent or perceived danger evoked a brain state, fear, which generates defensive behaviors to avoid or reduce potential harm. Defensive behaviors are a collection of conserved evolutionary reactions to threat across species. These include freezing [1,2], flight [3,4], defensive attack [5], and risk assessment [6] which are canonically known to depend on threat imminence and contextual factors such as the presence of available escape routes [7-9]. Defensive behaviors switch rapidly to adequately adapt to the changing threat levels or environmental challenges [7]. Threat that are distant are met with risk

assessment and freezing behaviors, whereas proximal and or fast approaching threat evokes escape behaviors such as running or jumping [10-12].

Moreover, defensive behaviors have been used as a read-out to study normal fear and maladaptive anxiety [13-16]. It has been a long-standing question in the research of fear and anxiety what are the neurobiological underpinnings; cellular, molecular, and brain circuits, and how these generate and regulate the various forms of defensive behaviors. Therefore, this study tries to elucidate one of the neurobiological underpinnings in light of astrocyte function and further support the fundamental role of the effective and appropriate defensive behaviors in animal survival.

1.1.2 Midbrain Periaqueductal Gray in Defensive Behaviors

The midbrain periaqueductal gray (PAG), a brain area located at the floor of the midbrain that surrounds the aqueduct, is found across the species under phylum Chordata (Figure 1) [17,18]. It has also been implicated in several functions that include pain modulation, vocalization, breathing, heart rate, hunting, and defensive behaviors [18-21]. Notably, previous studies have shown that midbrain PAG is actively involved in detection of threat and threat imminence, and generation of various forms of defensive responses such as risk assessment, freezing, flight and fight [22,23]. Clinical studies demonstrated increased BOLD activity of midbrain PAG upon threat imminence and freezing in humans [24-26]

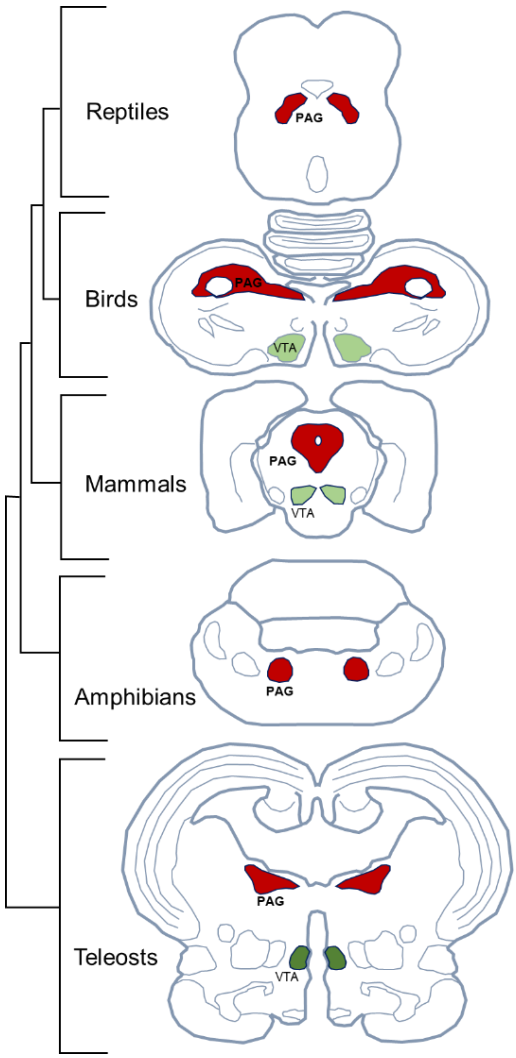

Figure 1. The midbrain periaqueductal gray is an evolutionarily conserved brain area present in vertebrate animals [17,18].

Based on the compilation of previous reports [17,18], the figure illustrates the PAG of animals under vertebrate classification that is responsible for animal survival behaviors particularly appetitive and defensive behaviors.

Previous studies put a great deal of effort toward understanding how columnar subdivisions of the PAG control and contribute to distinct defensive behaviors. The functional organization of PAG has been indicated according to its subregions namely dorsomedial (dm), dorsolateral (dl), lateral (l), and ventrolateral (vl) subregions of PAG (Figure 2) [27-30].

A study of Tovote et. al. suggested that vlPAG is necessary for conditioned freezing[23]. Though less explored than the vlPAG, optogenetic and electrical

stimulation of the lPAG column also elicits freezing [31,32]. Meanwhile, dorsomedial and dorsolateral PAG, which the author addressed in this study as dPAG, have key roles in controlling innate defensive behaviors including freezing, escape, and risk assessment [22,33,34]. Previous reports also demonstrated dPAG neurons expressing VGlut2 and CamKII encode the choice to escape and control escape vigor [3,4,22,23]. Moreover, these dPAG glutamatergic neurons receive direct inputs from brain areas that encode saliency of threat stimuli such as amygdala, hypothalamus, and medial superior colliculus, whereas GABAergic neurons in vlPAG control mice freezing behaviors [23]. These reports also paved questions whether PAG populations might also control and encode defensive behaviors. It was confirmed that PAG contains a diverse array of cell types exhibiting different neurochemical profiles and vary in anatomical location spanning PAG columns which lend insights into another axis of functional organization complementing the established anatomical columnar PAG subregions [35,36].

In addition, the PAG is positioned in an ideal location to integrate information from the higher brain regions down to the brain stem and spinal cord; receiving threat sensory information detected from environment (e.g. from retina, olfactory blub, superior colliculus) [3,37-39] which are then processed accordingly to its salience and emotional valence (e.g. amygdala, hypothalamus)[23,40-43] and lead to the generation of motor outputs as animal response from the downstream of midbrain PAG (VTA, PBGN, brainstem and spinal regions) [23,37,38]

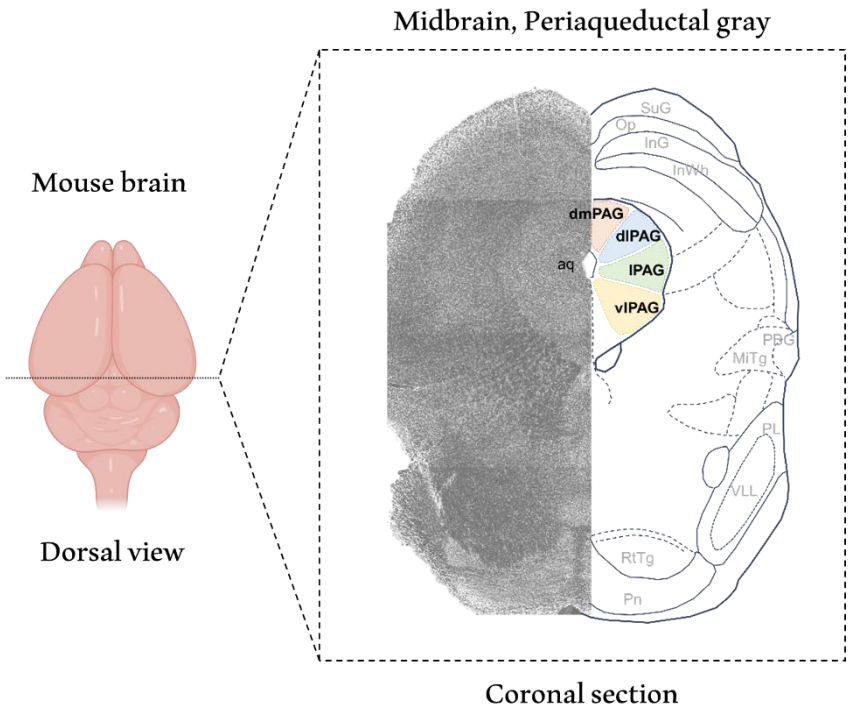

Figure 2. The midbrain region where PAG is located and its subregions.

In a mammalian brain, such that of the mouse (left image), PAG is located in the midbrain as shown in the coronal section (right). PAG subregions: Dorsomedial PAG, *dmPAG,* dorsolateral PAG, *dlPAG*, lateral PAG, *lPAG*, ventrolateral PAG, *vlPAG*, aqueduct, *aq*. Land mark midbrain areas includes superior colliculus: superficial gray layer, *SuG*, optic layer, *Op*, intermediate gray layer, *InG*, intermediate white layer, *InWh*. Parabigeminal nucleus, *PBG*, midbrain tegmentum, *MiTg*, paralemniscal zone *PL*, ventral nucleus of lateral lemniscus, *VLL*, reticulotegmental nucleus, *RtTg*, pontine gray nucleus, *Pn*.

1.1.3 Dorsal Periaqueductal Gray in Dysregulated Fear and Panic-related behaviors

Fear and anxiety responses are fundamental behaviors that animals used to respond and adapt to threatening environment and or real dangers. Dysregulation of

this healthy response results in 'marked, persistent, and excessive or unreasonable fear' [44,45] which culminates in a significant burden and interference in normal life that can be described as an anxiety disorder. Clinical studies described that the most common among these anxiety disorder subtypes are generalized anxiety disorder (GAD), post-traumatic stress disorder (PTSD), and panic disorder [44,46]. Notably, panic disorder is characterized by panic attacks of increased autonomic nervous symptoms, fear of dying, fear of losing control even in the absence of danger [7,44].Many behavioral symptoms, which often rely on verbal reporting, can hardly be modeled in animals. However, panic is described to be accompanied by an 'urge to escape' and panic disorder patients 'usually report an urgent desire to flee from where ever the attack is occurring'. It was further proposed that panic may occur when 'flight and fight' systems are strongly aroused but no apparent and perceived route for escape is available [47,48].

It was reported that neurosurgical patients who underwent electrical stimulation of midbrain PAG experienced panic-related symptoms [49]. In rodents, electrical and chemical stimulation of midbrain dPAG have been used to study panic-like behaviors [50-52]. It was also reported that exposure to panicogenic stimuli such as CO_2 induce increased Fos expression in dPAG [53].

In addition, based on clinical and animal observations of Deakin, Graeff and colleagues, it was suggested that activation of the midbrain dPAG leads to behavioral manifestation of defensive flight and escape jumping that are identified as panic-like [7,47,54,55]. The clinical and psychopharmacological characteristics of panic disorder in human patients demonstrates a remarkable similarity to the dysregulated defensive behavioral response elicited in experimental animals exposed to panicogenic agents.

The dPAG commands primitive fight and flight reactions to proximal threat, acute pain, or asphyxia [21]. The pharmacological profile of dPAG may not be different from the clinical findings suggesting the promise of certain drugs like benzodiazepines and selective serotonin reuptake inhibitors (SSRIs) [56]. Previous studies proposed that GABAergic and serotonergic systems play a crucial role in the regulation of the neural excitability in the PAG and its panicogenic consequences. Moreover, several known anti-depressive medications are being prescribed to panic disorder patients which include SSRI, serotonin-norepinephrine reuptake inhibitor (SNRI), benzodiazepines, and beta-blockers [47,57,58]. Unfortunately, several studies reported that these medications impose side effects for some and not a guaranteed solution against panic disorder and panic-related symptoms [57,59,60].

Despite the crippling effect of panic disorder and panic-related behaviors in society, knowledge on the neurobiological mechanisms is still elusive. Thus, highly effective treatment has not been established. My study suggests a novel finding of the crucial role of dPAG astrocyte in panic-related behaviors that advances our understanding on the biological basis of panic-related behaviors and panic disorder.

1.1.4 Astrocytes in Animal Brain and Behavior

Astrocytes are glial cells that outnumber neurons and tile the central nervous system. Astrocytes were once viewed principally as nutritive and supportive cells but are now understood to be functionally much more diverse and their role and influence in higher brain functions, synaptic plasticity, and neuronal circuitry is being re-evaluated [61]. The discovery of a more complex and closer interaction of astrocyte with neurons has been further elucidated when the concept of tripartite

synapse was proposed [62]. The pioneering studies which discovered the influence of astrocyte in neural functions through Ca^{2+} signals revolutionized the current neuroscience of astrocytes which began in the early 1990s. The concept of tripartite synapse suggests the communication of the pre-synapse and post-synapse as the neural components with intimate association with astrocytes regulating this communication (Figure 3) [62,63].

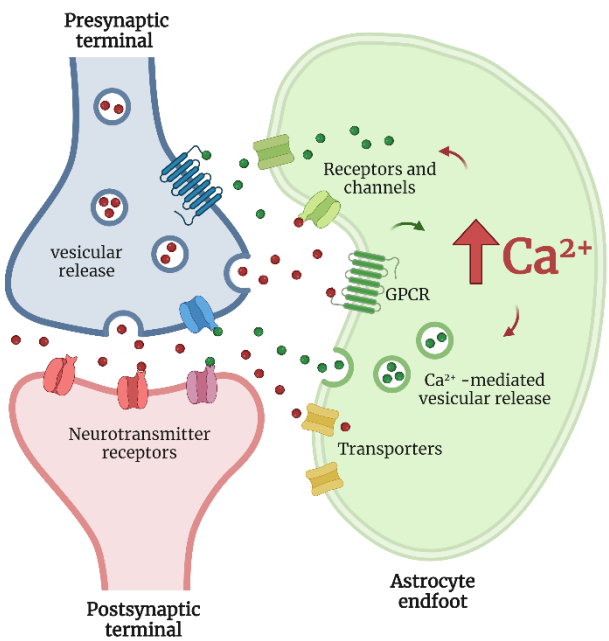

Figure 3. Schematics of the tripartite synapse.

The tripartite synapse consists of the presynaptic and postsynaptic terminals with astrocytic processes or endfoot enwrapping the synapses. The release of neurotransmitter from the presynaptic terminal acts on the postsynaptic terminal and astrocytic endfoot mediating an increase of Ca^{2+} activity on astrocyte and subsequently regulating the synaptic communication through neurotransmitter receptors and transporters.

To regulate synaptic transmission, it was further elucidated that astrocytes with their perisynaptic astrocyte processes (PAPs) express functional neurotransmitter receptors and transporters [64,65]. There are various mechanisms

involved in the generation of astrocytic Ca^{2+} signals which includes ionotropic glutamate receptors such as N-methyl-d-aspartate (NMDA) and α-amino-3-hydroxyl-5-methyl-4-isoxazole-propionate (AMPA), P2X purinergic receptors, and store-operated channels such as Orai [66-68]. Also, many of these receptors are of metabotropic type that are associated with G proteins such as metabotropic glutamate receptor 5 (mGluR5), P2Y purinergic receptors, α1-adrenergic receptors, which upon activation, stimulate phospholipase C and formation of inositol (1,4,5)-triphosphate (Ins(1,4,5)P_3), which increases the intracellular Ca^{2+} concentration through the release of Ca^{2+} from the Ins(1,4,5)P_3-sensitive Ca^{2+} stores [69-72]. Astrocytes generate robust intracellular Ca^{2+} signals that are suggested to be crucial regulators of astrocytic function [73]. This increase of intracellular Ca^{2+} level in astrocyte results in the release of gliotransmitters [74-77] such as ATP [78,79], glutamate [80,81], GABA [82,83], and D-serine [84] which regulates neuronal excitability and synaptic transmission [85]. Furthermore, increasing evidence suggests the putative involvement of astrocytes in animal behaviors and psychiatric disorders [86,87]. Studies showed that the disruption of astrocytic activity and regulation of neurons and synaptic transmission accompanies dysregulation of the brain thereby affecting animal behavior such as memory and learning [88,89], breathing [79,90], depressive-like behaviors [78], and fear and anxiety-like behaviors [91-96].

This study further emphasizes and supports the role of astrocyte in fear and anxiety behaviors. Using optogenetics to manipulate astrocyte activity, a recent study demonstrated that astrocytes in ventral tegmental area (VTA) orchestrate avoidance and approach behaviors by tuning glutamatergic signals to VTA GABAergic neurons to drive learned avoidance in mice [93]. In addition, chemogenetic

activation of astrocytes in central amygdala reduced mouse freezing behavior in a cued fear conditioning experiment through decreasing the firing rate of the central medial amygdala neurons [95]. Meanwhile, recent studies showed that hippocampal astrocyte activation using optogenetics reduced fear-related behavior accompanied with increased extracellular ATP and adenosine concentrations [94 96]. It was also reported that hippocampal astrocyte is implicated in the pathology of PTSD and proposed to reduce PTSD symptoms [91,97]. These studies further support the active involvement of astrocytes in the neural mechanisms and animal behaviors addressing fear and anxiety behaviors and its dysregulations.

Tools for genetic, pharmacological, molecular, and physiological assessments which have been adapted from their original purposes to study neurons, are now being developed and employed to comprehensively examine astrocyte biology in vivo [98]. One of these improved tools is optogenetics which utilizes genetically modified light-responsive ion channels such as channelrhodopsin-2 (ChR2), a non-selective cation channel which induces membrane depolarization and thus excites neurons upon blue-light (470 nm) illumination, and halorhodopsin (eHpHR), a light-responsive chloride channel which hyperpolarizes membrane potential upon illumination of yellow light (589 nm)[99]. Optogenetics allows non-invasive and temporally precise manipulation of neural activity [100] and has been adapted to study astrocytes [79,93,94,101]. Prior studies showed that illumination of ChR2-expressing astrocytes displayed robust increases of intracellular Ca^{2+} response and gliotransmitter release such as ATP and glutamate which enhanced or perturbed nearby neuronal activities or brain functions resulting in alteration of animal behaviors [79,96,101-103].

Other tools to manipulate astrocytes includes OptoSTIM [104], the use of DREADD and its specific ligands and melanopsin [105], which are employed to specifically target Gq and Gi pathways to increase and or inhibit astrocytic calcium activity [88,106,107]. In addition, there are several methods employed to inhibit astrocytic functions which includes (1) astrocyte pharmacological ablation of by L-alpha-aminoadipic acid (L-AAA), a glutamate homologue working as an astrotoxin, taken up by astrocyte via glutamate transporter and competitively inhibits glutamate synthetase and γ-glutamyl cysteine synthase thereby inhibiting glutamate cycling [108,109], and (2) Opto-vTrap, a reversible optogenetic tool that utilizes blue-light to induce vesicle-trapping system based on cryptochrome 2 (CRY2) and cryptochrome-interacting basic-helix-loop-helix 1 (CIB1) interaction which then traps synaptic vesicles in neurons and gliotransmitter-containing vesicles in astrocytes thereby disrupting the vesicular release machinery [110].

To this end, the author aimed to address in this study the role of midbrain dorsal PAG astrocytes in instinctive and survival behaviors particularly the optimal defensive actions mice perform to reduce harm and maximize the chance of survival. Although substantial progress has been made to interrogate the role of astrocytes in brain functions and mood disorder, much is still to be explored to address the regulation of defensive and panic-related behaviors.

1.2 Purpose of the Study

Upon exposure to threatening situations, efficient and appropriate defensive responses are crucial to animal survival. Dysregulation of fear and defensive responses have been used as measures to address psychiatric disorders such as maladaptive anxiety, panic-related behaviors, and post-traumatic stress disorder. Studies in both humans and rodents revealed that the midbrain dPAG is involved in fear and defensive response and its dysregulation produces aberrant fear and panic-related behaviors. Although there is increasing evidence which indicate glial cells, particularly astrocyte, actively influence neural activity, the role of astrocyte in midbrain PAG in defensive behaviors and its dysregulation is still unknown.

Therefore, it is reasonable to hypothesize that the midbrain dPAG astrocytes regulate defensive behaviors and its dysregulation. To address this hypothesis, the following specific aims were sought.

1. To investigate whether dPAG astrocyte is actively engaged in mouse defensive behaviors
2. To elucidate whether dPAG astrocyte is involved in the dysregulation of mouse safety-seeking defensive behaviors reminiscent of panic-like behaviors
3. To reveal possible mechanism to which dPAG astrocytes influence mouse defensive and panic-like behaviors

2. Materials and Methods

Animals

Six to 12-week old male CB7BL/6J and GFAP-CreERT2 mice were used in the experiments. GFAP-CreERT2 mice were obtained from the laboratory of Dr. Frank Kirchhoff (Max Plank Institute, Munich, Germany). For the optogenetic modulation of astrocytic activity, floxed-ChR2(H134R)-EYFP (#12569, Jackson Laboratory, Bar Harbor, ME, USA) mice were crossed with GFAP-CreERT2 mice (GFAP-ChR2). GFAP-ChR2 mice were intraperitoneally administered of 100 μg/g tamoxifen (#13258, Cayman Chemical, Ann Arbor, MI, USA) for 5 consecutive days starting at 6 weeks old. For the control group, vehicle (90% corn oil and 10% ethanol) was administered at the same volume as tamoxifen. All experiments were conducted within 2 months of the first tamoxifen injection. The animals were housed and maintained in a controlled environment at 22°C – 24°C and 55% humidity with 12-h light/dark cycles and fed with regular rodent chow and tap water *ad libitum*. All animal experiments were guided by the Seoul National University Institutional Animal Care and Use Committee.

Stereotaxic surgery

Animals that were subjected to implantation of probes and optic fibers, microinjection of virus or chemical were anesthetized with 1.5 ~ 2.0% isoflurane and secured in a stereotaxic apparatus (Stoelting Co., Wood Dale, IL, USA). For in vivo calcium activity recording experiments, holes with the size of the injection needle

were drilled unilaterally into the skull at ±0.40 mm from midline and at the level of lambda suture. Using a syringe pump (Stoelting Co.), 10 μl Hamilton syringe (Hamilton Co., Reno, NV, USA) delivered an 800 nl of pZac2.1-GfaABC1D-lck-GCaMP6f (#52924, Addgene, Watertown, MA, USA) to dPAG (AP: 0.00 mm ML: ±0.40 mm, DV +2.50 mm, from lambda). Virus was injected at a constant rate of 200 nl/min and the needle was left in place for 10 minutes after each injection to minimize the upward flow of the viral solution after raising the needle. This was followed by TCSPC probe implantation with the same coordinates but with DV +2.30 mm superior to the viral injection site. The implantation was fixed with zinc polycarboxylate dental cement. Similar protocol was used when injecting AAV-hSyn-oChIEF-tdTomato (KIST, Seoul, Korea) to dPAG of GFAP-ChR2 mice for neuronal manipulations. After 7 days, mice were implanted with 200-μm optic fibers (FP200URT; Thorlabs Inc., Newton, NJ, USA) with 1.25 mm ceramic ferule (CFLC230-10; Thorlabs Inc.) unilaterally or bilaterally on the same coordinates except depth with DV +2.30 mm superior to the viral injection site. Mice were given another 7 days for virus expression and recovery.

Similar protocol was applied when using AAVDJ-GFAP-Opto-vTrap (Addgene) injected to wild type mice and GFAP-ChR2 mice.

For L-AAA or PBS injection, mice dPAG (AP 0.00 mm ML ±0.40 mm, DV +2.50 mm, from lambda) were injected with 800 nl of either 0.1 M PBS or 20 μg/μl of L-AAA (A7275, Sigma-Aldrich, Burlington, MA, USA) using a syringe pump with a constant rate of 200nl/ min and needle was left in place for 10 min after the injection. After raising the needle, 3 sutures were applied to close the skin of the

head. Mice were allowed to recover for 1 to 2 days before subjecting to the behavioral or western blot experiments.

For optic fiber implantation, GFAP-ChR2 mice were implanted with 200 μm mono fiber-optic cannula with 1.25 mm ceramic ferrule (Thorlabs Inc.) bilaterally (angle 26°, AP 0.00 mm, ML ±1.40 mm, DV +2.40 mm, from lambda) or unilaterally (AP 0.00 mm, ML ±0.40 mm, DV +2.30 mm, from lambda) to dPAG or vPAG (DV +2.50~2.60 mm) and fixed with zinc polycarboxylate dental cement. Mice were given 7 days to recover before performing behavioral experiments.

For microdialysis guide cannula implantation, GFAP-ChR2 mice were implanted with CMA7 guide cannula (C315MN; CMA microdialysis, CMAP000137, Kista, Sweden) covered by its dummy (angle 26°, AP 0.00 mm, ML ±1.40 mm, DV +2.40 mm, from lambda) and a mono fiber-optic cannula (AP 0.00 mm, ML ±0.40 mm, DV +2.30 mm, from lambda) to simultaneously stimulate dPAG astrocyte and perform *in vivo* microdialysis. The implantations were secured using zinc polycarboxylate dental cement. Mice were given at least 3 days to recover before performing the microdialysis experiment.

Animals with mistargeted implantations or virus expression were excluded from the analyses.

TCSPC *in vivo* Ca^{2+} recording

Two weeks after virus expression of GCaMP6f and TCSPC probe implantation, a single wavelength TCSPC system (Becker & Hickl GmbH, Berlin, Germany) was used for *in vivo* astrocytic calcium signal acquisition. A 488-nm laser (BDL-488-SMN; Becker & Hickl GmbH) was used to excite GCaMP6f signal at 20

MHz through a single mode fiber (F200-Hybrid-FC-COLL-OPTC; Becker & Hickl GmbH) connected to a multi-mode probe (F05-MM-FP-OPTH; Becker & Hickl GmbH). The laser power was set to approximately 0.1 mW, as measured at the tip of the optic probe using an optical power sensor (PM100D-S121C; Thorlabs Inc.). Photons emitted from the brain tissue traversed the multi-mode fiber and were collected using a 16-channel multi-wavelength photodetector (PML-SPEC-1-C; Becker & Hickl GmbH) controlled by a detector controller (DCC-100; Becker & Hickl GmbH). The number of photons was counted at 0.1 Hz. The original data was smoothed with a Gaussian Filter and converted into Excel file using customized MATLAB codes (MathWorks). Data acquired were presented as z-score. The detected photon counts were denoted as x, and the mean and standard deviation of the photon count over the entire experimental session as μ and σ, respectively. The z-scored photon counts were then computed as $(x-\mu)/\sigma$.

Behavioral Experiments

In performing OFT, TST, FST, CPP and RTPP, animals were placed in the test room and left for acclimatization for at least 30 min before performing behavioral experiments. The behavioral experiments were monitored and recorded using a computerized tracking system (SMART 3-0, Panlab Harvard Apparatus, Holliston, MA, USA). All the behavioral experiments were analyzed automatically and/or manually by experimenters blinded to the experimental conditions.

Open field test (OFT)

The OFT apparatus is an all-white 40 x 40 cm square arena surrounded by 40 cm high walls. The mice were individually placed in the center of the arena and

their locomotion activity was monitored using an automatic system for 6 min. The distance traveled and time spent in each area were analyzed using an automated video tracking system. The arena was cleaned with 70% ethanol after each use to eliminate any olfactory cues from the previously tested mouse.

Tail suspension test (TST) and Forced swim test (FST)

To observe whether there are changes in depressive-like behaviors of mice, TST and FST were performed. The TST was conducted in an all-white rectangular chamber (height 30 cm, width 15 cm) by suspending the mouse tail using adhesive tape wrapped around its tail 1 cm from the tip and tied to a hook in the chamber. Each mouse was suspended for 6 min and the immobility was automatically measured. The chamber was cleaned with 70% ethanol after each use to eliminate any olfactory cues from the previously tested mouse. FST was conducted by placing each mouse individually in a transparent cylinder filled with water (23°C–25°C; depth 18 cm, height 30 cm) for 6 min. Immobility in FST was defined as a state in which the mouse only made necessary movements to keep its head above the water surface. The data acquired were automatically analyzed using a video tracking system.

Elevated plus maze (EPM)

To observe whether there are changes in anxiety-like behaviors of mice, EPM was performed. The EPM was conducted in an all-white apparatus consisted of two open arms and two closed arms (width 5 cm x length 30 cm) and elevated 50 cm above the floor. The mice were placed individually in the center of the maze facing the open arm and allowed freely to explore for 6 min. The distance travelled and the time spent in each arm was analyzed using a video tracking system. The

maze was cleaned with 70% ethanol after each test to prevent olfactory influence from the previously tested mouse.

Real time place preference (RTPP) and Conditioned place preference (CPP)

RTPP and CPP was performed in a rectangular apparatus consisting of two side chambers (25 × 25 × 30 cm each) with black stripes and gray circles on the walls, connected by a center corridor (10 × 10 cm). In RTPP experiment, mice were habituated (Pre-test, Day 1 to 3) and were allowed to freely explore the entire apparatus for 10 minutes for 3 days. On the test day (Day 4a), mice were placed in the center corridor and was given light stimulation (~3 mW, constant) only when they were within the designated light-paired chamber. Light was turned off when they remained in the chamber for more than 30 sec and was turned on again after 10 sec if they fail to get out of the light-paired chamber. This real-time place preference was consisted of 10-min session. For post-test session (Day 4b), another 10 min was given to mice to freely explore both chambers but without light stimulation pairings.

In CPP, another set of mice were used which were habituated (Pre-test, Day 1 to 3) for 10 min for 3 days allowing mice to freely explore the entire apparatus. On the conditioning day (Day 4), mice were first placed in the light-off-paired chamber for 12 min while blocking the corridor to the other chamber. After 12 minutes, corridor was open and mice were gently led to the other chamber. Once mice reach the other chamber, the corridor is blocked and light stimulation (~3 mW, constant) was delivered for 5 min after 2 min of mice exploration of the chamber and was then turned off until 12 min was reached. On the test day (Day 5), mice were placed in the center corridor and allowed to freely explore the apparatus for 10 min.

The preference of chamber was calculated as percentage of the time spent in

the stimulation chamber over the total time spent in both chambers. All behaviors were recorded using an automated video tracking system.

Threat and non-threat assays

Fox odor exposure. Predator odor, 2,5-dihydro-2,4,5-trimethylthiazoline (TMT, 2199185-5G, Sigma-Aldrich), a component of fox feces, was used as one of the innate threat stimuli. A cotton swab was dipped in a 100 ul TMT (1:10) and was put in a 15 ml conical tube which was tightly closed until exposure experiment starts. This was prepared according to number of animal subjects and on the day of the exposure experiment. Prior to exposure to fox odor, mice were placed in an all-white open arena (40 cm x 40 cm x 40 cm) and allowed to habituate in the open arena for 7 min the day before the exposure experiment. Habituation session was used as the pre-exposure session. On the exposure day, the conical tube-containing the cotton swab with fox odor was opened and put inside the open arena. Mice were brought to the test area one by one. The open arena was cleaned with 70% EtOH after each session. Mice behaviors were recorded and quantified with an automated tracking system. For cFOS detection experiment, mice were sacrificed 1 hr after exposure to fox odor.

RC car attack. For *in vivo* calcium activity recording, mice were placed in an open rectangular arena (length 85 cm x height 40 cm x width 40 cm) and allowed to habituate for 5 min. The recorded Ca^{2+} activity during habituation session was used as the baseline. After 5 min of habituation, a red remote-controlled car (length 20 cm x 5 cm height x width 8 cm) were placed in the corner opposite of where mice were positioned. RC car was controlled to make forward movement, mimicking an

attack, while mice were approaching or in the direction facing the RC car. Each session consisted of at least 3 trials. Mice behaviors were recorded and quantified with an automated tracking system. For cFOS detection experiment, mice were sacrificed 1 hr after 10 min session of RC car attack assay.

Hand attack. Mice were placed in the open arena (40 cm x 40 cm x 40 cm) for 5 minutes prior to experiment proper. For TCSPC recording, Ca^{2+} activity recorded in the habituation session was used as a baseline. Briefly after habituation, stimulus was applied by quickly touching the back of the mouse using the experimenter's hand. Hand attack was applied every 30 sec for 5 min. Hand attacks are innate threat that are not present in the open arena and cannot be investigated or approached by the mouse, unlike the RC car, which randomly attack the mouse from above mimicking previously reported looming stimulus used as a predator replica. The speed of the mice upon escaping from hand attack was automatically detected using the automated tracking system, SMART 3-0. For cFOS detection experiment, mice were sacrificed 1 hr after 5 min session of hand attack assay.

Carbon dioxide exposure. Mice were placed in a transparent box (height 30 cm x width 15 cm x 15 cm) with open top. Mice were habituated in the chamber for 5 min. After habituation, mice were exposed to either air or CO_2 delivered via 3-sec infusion of pure CO_2. The number of jumps, freezing, agonal breathing, and exploration were recorded and quantified manually using SMART 3-0 software.

Acute pain. Formalin injection in the paw is a widely used model of acute pain [111] and was used in this study as another aversive stimulus to observe whether it induces cFOS expression in dPAG. Paraformaldehyde in 0.1 M PBS (4%, 10 μl) was injected into the plantar surface of the left hind paw of mice. Few minutes after

injection, the injected paw was observed with redness and swelling and was then held and licked by the mouse. One hour after the paw injection, mice were sacrificed for cFOS immunostaining.

Fear conditioning. Fear Conditioning. The experiment measured mice freezing response to a conditioned stimulus (cue) which was associated with an unconditional stimulus (mild foot shock) presented during training session. Fear conditioning was conducted in fear-conditioning boxes that consisted of one clear plexiglass wall, three aluminum walls, and a stainless-steel grid as a floor (28 x 28 x 28 cm, Coulbourn Instruments, Holliston, MA, USA).

On the conditioning (training day), mice were placed in the chamber for 2 min and were exposed to series (2 pairing, 110-sec intertrial interval) of cue presentation (2.9 kHz pure tone, 20 sec duration) that co-terminated with a mild foot shock (0.4 mA, 2 sec duration), after 30 sec, mice were placed back to the home cages.

For contextual fear conditioning test, 24 hr after conditioning, mice were placed in the original conditioning chamber and freezing was measured for 5 min.

For auditory-cued fear conditioning, mice were placed in the test chamber with modified contextual elements (floor and walls). Freezing was measured in 150 sec for baseline followed by a 150-sec cue (2.9 kHz pure tone) exposure period.

The grid and the waste tray were cleaned with 70% ethanol between runs. Mice behaviors were recorded using a digital video camera mounted above the chamber and scored automatically for freezing response using FREEZEFRAME software (AM1-FF04, Lafayette Instrument, Lafayette, IN, USA). Data were presented as percentage of freezing response.

Home cage and sucrose. For dPAG cFOS expression experiment, mice that were not exposed to any other stimuli but only to their normal home cages were used as the control group and was sacrificed together with other mice exposed to various stimuli. For sucrose stimulus, mice were constricted of drinking water for 12 hr prior to giving 10% sucrose solution contained in mouse normal drinking bottles. Mice were allowed to access 10% sucrose solution for 30 min and were sacrificed 1 hr after the onset of sucrose exposure.

Female conspecific and novel object exposure. For TCSPC recording, mice were habituated to an open arena (40 cm x 40 cm x 40 cm) for 5 min prior to introduction of female or novel object stimuli. For female conspecific exposure, female mice were habituated for at least 5 min in a wired cup (height 16 cm, diameter 8 cm) with a white lid. After the 5 min habituation of subject mice, female mouse in a wired cup was placed in the open arena. Subject mice were exposed to female conspecific and were allowed to explore and interact with the stimulus for 7 min. The open arena was cleaned by 70% EtOH after each session to remove olfactory cues from previous mice.

For novel object exposure, a cartoon figure with similar size of subject mice and a height of 4 cm, was affixed in the open arena using an adhesive tape, and was used as a novel object. Subject mice were exposed to the novel object and were allowed to explore and interact with the object for 7 min. The open arena was cleaned by 70% EtOH after each session to remove olfactory cues from previous mice. Mice behaviors were recorded and the duration and the number of times mice spent sniffing the stimuli were quantified using SMART 3-0. For cFOS expression experiment, subject mice were sacrificed 1 hr after the exposure to the stimuli.

OFT with optogenetic stimulation

Seven days after recovery from stereotaxic implantation of optic fiber into dPAG or vPAG, GFAP-ChR2 or control mice were placed in the test room 30 min before starting the experiment. Mice with optic fibers connected to a laser were subjected to an open field arena (40 cm x 40 cm x 40 cm) and habituated for 5 min. The last 2 min of the habituation was considered the first light-off epoch followed by a 2 min light-on epoch consisting of ~3 mW of either continuous, 0.5 Hz 10 ms, 20 Hz 10 ms, 40 Hz 10ms, or 100 Hz light stimulation per session. This cycle was repeated to complete the10 min session (2 min off – 2 min on – 2 min off – 2 min on – 2 min off). Freezing response was defined as drastic immobility in an inflexible posture aside from breathing. Fleeing response was characterized as jumping and rapid changes of direction. Retreat response was defined as avoidance-like responses described as backward movements. Lastly, tail rattling response was characterized by stiff followed by fast waving movement of the tail. Behaviors of animals were recorded and manually quantified using SMART 3-0 by an experimenter blinded of the experimental conditions of mice.

Available shelter and optogenetic stimulation

GFAP-ChR2 and control mice were habituated in an open field arena (40 cm x 40 cm x 40 cm) with a white-colored-outside and black-colored-inside shelter (length 18 cm x height 12 cm x width15 cm) for 5 min for 3 days. Habituated mice approached the shelter upon its availability (placed by the experimenter) in the open arena. Successful escape was scored when mice reached the shelter within 5 sec upon shelter availability. On the stimulation day, constant light stimulation was delivered when mice approached and before it finally reached the shelter. Light stimulation

was delivered for 10 sec and was turned off when mice reach the shelter. At least 2 trials were performed for each mouse and each trial was made up of 30 sec. Successful escape bouts, latency to reach the shelter, freezing, fleeing, retreat, and tail rattling were quantified manually by a blinded experimenter using SMART 3-0 Panlab software.

Available shelter and threat with optogenetic stimulation

On the experiment day, mice were habituated in an open field arena (length 85 cm x height 40 cm x width 40 cm) with a gray-colored outside and black-colored inside shelter with a dark gray-tinted lid (20 cm x 20 cm x 20 cm) for 10 min and then an RC car (length 20 cm x 5 cm height x width 8 cm) was introduced at the opposite side of the shelter. Mice were allowed to explore the area with the RC car for 8 min until mice were able to approach and sniff the object. After 8 min, mice which were approaching were randomly attacked to evoke immediate escape to shelter. Successful escape was scored when mice reach the shelter within 5 sec upon the onset of RC car attack. For light-on epochs, constant light stimulation (~3mW) was delivered when mice were approaching the RC car. The successful escape, latency to reach the shelter, and defensive-like behaviors were quantified by an experimenter blinded with the condition of experimental groups.

Simultaneous stimulation of neurons and astrocyte

GFAP-ChR2 mice were injected with hSyn-oChIEF-tdTomato or control virus. After 7 days, mice were implanted with optic fibers into the dPAG. Mice were allowed to recover for another 7 days. After recovery period, mice were subjected into an escape experiment through an all-white rectangular open arena (length 85 cm x height 40 cm x width 40 cm) that consisted of a gray-colored outside and black-

colored inside shelter with a dark gray-tinted lid (20 cm x 20 cm x 20 cm) and a stimulation zone with a mouse-sized novel object affixed at the center of the stimulation zone to enrich the open arena and engage mice to explore. hSyn-oChIEF-tdTomato -injected GFAP-ChR2 mice were placed in the arena and given 10 min to freely explore the environment. After the 10 min habituation session, blue light stimulation, ~3mW, 10 ms 40 Hz, constant light, or no light, was delivered when the mice entered the stimulation zone. Light was turned off when mice leave the stimulation zone. Successful escape or flight response was scored when mice reach the shelter within 5 sec at the onset of light stimulation. The experiment session lasted 30-40 minutes per mouse with at least 5 trials for each light condition. Twenty-four hours after the first escape experiment, the same GFAP-ChR2 mice were injected with 100 μg/g tamoxifen or vehicle for control group, for 5 days to express ChR2-eYFP on astrocytes. Two days after the last injection of tamoxifen, the same mice, now expressing both hSyn-oChIEF and GFAP-ChR2, were subjected to the same escape experiment. The same procedures were performed on the same mice. Light stimulation (~3mW, 10 ms 40 Hz or continuous light) lasted for 1 min and resumed after 30 sec if the mice did not leave the stimulation zone. This second escape experiment session lasted 30-40 minutes per mouse with at least 5 trials for each light condition. The percentage of successful escape, latency to reach the shelter, and the observed defensive-like behaviors were recorded and quantified using SMART 3-0 software by an experimenter blinded to experimental conditions.

Neuronal stimulation and astrocyte ablation

C57BL/6 mice were injected with hSyn-oChIEF-tdTomato into dPAG and after 14 days of virus expression, 0.1 M PBS or 20 ug/ul of L-AAA was injected on

the same site followed by unilateral implantation of an optic fiber. Mice were given 2-3 days to recover before performing the escape experiment. On the experiment day, mice were placed in the rectangular arena (length 85 cm x height 40 cm x width 40 cm) that consisted of a gray-colored outside and black-colored inside shelter with a dark gray-tinted lid (20 cm x 20 cm x 20 cm) and a stimulation zone with a mouse-sized novel object affixed at the center of the stimulation zone to enrich the open arena and engage mice to explore. Mice were given 10 min to habituate and explore the environment. L-AAA- and PBS-injected mice with hSyn-oChIEF-tdTomato were given light stimulation (~3mW, 10ms 40 Hz or constant light or light-off) randomly when they entered the stimulation zone. Light was turned off when mice moved outside the stimulation zone. Successful escape or flight response was scored when mice reach the shelter within 5 sec at the onset of light stimulation. The experiment session lasted 30-40 minutes per mouse with at least 5 trials for each light condition. The percentage of successful escape, latency to reach the shelter, and the observed defensive-like behaviors were recorded and quantified using SMART 3-0 software by an experimenter blinded to experimental conditions.

Opto-vTrap stimulation

After recovery period, wild type mice or GFAP-ChR2 mice injected with GFAP-Opto-vTrap were subjected to behavioral experiments. Opto-vTrap-injected mice were placed in the test room 30 min before starting the experiment. Mice with optic fibers connected to a laser were subjected to an open field arena (40 cm x 40 cm x 40 cm) for a 5 min session. The first 2 min of the session was considered the first light-off epoch followed by a 2 min light-on epoch consisting of 3 mW of constant blue light. Then, at the last min, light was turned off. Behaviors of animals

were recorded and automatically quantified using SMART 3-0 while freezing behavior was quantified manually.

Hot plate and CO_2 assay with escape route

The hot plate assay was done using a metallic heating plate (MSH-20A, Daihan Scientific, Daegu, South Korea) heated at about 40C or at room temperature. A transparent box (18 cm x 18 cm x 30 cm) that has open top and bottom was placed on top of a heated plate. A rope, attached from the sides of the transparent box, was used for mouse to climb as an escape route to avoid the heat. The mice were habituated in the set-up one day prior to the experiment day. On the experiment day, mouse was placed in the set-up in either heated or room temperature for a 15 min session. To avoid the heated plate, mice climbed the rope and went back to the heated floor than hang on the rope with their weight. The number of climbs and the average latency of climbing since touching the hot plate was quantified.

In vivo microdialysis with light stimulation

After surgery, a CMA7 microdialysis probe (shaft length 5 mm; shaft outer-diameter 0.58 mm) was implanted through the guide cannula. The probe was connected to a CMA100 microinjection pump (CMA Microdialysis) using polyethylene tubing (PE 50) and FEP tubing (INSTECH, Plymouth Meeting, PA, USA). ACSF was used as the microdialysis fluid (in mM: 149 NaCl, 2.8 KCl, 1.2 MgCl2, 1.2 CaCl2, and 5.4 glucose, pH7.4) which was perfused into the inlet of the probe at a flow rate of 1.5 μl/min. Perfusates from the outlet of the tubing were automatically collected in plastic vials at 8°C using a CMA470 refrigerated fraction

collector. Dialysates were collected over 20 min during light-off and light-on epoch. Dialysates were stored at −80°C until used for gliotransmitter assays

GABA, Glutamate, D-serine, and extracellular ATP assays

GABA concentrations were obtained using LC/MS performed by Neurovis Co. (Cheonan, Korea). Glutamate, D-serine, and extracellular ATP concentrations were measured using kits according to the respective manufacturer's instruction. All assays were performed using a 96-well microplate. Glutamate was measured using a colorimetric assay kit (#K629-100; Biovision, Milpitas, CA, USA), and D-serine with a fluorometric assay kit (#K743-100; Biovision).

For extracellular ATP assays, briefly, using acute brain slices, dPAG slices were collected from ChR2-expressing GFAP-ChR2 mice. The dPAG slices were incubated in ice-cold oxygenized ACSF for 10 min and samples were collected and labeled as 'light-off'. Ice-cold oxygenated ACSF was replaced and dPAG slices were subjected to light stimulation for 10 min with similar procedures with slight modification performed in previous report [112]. The ACSF was then collected and temporarily stored to -80°C. The ATP level was determined using a bioluminescent ATP assay kit (FF2000; Promega, Madison, WI, USA) and measured using luminometer (SPARK 10M, Tecan, Grödig, Austria). The GABA, Glutamate, D-serine, and ATP amounts were normalized to the total protein amounts of each sample.

Primary astrocyte culture and in vitro Ca^{2+} assay

Primary astrocytes were isolated from the cortical area, midbrain, and brainstem of postnatal day 1 GFAP-ChR2 mice and prepared using a modified established protocol [113]. Briefly, after removing the meninges from the cerebral hemisphere, the tissue was dissociated into a single-cell suspension by gentle repetitive pipetting and was filtered through a 70 μm filter (#352350, Falcon, NY, USA). The cells were cultured in DMEM supplemented with 10 mM HEPES, 10% FBS, 2 mM L-glutamine, and 1x antibiotic/ antimycotic in 75 cm^2 flasks at 37° C in a 5% CO2 incubator. The medium was changed every 5 days. After 3 weeks, the flask was shaken at 250 rpm for 2 hr at 37° C, treated with 100 mM L-leucine methyl ester for 60 min to remove microglial cells, and harvested using trypsinization (0.25% trypsin, 0.02% EDTA). Primary cells were plated on PDL-coated cover glasses and incubated. After seeding, the cells were treated with 4-OH-tamoxifen (1 mM, #H7904, Sigma-Aldrich) ofr2 days with a new medium. Calcium activity of astrocyte expressing ChR2 was measured by a single-cell calcium imaging using Rhod-2-AM (Invitrogen, Carlsbad, CA, USA). Cells were incubated for 30 min at 37° C with 2μm Rhod-2-AM in HBSS containing 25 mM HEPES (pH 7.5) and washed with HBSS-HEPES before Ca^{2+} assays. A baseline reading was taken for 2 min before blue light (473 nm, ~3 mW) stimulation. Intracellular calcium levels were measured via a digital video microfluorometry with an intensified charge-coupled device camera (CasCade, Roper Scientific, Trenton, NJ, USA) coupled to a microscope and analyzed with MetaFluor software (Universal Imaging Corp., Downtown, PA, USA). The fluorescence intensity data were z-scored for each trace.

Immunohistochemistry

Mice were transcardially perfused with ice-cold 0.1 M phosphate-buffered saline (PBS; pH 7.4) until all blood was removed, followed by perfusion with ice-cold 4% paraformaldehyde in 0.1 M PBS. Whole brains were post-fixed in 4% paraformaldehyde in 0.1 M PBS overnight at 4°C and cryoprotected with 30% sucrose for 3 days. Brains were cryosectioned to 40-μm-thick coronal sections and incubated in cryoprotectant at –20°C until immunohistochemical staining was performed. The sections were incubated in a blocking solution containing 5% normal donkey serum (Jackson ImmunoResearch, Bar Harbor, ME, USA), 2% BSA (Sigma-Aldrich), and 0.1% Triton X-100 (Sigma-Aldrich) for 1.5 hr at room temperature. Subsequently, the sections were incubated with mouse anti-NeuN (MAB377B, 1:1,000; Millipore, Billerica, MA, USA), mouse anti-GFAP (MAB360, 1:1,000; Millipore), rabbit anti-S100ß (ab52642, 1:500; Abcam, Cambridge, MA, USA), rabbit anti-Iba1 (019-19741, 1:1,000; Wako, Richmond, VA, USA), and rabbit anti-cFos (PC05-100UG, 1:1,000; Millipore) antibodies overnight at room temperature in a blocking solution. After washing with 0.1 M PBS containing 0.1% Triton X-100, the sections were incubated for 1 hr with FITC-, cy3-, or cy5-conjugated secondary antibodies (1:200, Jackson ImmunoResearch) in a blocking solution at room temperature, washed three times, and then mounted on gelatin-coated glass slides using Vectashield (Vector Laboratories, Inc., Burlingame, CA, USA). Fluorescent images of the mounted sections were obtained using a confocal microscope (LSM800; Carl Zeiss, Jena, Germany).

Image acquisition and quantification

Image acquisition was performed using Carl Zeiss confocal laser scanning microscope. Image quantification was performed on images collected using the 20x objective. Laser intensity and gain were kept constant between experiments. Quantification of the number of cells were performed manually using the Event function of ZEN 2.0 software within a defined region of interest (ROI) in each tissue section. Quantification data were obtained using at least 3 mice, and at least 4 tissue sections per mouse, for each experimental group. Cell density quantification were normalized and presented as fold change compared to designated control group.

Western blot assay

The brains were removed from mice 2 days after PBS or L-AAA injection, and rostral to caudal region of dPAG was dissected on an ice-cold metal stage and frozen at -80°C until further processing. To extract proteins for GFAP analyses, individual tissue samples were weighed and homogenized in 5 volumes of ice-cold buffer containing 20 mM Tris (pH 7.5), 5% glycerol, 1.5 mM EDTA, 40 mM KCl, 0.5 mM dithiothreitol, and protease inhibitors (No. 539131, Calbiochem, San Diego, CA, USA). Homogenates were centrifuged at 14,000 rpm for 1 h at 4°C. The supernatant was removed from each sample, and an aliquot was collected for determination of total protein concentration using the Pierce BCA assay (Thermo Fisher Scientific, Hampton, NH, USA). The proteins were separated using sodium dodecyl sulfate (SDS)-polyacrylamide gel electrophoresis and transferred to a polyvinylidene difluoride (PVDF) membrane. Membranes were incubated with primary antibodies against GFAP (1:1,000, DAKO) and β-actin (1:5,000, Sigma-

Aldrich). Proteins were detected with horseradish peroxidase-conjugated secondary antibodies using the West Save Gold western blot detection kit (Ab Frontier, Seoul, Korea). Signals were visualized using MicroChemi (DNR Bio-imaging Systems, Jerusalem, Israel). The relative expression level of GFAP was determined using densitometry and normalized to the β-actin expression level.

Statistics

Briefly, depending on the normality of data distribution, statistical significance for comparisons between two groups was determined using Independent or Paired t-test. For multiple comparisons, one-way analysis of variance (ANOVA) followed by LSD post-hoc analysis unless otherwise mentioned in the figure legends. All data are represented as mean ± standard error of the mean (SEM), and differences were considered statistically significant if the p value is less than 0.05. Statistical analyses were performed using SPSS (v25, IBM SPSS Statistics).

3. Results

dPAG astrocyte Ca^{2+} activity increases in threatening situations

To determine whether astrocytes in dPAG is involved in mice defensive responses to threatening situations, mice were exposed to different threat stimuli. Previous studies have shown that exposure to threat stimuli induce cFos expression in dPAG [4,114]. Similarly, the threat stimuli (described in Chapter 2) used in this research were validated as the author observed the increased level of cFos in dPAG compared to control environment, the home cage. cFos level was significantly increased after exposure to foot shock, fox odor, hand attack, and RC car (Figure 4A). Meanwhile, dPAG cFos level after exposure to acute pain, novel object, female mouse, and sucrose did not show significant difference when compared with control, home cage group (Figure 4A). Quantification of the $cFos^{+}$ cells fold change compared to home cage control group was illustrated in Figure 4B.

To test whether astrocytes in dPAG are engaged in mice defensive responses to threatening situations, in vivo fiber photometry method was performed using time correlated single photon counting (TCSPC) to measure intracellular Ca^{2+} activities dPAG astrocyte-expressing GCaMP6f virus during mouse exposure to various threat stimuli (Figure 5A). dPAG was targeted by local injection of adeno-associated viruses (AAV) expressing GfaABC1D-GCaMP6f followed by implantation of TCSPC optic fiber probe (Figure 5B). Histology data showed that GCaMP6f is

mostly colocalized with S100β+ astrocytes, with negligible expression in NeuN^{+} neurons or Iba-1^{+} microglia (Figure 5C, D).

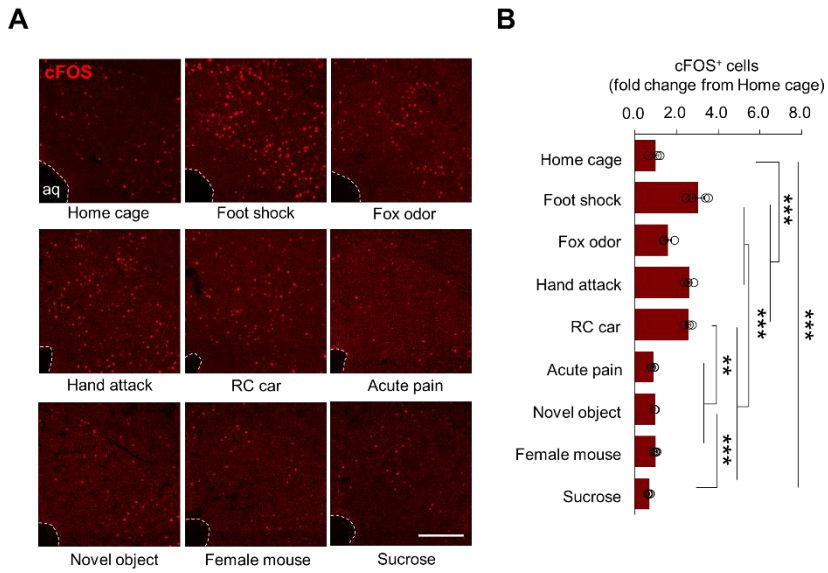

Figure 4. Validation of threat stimuli via cFOS expression in dPAG

(**A**) Representative images of dPAG tissue sections stained with anti-cFOS (red) from mice exposed to various stimuli. Scale bar, 200 μm. aq: aqueduct (**B**) Quantification of the number of the cFOS^{+} cells fold change from control group 'Home cage' in dPAG upon exposure to various stimuli (n = 4 mice, 3 - 4 dPAG slices per mouse; one-way ANOVA followed by LSD post-hoc test, **$p < 0.01$, ***$p < 0.001$; data are presented as mean ± SEM).

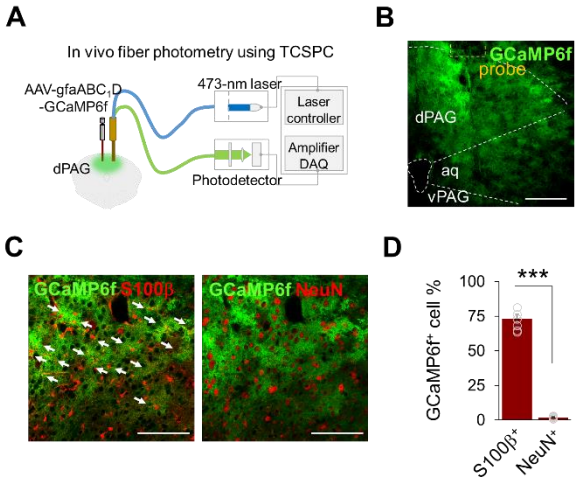

Figure 5. *In vivo* Ca^{2+} activity measurement using TCSPC

(A) Schematic diagram of *in vivo* Ca^{2+} recording using TCSPC. Mouse dPAG were injected with GfaABC1D-GCaMP6f and implanted with TCSPC probe connected to a laser controller emitting 473 nm blue light and a photodetector for Ca^{2+} activity detection. (**B**) Representative image of GfaABC1D-GcaMP6 virus expression in dPAG and probe implantation. vPAG: ventral periaqueductal gray, aq: aqueduct. Scale bar, 200 μm. (**C**) Representative images of the dPAG astrocyte injected with GcaMP6f (green) and its colocalization with $S100\beta^+$ astrocytes (red, left image) and $NeuN^+$ neurons (red, right image). White arrows indicate merged signals with GcamP6. Scale bar, 100 μm. (**D**) Quantification of the percentage of $S100\beta^+$ and $NeuN^+$ cells colocalized with GcaMP6f in dPAG ($S100\beta^+$, n = 6 mice; $NeuN^+$, n = 6 mice; 2 dPAG slices per mouse; independent T-test ***$p<0.001$).

Mice were exposed to various threatening situations while simultaneously measuring dPAG astrocyte Ca^{2+} activities in vivo. Mice were placed in an open field arena and exposed to a predator odor using 2,5-dihydro-2,4,5-trimethylthiazoline (TMT), a component of fox feces (referred to as 'fox odor', Figure 6A). Previous studies have shown that TMT induced fear and defensive behaviors, indicating that it is an innate threat stimulus [115]. Data showed that upon exposure to fox odor, mice elicited a significant increase of freezing percentage compared to pre-exposed mice (Figure 6B). Also, dPAG astrocyte significantly increased Ca^{2+} activity upon exposure to fox odor compared to baseline level, recorded during exposure to only unscented water (Figure 6C). Individual mouse used in this experiment and each mouse's dPAG astrocyte Ca^{2+} activity was illustrated further in Figure 6D and E, exposure to only unscented water and fox odor.

Furthermore, mice were exposed to a remote controlled (RC) car (Figure 7A) which was presented as an innate threat described as a large moving object [116,117]. The presence of RC car as a large moving novel object in the open arena evoked vigilance and or risk assessment behavior in mice (Figure 7B). Mice that were approaching and risk assessing the RC car were randomly attacked by the RC car, which led mice to flee away from the stimulus (Figure 7C). Correspondingly, in vivo fiber photometry data showed dPAG astrocyte Ca^{2+} activity significantly increased when mouse started risk assessing and approaching the RC car (Figure 7D) compared to the baseline level, recorded before exposure to RC car. Individual mouse's dPAG astrocyte Ca^{2+} activity recording during risk assessing and approaching were illustrated in Figure 7G and baseline recordings of each mouse in Figure 7F. Moreover, dPAG astrocyte evoked a strong Ca^{2+} activity increase upon

fleeing from the RC car attack (Figure 7E), which went down to baseline level when mice reached the corner of the open arena. Individual mouse recording during the flight from RC car attack was illustrated in Figure 7H. Meanwhile, this significant increase in Ca^{2+} activity was not observed when mice were exposed to a small inanimate object (Figure 10).

Another threat stimulus was applied by quickly touching the back of the mouse using the experimenter's hand which was previously used in other studies of fear and defensive behaviors [118]. It was referred to as "hand attack" in figures (Figure 8A). Compared to RC car, hand attacks are innate threat stimuli that are not presented in the open arena and cannot be approached by the mouse in the open field but a threat stimulus which randomly attack the mouse from above mimicking looming predators. Data showed that hand attack elicited escape or fleeing behaviors in mice (Figure 8B) and evoked a strong increase of dPAG astrocyte Ca^{2+} activity (Figure 8C). Individual mouse's dPAG astrocyte Ca^{2+} activity recording at baseline or before experiencing hand attack, and recoding when mouse was attacked were shown in Figure 8D and E.

Moreover, mice were also exposed to non-threatening stimuli such as a female conspecific (Figure 9A) and a small novel object (Figure 10A), as these stimuli might trigger activity in midbrain PAG area according to previous studies [119,120] However, dPAG astrocyte Ca^{2+} activity did not show a significant increase compared to the baseline level when mice were interacting with a female conspecific by sniffing behavior (Figure 9B, C). Individual mouse during baseline, before female mouse exposure, and during exposure to female mouse were shown in Figure 9D and E. Similarly, mice exposed to a small novel object (Figure 10A) with little to no

threat value did not evoke any significant increase in dPAG astrocyte Ca^{2+} activity during exposure and sniffing of the small object (Figure 10B, C). Individual mouse recording during the baseline and exposure to small novel object were shown in Figure 10D and E. These data suggest that the observed Ca^{2+} elevations of dPAG astrocyte are specifically evoked by threatening stimuli.

Taken together, these results demonstrate that upon exposure to various threat stimuli and exhibiting the consequent defensive behaviors, dPAG astrocyte remarkably responds by increasing Ca^{2+} activity. These data suggest a novel finding of the active response and involvement of dPAG astrocyte under threatening situations.

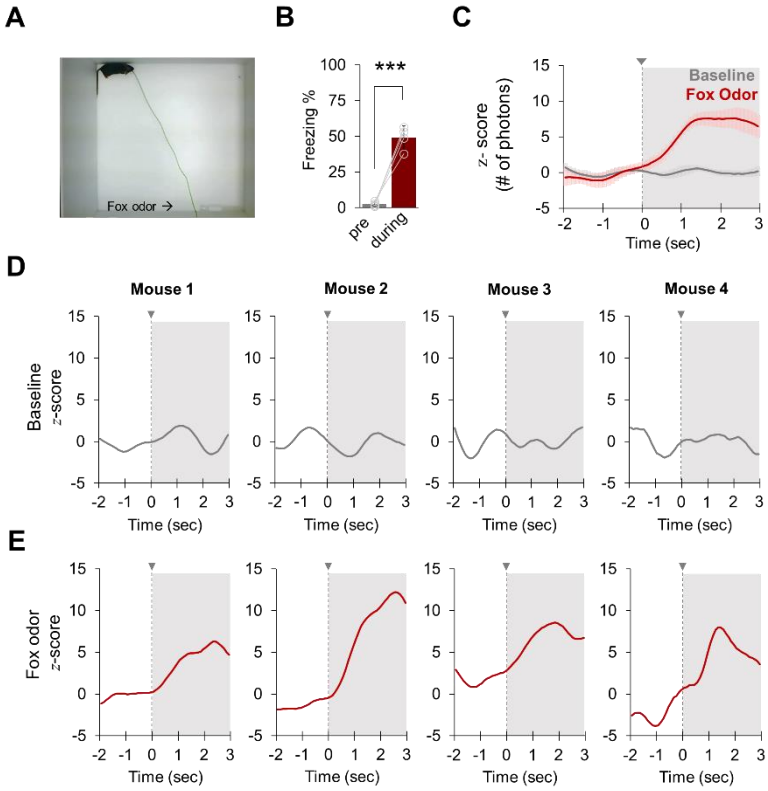

Figure 6. dPAG astrocyte Ca^{2+} activity increased upon exposure to predator odor

(**A**) Illustration of mouse exposure to fox odor in an open field arena. (**B**) Percentage of freezing response of mice pre and during fox odor exposure (n = 4, Paired t-test ***$p < 0.001$). (**C**) dPAG astrocyte Ca^{2+} activity mean trace presented as z-score before fox odor exposure (Baseline or no scent, gray line) and during fox odor exposure (Fox Odor, red line) indicated with gray shade at onset 0 sec. (**D**) Individual mouse Ca^{2+} activity trace used in the experiment, activity is presented as z-score before fox odor exposure. Gray shade and broken gray line indicate exposure to no/ neutral scent stimulus at onset 0 sec. (**E**) Individual mouse Ca^{2+} activity trace used in the experiment, activity is presented as z-score upon fox odor exposure. Gray shade and broken gray line indicate exposure to fox odor at onset 0 sec.

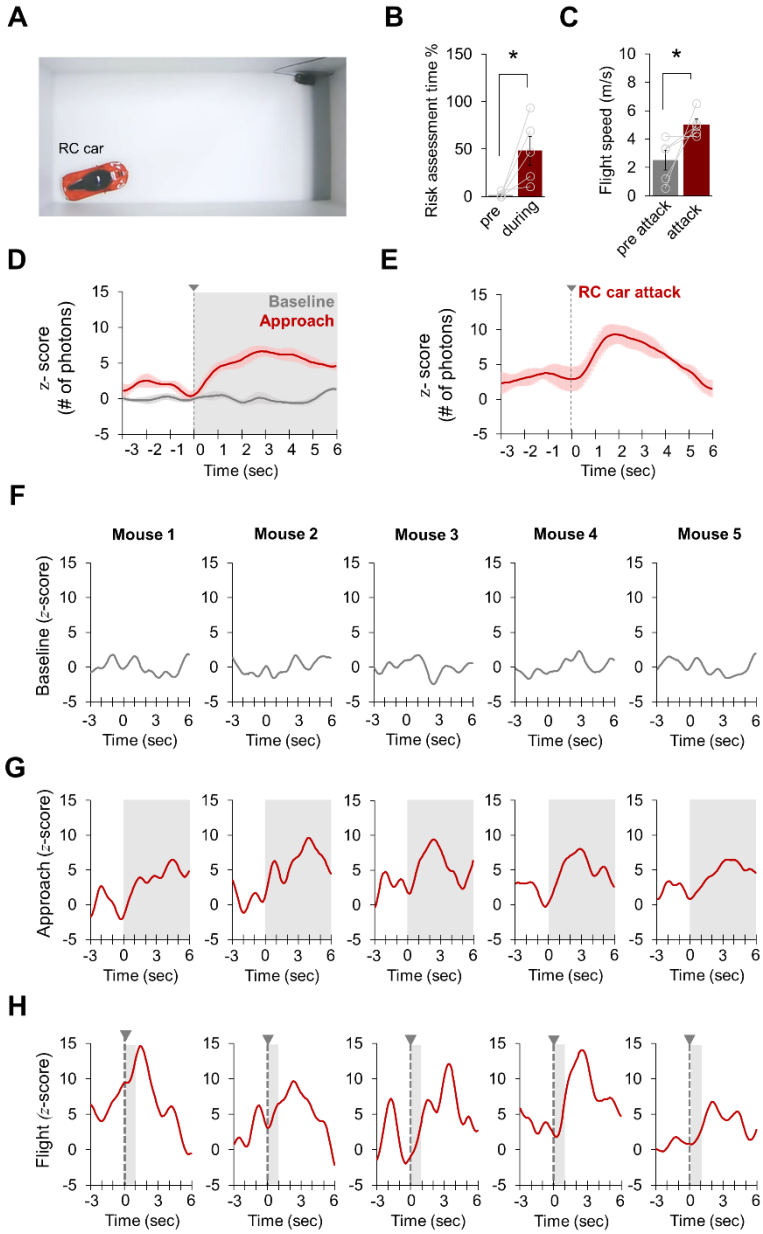

Figure 7. dPAG astrocyte Ca^{2+} activity increased upon mouse risk assessment and flight from a threatening object

(**A**) Illustration of mouse exposure to RC car in a rectangular open arena. (**B**) Percentage of mice risk assessment before and during exposure to RC car. (**C**) Speed of flight response before and upon RC car attack (n = 5 mice, Paired t-Test, *$p < 0.05$) (**D**) Ca^{2+} activity mean traces when mice risk assessed and approached the RC

car (Approach onset is at 0 sec and behavior is ongoing along gray shaded area time) compared to when mice were away from the RC car (Baseline, gray line). (**E**) Ca^{2+} activity mean trace when the same mice were attacked by the RC car (Attack, onset is at 0 sec indicated by gray broken line). (**F**) Individual mouse Ca^{2+} activity trace used in the experiment. Activity is presented as z-score before RC car exposure. (**G**) Individual mouse Ca^{2+} activity trace used in the experiment, activity is presented as z-score upon mouse risk assessment behavior toward RC car. Gray shade indicates mouse stretch-approach position towards the RC car at onset 0 sec. (**H**) Individual mouse Ca^{2+} activity trace used in the experiment, activity is presented as z-score upon mouse flight against RC car attack. Gray broken line indicates onset of RC car attack and gray shade indicates mice flight behavior in response to attack.

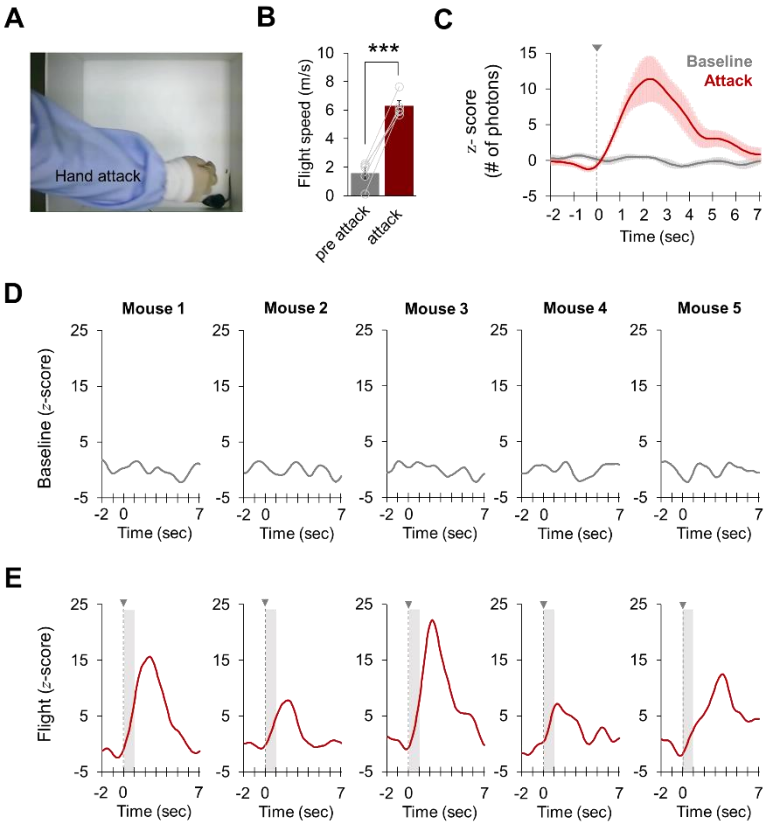

Figure 8. dPAG astrocyte Ca^{2+} activity increased upon fleeing from a looming and attacking stimuli

(**A**) Illustration of the hand attack assay (**B**) Speed of mouse flight response upon hand attack compared to mouse normal speed in the arena (n = 5, Paired t-Test, ***p < 0.001) (**C**) Hand attack assay Ca^{2+} activity mean traces before the stimulus (Baseline, gray line) and when experimenter attack the mice (Attack, red line; attack onset at 0 sec). (**D**) Individual mouse Ca^{2+} activity trace used in the experiment, activity is presented as z-score during baseline or before exposure to threat stimulus (**E**) Individual mouse Ca^{2+} activity trace used in the experiment, activity is presented as z-score upon mouse flight response against the hand attack. Gray broken line indicates onset of hand attack and gray shade indicates mice flight behavior in response to attack.

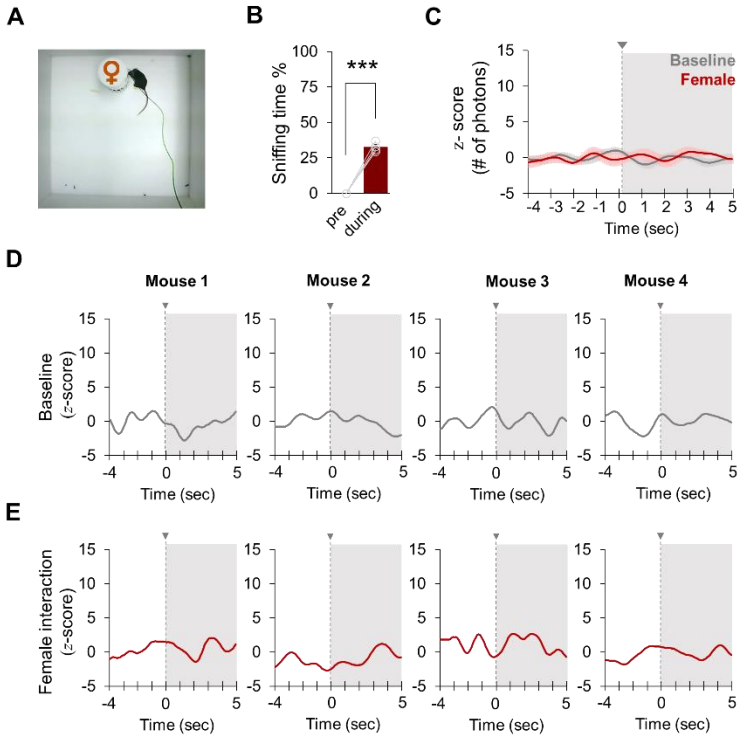

Figure 9. dPAG astrocyte Ca^{2+} activity did not change upon mouse exposure to female conspecific

(**A**) Illustration of the female mouse exposure where female conspecific was placed in a wired cup and the subject mouse was freely approaching the cup. (**B**) Percentage of mouse sniffing time to stimulus before and during female mouse exposure (n = 4, Paired t-test, ***$p < 0.001$). (**C**) Female mouse exposure assay Ca^{2+} activity mean traces before mice were exposed to a female mouse (Baseline, gray line) and when mice were exposed and sniffing the female mouse (Female, red line; sniffing onset at 0 sec; sniffing behavior is indicated with gray shade) (**D**) Individual mouse Ca^{2+} activity trace used in the experiment, activity is presented as z-score during baseline or exposure to only the conspecific container (**E**) Individual mouse Ca^{2+} activity trace used in the experiment, activity is presented as z-score upon mouse interaction with female conspecific in the social cup. Gray broken line and gray shade indicate onset of sniffing behaviors to stimuli.

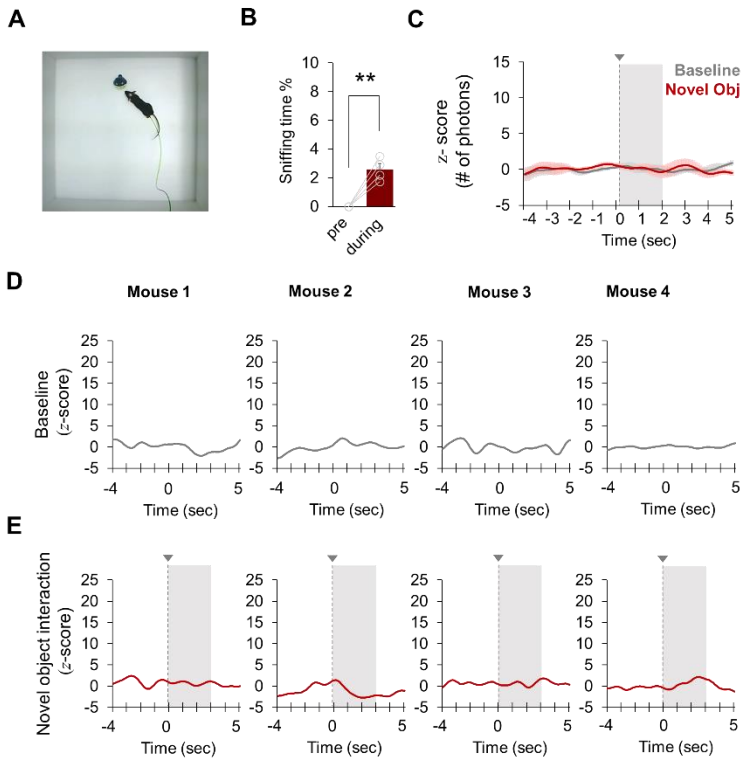

Figure 10. dPAG astrocyte Ca^{2+} activity did not change upon mouse exposure to small novel object

(**A**) Illustration of the novel object exposure assay. (**B**) Percentage of mouse sniffing behavior before and during exposure to a novel object (n = 4, Paired t-Test, **p < 0.001) (**C**) Novel object exposure assay: Before mice were exposed to novel object (Baseline, gray line) and when mice were exposed and started sniffing the novel object (Novel Obj, red line; sniffing onset at 0 sec; sniffing behavior is indicated with gray shade) (**D**) Individual mouse Ca^{2+} activity trace used in the experiment, activity is presented as z-score during baseline or before exposure to the small novel object (**E**) Individual mouse Ca^{2+} activity trace used in the experiment, activity is presented as z-score upon mouse sniffing to the novel object. Gray broken line and gray shade indicate onset of sniffing behaviors to stimulus.

dPAG astrocyte is required for optimal defensive responses to threat

To investigate whether dPAG astrocyte is necessary in executing defensive responses to threatening situations, dPAG astrocytes were pharmacologically ablated using L-α-aminoadipate (L-AAA), a glutamate homologue acting as an astrotoxin[108,121]. L-AAA (20 ug/ul) injection into mouse dPAG reduced S100β^{+} astrocytes but not NeuN^{+} cells as demonstrate in histology data (Figure 11A). Likewise, GFAP protein expression from western blot experiment was significantly reduced in dPAG of L-AAA -injected mice compared to PBS-injected mice (Figure 11B) with no influence on neuronal density as demonstrated from the manual quantification of NeuN^{+} cells of the histology samples (Figure 11C).

Two to 3 days after L-AAA or PBS injection, mice were subjected to various threat stimuli and defensive behaviors were observed. As a general test of fear behavior to observe freezing response in mice, auditory-cued fear conditioning was performed where mice were placed in a chamber and received a foot shock associated with an auditory cue. After 24 hr, mice were subjected to a novel chamber where freezing percentage was recorded before and during presentation of only the conditioned auditory cue (Figure 12A). During presentation of the conditioned auditory cue, L-AAA-injected mice showed a significantly reduced freezing response compared to PBS-injected mice (Figure 12B) which was not seen in hippocampal-dependent contextual fear/memory test (Figure 14E). Moreover, L-AAA injected mice showed significantly decreased freezing and increased exploration in the periphery of arena during exposure to fox odor compared to PBS-injected mice (Figure 12C-E). In the hand attack and RC car assays, L-AAA-injected

mice fled from the hand attack with a significantly reduced speed compared to PBS-injected mice (Figure 12F, G).

Meanwhile, when mice were exposed to non-threatening stimuli such as female mouse conspecific (Figure 13A) and or a small novel object (Figure 13C), L-AAA- and PBS-injected mice showed no significant difference in the percentage of time spent in the zone of stimulus (Figure 13B, D). Time spent in the stimulus zone suggests the duration of mice approaching and sniffing the stimulus.

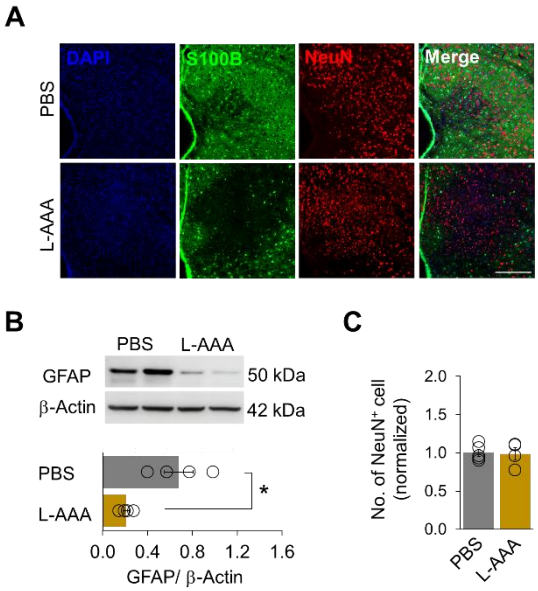

Figure 11. dPAG astrocyte ablation using L-AAA

(**A**) Representative images of mouse dPAG slice injected PBS or L-AAA showing DAPI (blue), S100β^{+} astrocytes (green), NeuN^{+} cells (red) and the merged images. Scale bar, 200 μm. (**B**) Upper: representative western blots of GFAP and β-actin expressions in PBS and L-AAA -injected mouse dPAG. Lower: quantification of the fold expression of GFAP over β-actin levels in PBS and L-AAA -injected mouse dPAG (n = 4 mice; *$p < 0.05$). (**C**) Quantification of NeuN^{+} cell density in PBS and L-AAA -injected mice (PBS n = 5, L-AAA n = 4, 3 slices per mouse, Independent t-Test).

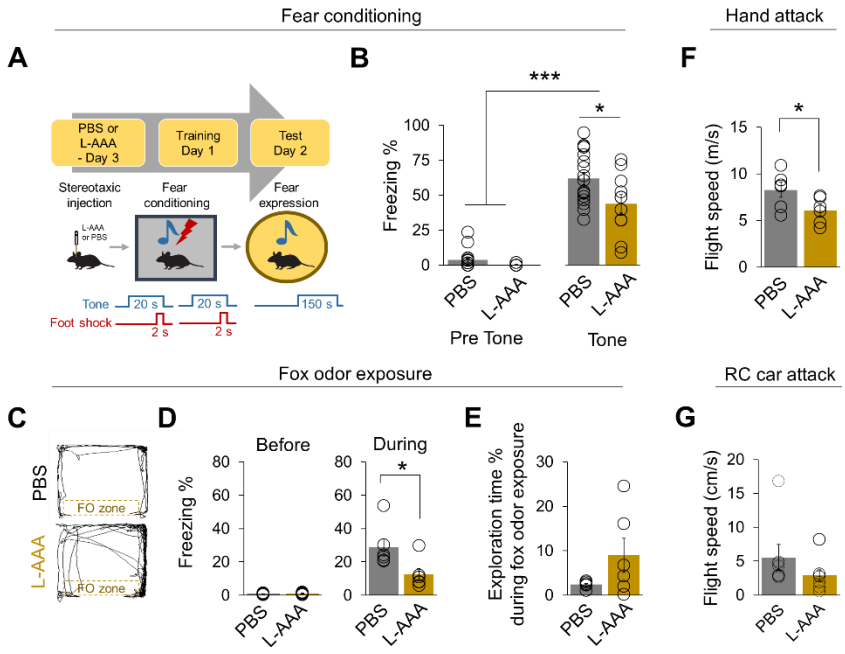

Figure 12. dPAG astrocyte ablation reduced mouse defensive response against threat stimuli

(**A**) Schematic illustration of the fear conditioning paradigm. PBS or L-AAA -injected mice were fear conditioned on the training day in 2 trials consisting of a 20-s sound cue co-terminating with a 2-s foot shock. Fear behavior was tested in Day 2 from 150-s pre-tone and 150-s tone exposure. (**B**) Freezing percentage of PBS and L-AAA -injected mice in auditory fear conditioning: pre-auditory cue exposure and auditory cue exposure sessions (PBS n = 11 mice, L-AAA n = 17 mice, Two-way ANOVA, Independent t-Test, ***$p < 0.001$, *$p < 0.05$). (**C**) Sample trace of PBS and L-AAA -injected mice exploration in an open arena with fox odor. (**D**) Freezing percentage of PBS and L-AAA -injected mice before and during exposure to fox odor (n = 7 mice per group; Independent t-Test, $p < 0.05$). (**E**) Percentage of exploration time in the fox odor zone of PBS and L-AAA -injected mice. (**F**) Speed of flight response against hand attack of PBS and L-AAA -injected mice (**G**) Speed of flight response against RC car attach of PBS and L-AAA – injected mice.

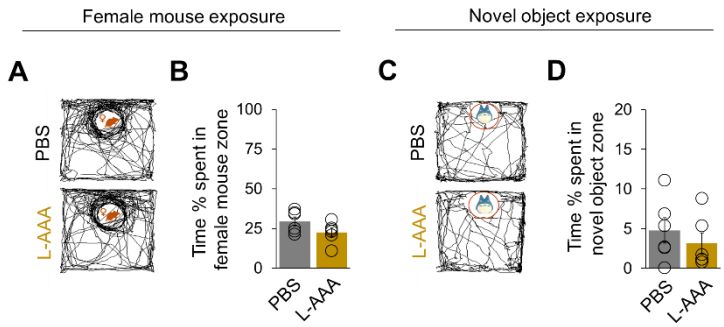

Figure 13. dPAG astrocyte ablation did not change mouse behavior upon exposure to non-threatening stimuli

(**A**) Sample trace of the exploration of PBS and L-AAA -injected mice in an open arena with a female conspecific. (**B**) Percentage of time spent in the female mouse zone between PBS and L-AAA -injected mice (n = 7 mice per group; Independent t-test). (**C**) Sample trace of the exploration of PBS and L-AAA -injected mice in an open arena with an inanimate novel object. (**D**) Percentage of time spent in the novel object zone between PBS and L-AAA -injected mice.

In addition, to test whether L-AAA or PBS injection to dPAG will affect other behaviors, mice were subjected to a series of general behavioral tests. Data showed that both groups did not vary in total distance travelled and time spent in the center of an empty open arena, suggesting that neither PBS nor L-AAA injection had any effect on locomotor activity and anxiety-like behavior of mice against the open space in the open field test (Figure 14A, B). Also, L-AAA and PBS-injected mice showed no significant differences in immobility duration which is a parameter of depressive-like behaviors in a helpless environment such as the tail suspension test (TST, Figure 14C) and forced swim test (FST, Figure 14D). Moreover, mice were also subjected to the contextual conditioning test, also known as a hippocampal-

dependent contextual memory test. Compared to baseline, both mice showed significant increase of freezing percentage when exposed to the context where they received foot shock 24 h prior to test, however, there was no significant difference in the freezing percentage between the groups when exposed to the conditioned context (Figure 14E). Likewise, there were no significant differences observed in the time spent in the center (Figure 14F), open arms (Figure 14G), and closed arms (Figure 14H) of the elevated plus maze (EPM) which is one of the general behavioral tests to measure anxiety-like behaviors. These data suggested that pharmacological ablation of dPAG astrocyte through injection of L-AAA did not affect other mouse behaviors besides defensive behaviors.

Notably, behavioral tests involving salient threatening stimuli highlighted defensive responses of mice which were significantly attenuated and reduced upon dPAG astrocyte ablation through L-AAA. These results denote that dPAG astrocytes are required for efficient and optimal defensive responses against threatening stimuli.

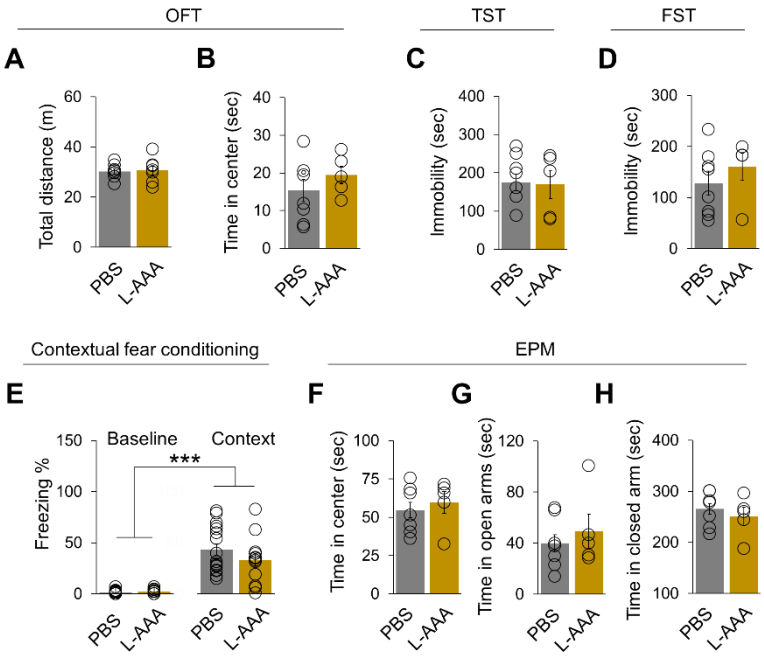

Figure 14. dPAG astrocyte ablation did alter other mouse behaviors

(**A**) Total distance travelled of PBS or L-AAA -injected mice in open field arena (PBS n = 8, L-AAA n = 7, Independent t-Test) (**B**) The time mice spent in the center of the open field test (OFT) (**C**) Duration of immobility in tail suspension test (TST) between PBS and L-AAA -injected mice (n = 7 mice per group; Independent t-Test). (**D**) Duration of forced swim test (FST) immobility between PBS and L-AAA -injected mice (PBS n = 8, L-AAA n = 7) (**E**) Freezing percentage between PBS and L-AAA -injected mice in baseline and exposure to the hippocampal-independent context fear conditioning (PBS n = 17, L-AAA n = 13, Independent t-Test) (**F**) The time mice spent in the center of elevated plus maze (EPM) (**G**) The time mice spent in the open arms of EPM (**H**) The time mice spent in the closed arms of EPM (n = 7 per group, Independent t-Test)

Optogenetic stimulation of dPAG astrocyte evokes defensive-like responses

The role of dPAG astrocytes was further elucidated by utilizing optogenetics to explore whether dPAG astrocytes activation directly influence mouse defensive responses. To this end, an astrocyte-specific channelrhodopsin 2 (ChR2)-expressing mice (GFAP-ChR2) crossed with hGFAP-CreERT2 mice with floxed-stop-ChR2-eYFP mice was generated (Figure 15A). Intraperitoneal injection (i.p) of 100 mg/kg Tamoxifen for 5 consecutive days facilitates action of the Cre recombinase. The expression of ChR2 in mouse brain and its expression in midbrain PAG was also observed in tamoxifen treated mice but not in vehicle-treated mice (Figure 15B). To validate the system, histology data showed that ChR2-eYFP expression was colocalized with $GFAP^+$ and $S100\beta^+$ astrocytes, not with $NeuN^+$ neurons or Iba-1^+ microglia (Figure 15C) and was further confirmed by manual quantification (Figure 15D). It was also observed that the intensity of the EYFP signal varied depending on specific brain areas such as the hippocampus, prefrontal cortex, striatum, amygdala, thalamus, and cortex (Figure 15E).

To confirm astrocyte intracellular Ca^{2+} elevation by optogenetic stimulation, primary astrocytes were cultured from GFAP-ChR2 pups and treated with tamoxifen to induce ChR2 expression (Figure 16A). Astrocytes elicited Ca^{2+} increase as observed by Rhod-2AM signal after receiving blue light stimulation (Figure 16B). These Ca^{2+} signals were quantified from primary astrocytes derived from the midbrain (Figure 16C) and brainstem (Figure 16D), which are the precursor brain region of PAG. Likewise, increased Ca^{2+} signals in the cortex were also observed

(Figure 16E). Data show that astrocytes derived from GFAP-ChR2 mouse line demonstrated intracellular Ca^{2+} elevation in response to optogenetic stimulation.

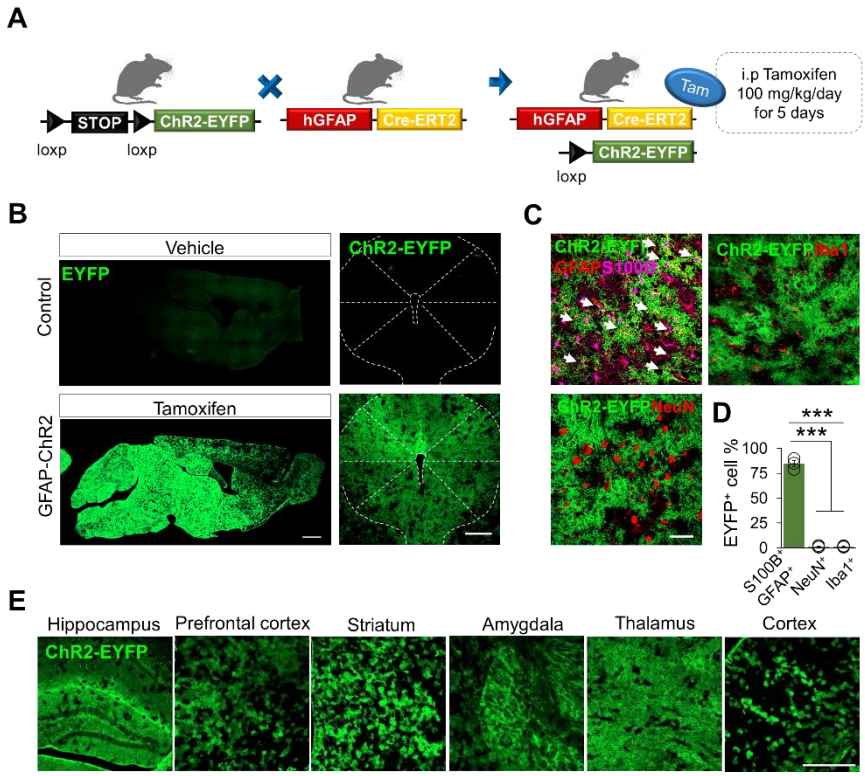

Figure 15. Characterization of GFAP Cre ERT2 x ChR2-EYFP mouse for optogenetic manipulation of dPAG astrocyte

(**A**) Schematic illustration of the generation of GFAP-ChR2 mice from crossing hGFAP Cre ERT2 with ChR2-EYFP mouse where expression is induced by intraperitoneal injection of 100 mg/kg tamoxifen daily for 5 days. (**B**) Left: Representative images of the whole brain of mouse injected with vehicle ('control') or tamoxifen ('GFAP-ChR2') showing the expression of ChR2 (green) Scale bar, 1000 μm. Right: ChR2 expression in the midbrain PAG of mouse injected with vehicle or tamoxifen. Scale bar, 200 μm. (**C**) Representative images of ChR2-EYFP (green) expression colocalized with $S100\beta^{+}$ (purple) and $GFAP^{+}$ (red) astrocytes but

not in Iba-1$^+$ (red) and NeuN$^+$ (red) cells. White arrows indicate merge with ChR2-eYFP; Scale bar, 50 μm. (**D**) Percentage of S100β$^+$ and GFAP$^+$, NeuN$^+$, and Iba-1$^+$ cells expressing ChR2-EYFP (n = 3 mice, 4 slices per mouse; One-way ANOVA followed by Bonferroni post-hoc test ***$p < 0.001$) (**E**) Representative images of ChR2-EYFP (green) expression in other brain regions. Scale bar, 100 μm.

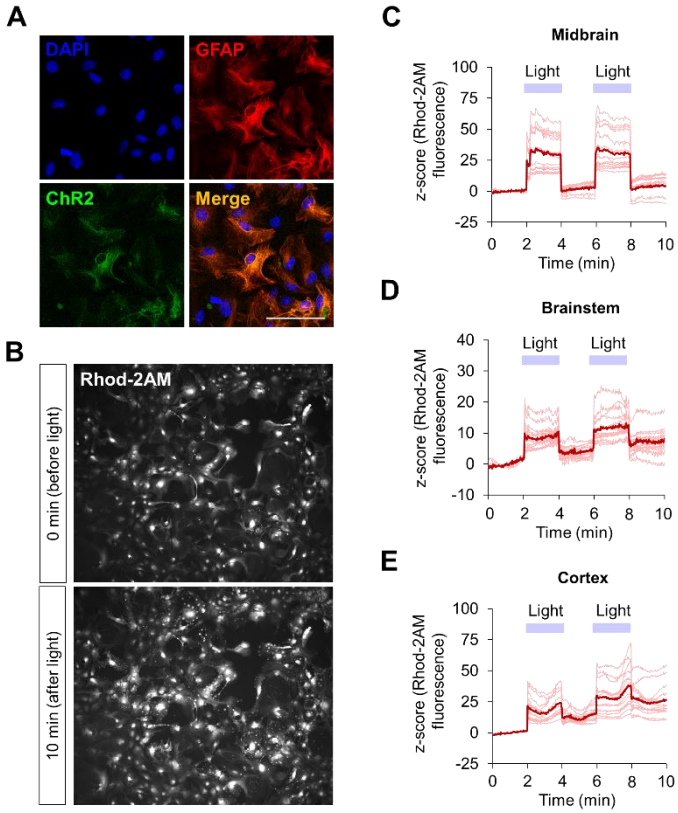

Figure 16. Optogenetic stimulation of primary astrocytes from GFAP-ChR2 pups evoked Ca^{2+} elevations

(**A**) Representative images of GFAP-ChR2 pup midbrain primary astrocytes expressing ChR2 (green) stained with DAPI (blue) and GFAP (red). Scale bar, 100 µm. (**B**) Representative image of the Rhod-2-AM signal from in vitro Ca^{2+} imaging before and after light exposure. (**C**) In vitro Ca^{2+} activity traces presented in z-score, from midbrain, (**D**) brainstem, and (**E**) cortical primary astrocytes of GFAP-ChR2 pups upon light stimulation of constant 2 mW 473 nm blue light.

Given that midbrain dPAG astrocyte Ca^{2+} activity was observed with mouse defensive responses against threat stimuli in prior figures presented, dPAG astrocyte Ca^{2+} signal activation by optogenetics and mouse behaviors were further explored. Optic fibers were unilaterally and or bilaterally implanted in dPAG (Figure 17A) of both the vehicle-injected control mice and the tamoxifen-injected GFAP-ChR2 mice (Figure 17B). GFAP-ChR2 mice were then subjected to an open arena to observe freezing defensive behaviors while receiving 6 min session of 2 min light-off followed by 2 min light-on and 2 min light-off epochs. Two-minute light-on stimulation was conditioned to 1 Hz, 20 Hz (10 ms duration, 40 ms interval), or continuous (constant, no intervals) with 2~3 mW light intensity. Data showed that 1 Hz stimulation showed an increased tendency of freezing bouts (Figure 17C upper panel) and a significantly increased total duration of freezing (Figure 17C lower panel) compared to light-off epochs. However, 20 Hz light stimulation did not show significant differences in freezing number and duration among the epochs observed (Figure 17D). Interestingly, mice showed a significantly increased freezing number and duration upon receiving the continuous light stimulation but not in light-off epochs (Figure 17E). These data showed that the *in vivo* optogenetic stimulation of dPAG astrocyte with longer duration and or constant light stimulation evokes drastic freezing behaviors in mice.

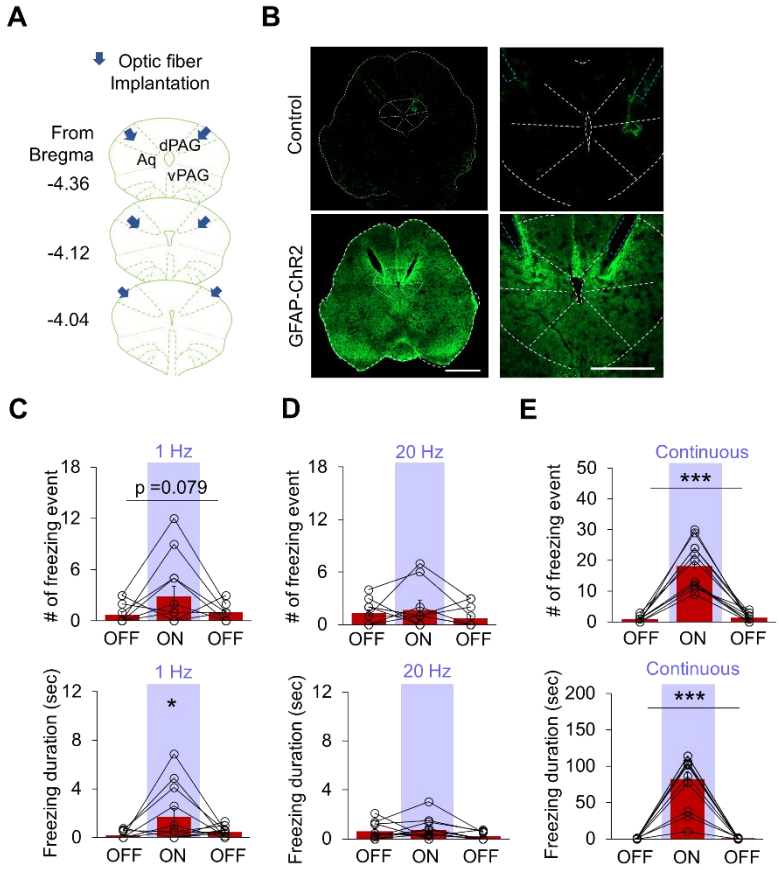

Figure 17. In vivo optogenetic stimulation of dPAG astrocyte increased freezing behavior

(**A**) Optic fiber placement in dPAG indicated by blue arrow. Implantations were found from slices 4.04 mm – 4.36 mm posterior to Bregma. (**B**) Representative images of the optic fiber placement in the midbrain region (left, scale bar, 1000 µm) particularly the targeted dPAG area (right, scale bar, 500 µm) in control and GFAP-ChR2 mice. (**C**) The number (upper) and duration (lower) of freezing bouts evoked by GFAP-ChR2 in light-off and 1 Hz, 10 ms light-on, (**D**) 20 Hz, 10 ms, and (**E**) constant 2 min light-on epochs (n = 12 mice, One-way ANOVA followed by LSD, * $p < 0.05$, ***$p < 0.001$)

Therefore, constant light stimulation was employed and further investigated various defensive behaviors of mice. Mice were subjected in open field arena in a 10-min session where mice received 2 min light-off and light-on epochs (Figure 18A). During 2-minute light-on epochs (2 mW, 473 nm/ blue continuous light stimulation), GFAP-ChR2 manifested significant increases in frequency and duration of freezing response (Figure 18B, C) characterized as drastic immobility in an inflexible posture aside from breathing. The freezing response of GFAP-ChR2 mice gradually went back to baseline level when light was turned off. Meanwhile, this increase and change in freezing response were not seen in control mice. The total duration and total number of freezing responses in the 10-min session was significantly increased in GFAP-ChR2 mice compared to control mice (Figure 18B, C). Furthermore, other defensive-like behaviors in between freezing bouts were observed. GFAP-ChR2 mice manifested increased duration and frequency of fleeing which involved aimless jumping and rapid changes of direction during light-on epochs, which were not observed in light-off epochs or in control mice (Figure 18D, E). Also, increased frequency and duration of retreat or avoidance-like responses described as backward movements were observed during light-on epochs (Figure 18F, G). Lastly, tail-rattling response was noticed during light-on epochs which is putatively known as a territorial behavior in response to a threat [122] and is characterized by stiff- followed by fast-waving movement of the tail. Light stimulation evoked a significant increase of tail-rattling number and duration in GFAP-ChR2 but not in control mice (Figure 18H, I). These data indicate that optogenetic activation of dPAG astrocyte evokes defensive-like responses in mice.

Moreover, it was observed that the defensive-like behaviors were dominated by the strong freezing behavior of mice in reponse to optogenetic stimulation of dPAG astrocytes. Data showed that freezing response accounted for the highest percentage of frequency and duration among the defensive-like behaviors observed in GFAP-ChR2 mice (Figure 19A, B). Furthermore, among the defensive-like behaviors monitored, freezing behavior was consistently observed in all GFAP-ChR2 mice (100%) used in the experiment (Figure 19C). However, retreat behavior was demonstrated by only 86% of the mice population, fleeing was seen in only 45%, and tail rattling was observed in only 43% of the GFAP-ChR2 mice examined in this experiment (Figure 19C).

These data further implicate that the optogenetic activation of dPAG astrocyte is sufficient to bias defensive responses towards more passive freezing defensive behaviors. However, other defensive-like behaviors such as the retreat, tail rattling, and fleeing may be due to the influence of the optogenetic astrocytes stimulation to various and nonselective cell types in PAG associated with other brain area projections that are partly responsible for active defensive responses. In addition, these active defensive-like behaviors might be due astrocyte indirect effect to the neural projections in dPAG coming from the amygdala [123] and hypothalamus [42], and superior colliculus [3] which are brain areas previously reported to carry out integration of signals necessary to orchestrate action selection between active and passive defensive responses.

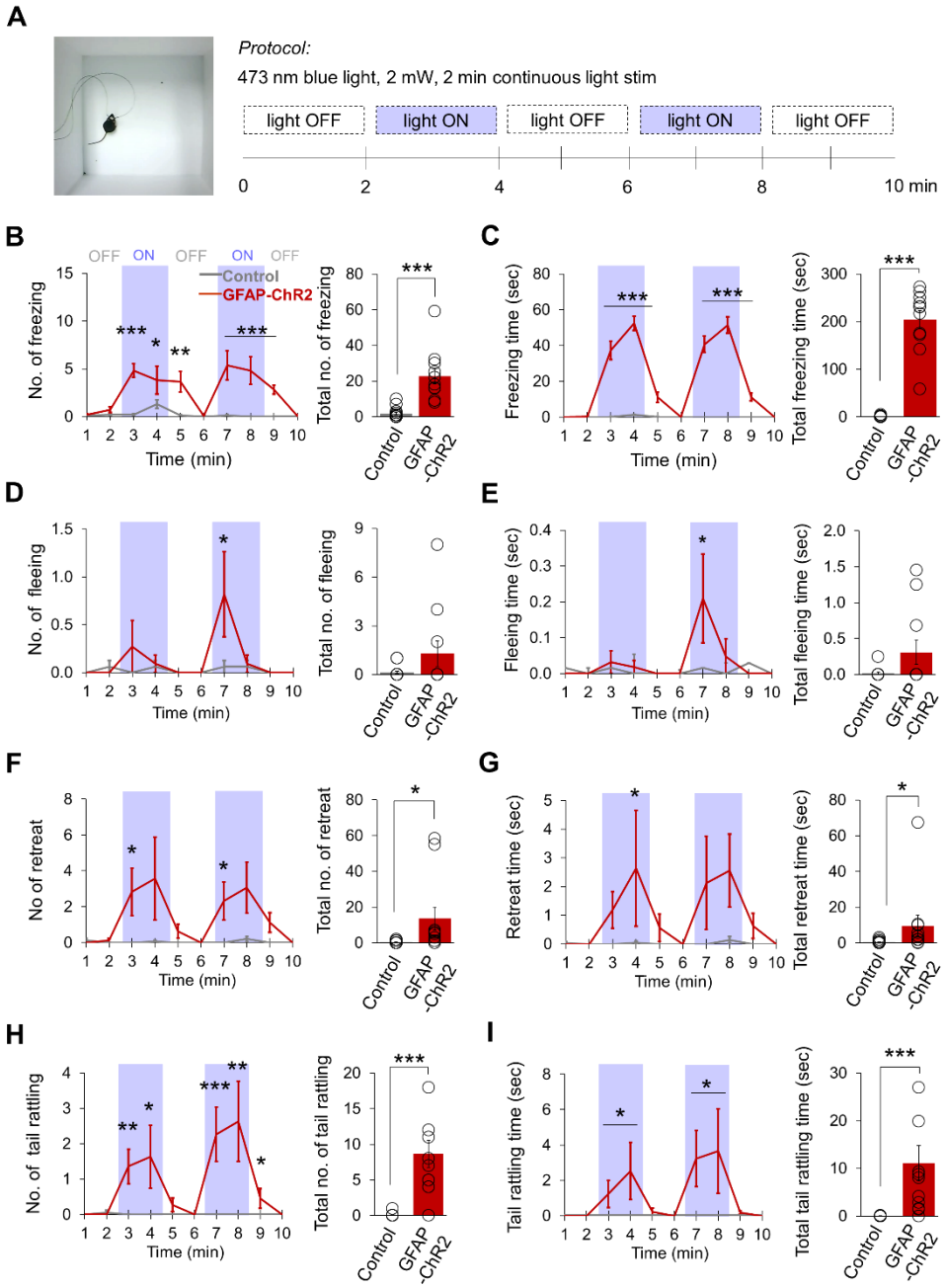

Figure 18. Optogenetic stimulation of dPAG astrocyte evoked defensive-like responses

(**A**) Schematic illustration of the protocol of mouse dPAG astrocyte optogenetic stimulation consisting of 473 nm constant 2 min light-off and 2 min light-on cycle

in a 10 min session in an empty open arena. (**B**) Left: the number of freezing events between control (gray line) vs GFAP-ChR2 mice (red line) in each minute across 10 min session with 2 min light-off and light-on (shaded area) epochs. Right: the total freezing events of control and GFAP-ChR2 mice in the whole 10 min session. (**C**) Left: the duration of freezing in control vs GFAP-ChR2 mice in each minute across 10 min session with 2 min light-off and light-on (shaded area) epochs. Right: the total freezing duration of control and GFAP-ChR2 mice in the whole 10 min session. (**D**) The number and (**E**) the duration of fleeing response in control and GFAP-ChR2 mice upon light-off and light-on epochs. (**F**) The number and (**G**) the duration of retreat or avoidance response of control and GFAP-ChR2 mice upon light-off and light-on epochs.(**H**) The number of events and (**I**) the duration of tail rattling reponse of control and GFAP-ChR2 mice upon light-off and light-on epochs (Control n = 16 mice, GFAP-ChR2 n = 17 mice, Independent t-Test between control and GFAP-ChR2, *$p < 0.05$, **$p < 0.01$, ***$p < 0.001$)

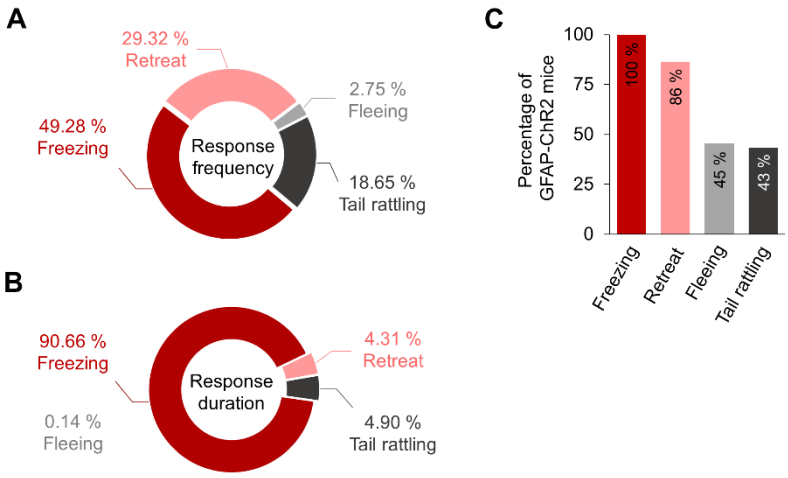

Figure 19. Optogenetic stimulation of dPAG astrocyte dominantly induced freezing behavior

(**A**) The percentage of the frequency of defensive-like responses; freezing, retreat, fleeing, and tail rattling in GFAP-ChR2 mice upon dPAG astrocyte light stimulation. (**B**) The percentage duration of the various defensive-like behaviors observed upon dPAG astrocyte light stimulation in GFAP-ChR2 mice. (**C**) The percentage of GFAP-ChR2 mice expressing defensive-like behaviors freezing, retreat, fleeing, and tail rattling. (n = 17 GFAP-ChR2 mice)

Then, author investigated the effects of light stimulation of dPAG astrocytes on other mouse behaviors. Mice were subjected to tail suspension test (TST), forced swim test (FST) and elevated plus maze test (EPM) right after they received a continuous 2 mW blue light stimulation for 5 min in their home cage (Figure 20A). Data showed that there were no significant differences observed between control and GFAP-ChR2 mice in time they spent immobile in the TST (Figure 20B) and FST (Figure 20C), both of which are general behavioral test to assess depressive-like behaviors. Also, there was no significant differences between control and GFAP-ChR2 mice in EPM observing the time they spent in the center (Figure 20D), open arms (Figure 20E), closed arms (Figure 20F), and the total distance the mice travelled in the apparatus (Figure 20G). These data suggest that optogenetic activation of dPAG astrocytes does not significantly affect depressive- or anxiety-like behaviors in mice.

Moreover, mice were also subjected to conditional place preference test (CPP, Figure 20H) where they were habituated in the apparatus for 3 days and allowed to freely explore the chambers. At the conditioning day, mice received dPAG stimulation in one chamber (light-paired chamber) for 5 min in a 12 min session. Mice were put to the center and guided to the light-paired chamber. Mice were allowed to explore the light-paired chamber for 2 min light-off epoch followed by a 5 min constant light-on stimulation. After the light stimulation period, mice were allowed to explore the light-paired chamber for another 5 min without light stimulation. Data showed the significantly increased freezing time of GFAP-ChR2 mice compared to control mice in the 12 min session of conditioning upon receiving light stimulation which was sustained until the session ended (Figure 20I). The total

freezing time was shown in Figure 20J. However, data showed that in the test day, conditioned GFAP-ChR2 and control mice showed no significant difference in the time spent in the light-paired chamber. Also, there was no significant difference between pre-test and test sessions (Figure 20K-L). The preference or aversion of mice were further explored with real-time place preference (RTPP) by first habituating mice in the apparatus for 3 days (Figure 20M). On the test day, mice were allowed to freely explore the chamber. When mouse enters the pre-determined light-paired chamber, it receives a continuous light stimulation with maximum duration of 1 min. Light will be turned off after 30 sec and will be turned on again if the mouse stays in the light-paired chamber. Real-time place preference/aversion test was performed in a 5 min session and a post-test, a session without light stimulation, was done right after the RTPP test (Figure 20M). Similar with CPP data, GFAP-ChR2 and control mice showed no significant differences in the time spent in the light-paired chamber during the RTPP pre-test, test, and post-test (Figure 20N-O). Although there was a slight increase of time percentage showed by the GFAP-ChR2, it was due to the freezing response of GFAP-ChR2 mice upon receiving light during real time test when they entered the light-paired chamber. These data reveal that even though optogenetic stimulation of dPAG astrocyte evoked drastic freezing behavior, it does not induce place preference to the chamber opposite to the light-paired chamber and or aversion from light stimulation. However, the author does not exclude the possibility that a prolonged or longer duration of conditioning with light stimulation might change mouse behavior and possibly induce aversion against light stimulation.

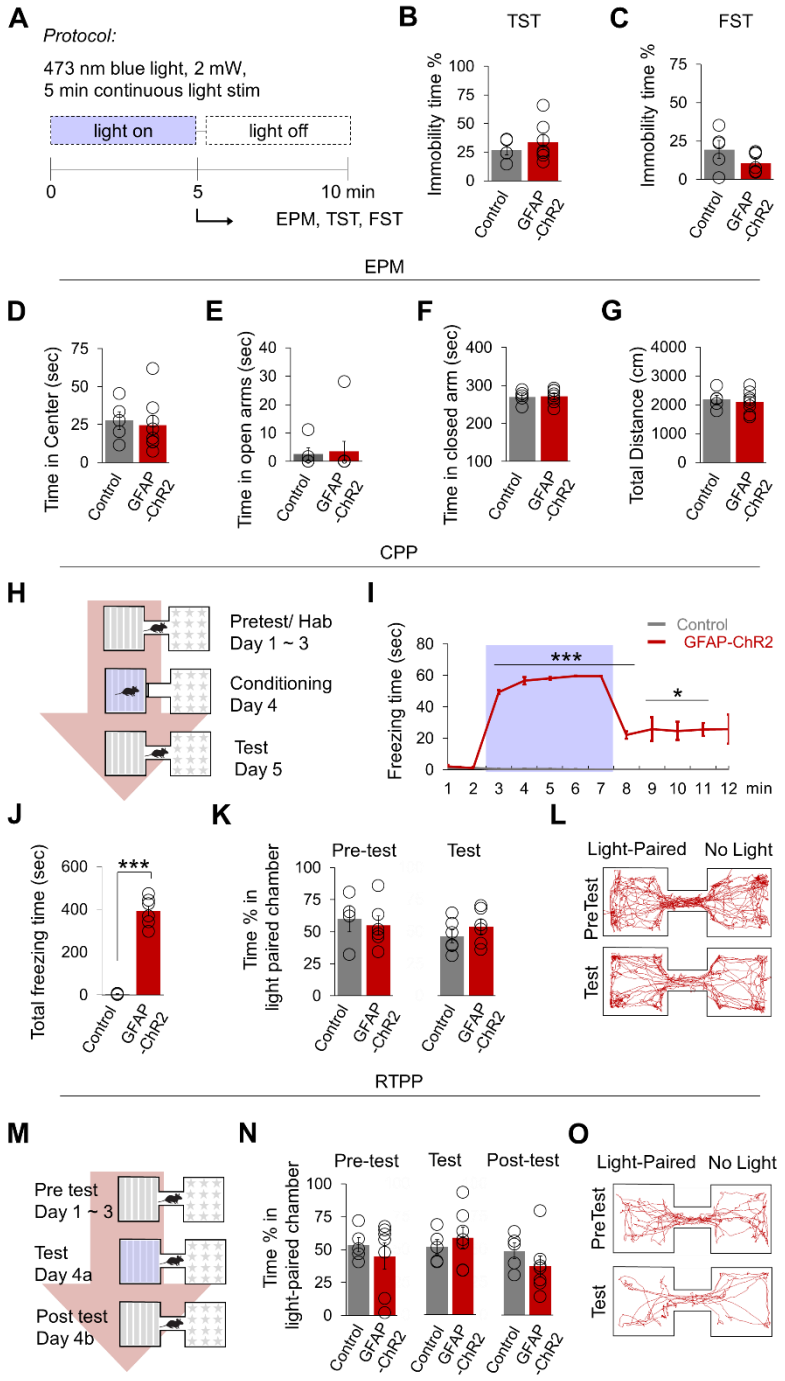
A
Protocol:
473 nm blue light, 2 mW,
5 min continuous light stim
light on
light off
0
5
10 min
EPM, TST, FST
B
TST
Immobility time %
Control
GFAP -ChR2
C
FST
Immobility time %
EPM
D
Time in Center (sec)
E
Time in open arms (sec)
F
Time in closed arm (sec)
G
Total Distance (cm)
CPP
H
Pretest/ Hab
Day 1 ~ 3
Conditioning
Day 4
Test
Day 5
I
Control
GFAP-ChR2
Freezing time (sec)
min
J
Total freezing time (sec)
K
Pre-test
Test
Time % in
light paired chamber
L
Light-Paired
No Light
PreTest
Test
RTPP
M
Pre test
Day 1 ~ 3
Test
Day 4a
Post test
Day 4b
N
Pre-test
Test
Post-test
Time % in
light-paired chamber
O
Light-Paired
No Light
PreTest
Test

Figure 20. Optogenetic stimulation of dPAG astrocyte did not affect other mouse behaviors

(**A**) Scheme of experiment giving mice 2 mW constant blue light stimulation for 5 min and subjecting mice to behavior tests (**B**) The time percentage mice are immobile in TST (control n = 5, GFAP-ChR2 n = 7, Independent t-Test). (**C**) The time percentage mice are immobile in FST. (**D**) The time mice spent in the center of EPM (**E**) The time mice spent in the open arms and (**F**) closed arms. (**G**) The total distance mice travelled in EPM apparatus. (**H**) The schematics of conditional place preference test (CPP). (**I**) The duration of freezing response of mice upon light stimulation during conditioning for CPP test (control n = 5, GFAP-ChR2 n = 6, Independent t-Test between control and GFAP-ChR2 mice each minute, *$p < 0.05$, ***$p < 0.001$) (**J**) The total time of freezing duration between control and GFAP-ChR2 mice during the 12 min session (**K**) The percentage of time the control and GFAP-ChR2 mice spent in the light-paired chamber during pre-test and the test sessions. (**L**) Sample traces of GFAP-ChR2 mouse exploration in CPP apparatus during pre-test and test sessions. (**M**) The schematics of real-time place preference test (RTPP). (**N**) The percentage of time the control and GFAP-ChR2 mice spent in the light-paired chamber during pre-test, test, and post-test sessions. (**O**) Sample traces of GFAP-ChR2 mouse exploration in the apparatus during pre-test and test sessions.

Previous studies reported the different functional role of PAG which suggested that ventral PAG is involved in mouse defensive responses, particularly freezing response [23,31]. To this end, author checked whether optogenetic stimulation of ventral PAG (vPAG) astrocyte affects mouse defensive behaviors. Optic fibers were implanted to vPAG to both control and GFAP-ChR2 mice (Figure 21A). Mice were subjected to open field arena and received 2 mW constant light stimulation with the same protocol used in dPAG stimulation (Figure 18A). Data showed that vPAG astrocyte light stimulation evoked significantly increased freezing behaviors in GFAP-ChR2 mice but not in control mice along the 10 min session. (Figure 21B, left). It was also shown that the total duration and number of freezing bouts were significantly increased in GFAP-ChR2 mice but not in control mice (Figure 21B, middle and right). Similarly, bouts of retreat responses in between freezing reponse were observed upon light stimulation of vPAG astrocyte. GFAP-ChR2 mice showed a significantly increased total duration and number of retreat response compared to control mice (Figure 21C). In addition, author also observed a tendency of increased tail rattling behaviors in response to light stimulation in GFAP-ChR2 mice but not in control mice (Figure 21D). vPAG astrocyte stimulation did not evoke fleeing or jumping behaviors in mice in contrast to dPAG astrocyte stimulation. These data suggest that optogenetic stimulation of vPAG astrocyte showed similar defensive-like behaviors with dPAG astrocyte stimulation.

Taken together, the results suggest that optogenetic stimulation of midbrain dPAG astrocyte is sufficient to evoke defensive-like responses even in the absence of a threat stimulus without altering other affective behaviors and preference or aversion in mice.

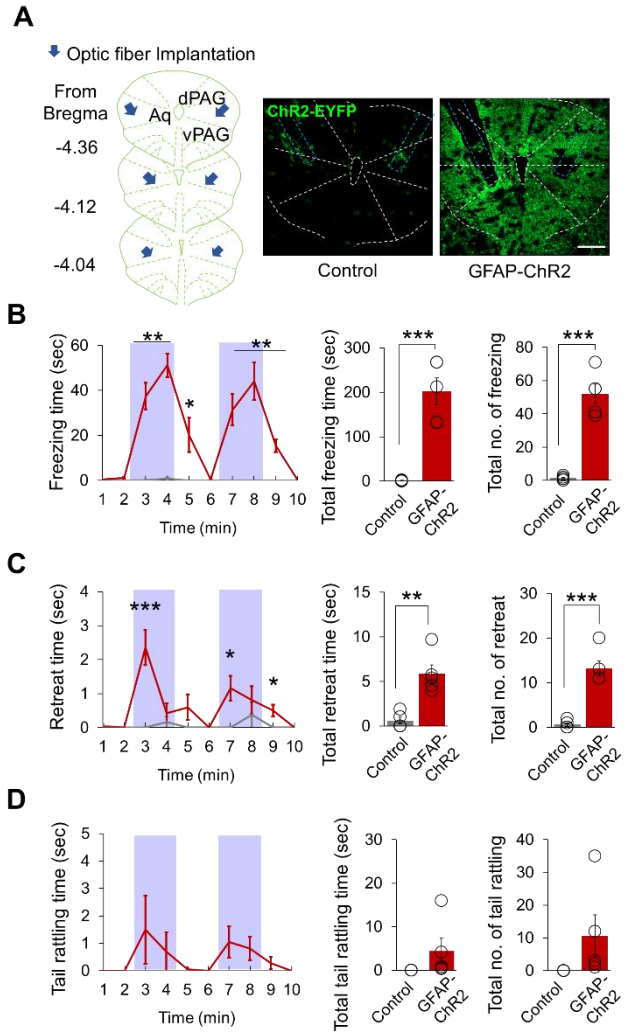

Figure 21. Optogenetic stimulation of vPAG astrocyte showed similar defensive-like behaviors with dPAG astrocyte stimulation

(A) Left: optic fiber placement in vPAG indicated by blue arrow. Implantations were found from slices 4.04 mm – 4.36 mm posterior to Bregma. Right: representative images of ChR2 expression and vPAG implantation in control and GFAP-ChR2 mice. Blue broken lines indicate implantation. Scale bar, 200 μm. (**B**) Left: the duration of vPAG astrocyte stimulation-induced freezing response between control vs GFAP-ChR2 mice in each minute across 10 min session with 2 min light-off and light-on (shaded area) epochs. Middle: the total freezing duration of control and

GFAP-ChR2 mice in a 10 min session. Right: the total number of freezing events of control and GFAP-ChR2 mice (n = 5 per group, Independent t-Test for each minute between control and GFAP-ChR2, *$p < 0.05$, ** $p < 0.01$, ***$p < 0.001$) (**C**) Left: the duration of retreat response in each minute across 10 min session with 2 min light-off and light-on epochs, middle: the total retreat duration, and right: the total number of retreat events of control and GFAP-ChR2 mice (**D**) Left: the duration of tail rattling response between control and GFAP-ChR2 in each minute across 10 min session with 2 min light-off and light-on (shaded area) epochs, middle: the total retreat duration, and the right: the total number of retreat events of control and GFAP-ChR2 mice.

Optogenetic stimulation of dPAG astrocyte elicits aberrant defensive-like responses against threat

Upon detection of threat and exposure to a potentially dangerous environment, it is an instinctive behavior of mice to elicit a defensive response to seek and secure safety [3,4,9,124]. In this regard, mice were subjected to an open arena, a general anxiogenic environment where mice were more easily exposed to predators. In the open field arena, a shelter (safe zone) was added where they can hide and escape from the open arena (Figure 22A). Author then tested the effects of dPAG astrocyte activation on the instinctive and natural behavior of mice to escape and seek safety against a potentially threatening environment. After habituation with the shelter in open arena, mice naturally preferred and escape to the shelter rather than explore the open arena. After 3 days of habituation, author allowed the mice to approach the shelter first which was followed by dPAG astrocyte light stimulation and checked whether dPAG astrocyte stimulation affects mouse instinctive behavior to seek safety. Trials were classified as successful escape if the mouse reached the shelter within 5 seconds upon shelter availability. Data showed that control mice went straight to the shelter to seek safety even upon receiving light stimulation as demonstrated in Figure 22B with significantly higher percentage of successful escape and shorter latency to reach the shelter (Figure 22B, C). Interestingly, upon delivery of a light stimulation to dPAG astrocyte, GFAP-ChR2 mice failed to successfully escape to shelter and it took significantly longer time to reach the shelter compared to control mice or light-off epoch (Figure 22B, C). Intriguingly, the failure to escape and the increased time to reach the shelter were due to defensive-like behaviors such as freezing (Figure 22D), retreat (Figure 22E), fleeing (Figure 22F),

and tail rattling (Figure 22G) during light stimulation in GFAP-ChR2 mice. Thus, the behaviors elicited by the dPAG astrocyte stimulation were regarded as aberrant defensive response. Therefore, heightened and aberrant behavior was further confirmed by exposing mice to an innate threat and an available shelter in the rectangular open arena (Figure 23A). Mice were habituated in the apparatus with only the shelter for 5 min in 3 days. On the test day, mice were exposed to a large moving object, the RC car. Mice were allowed to risk assess and approach the car which was the experimenter's cue to deliver light stimulation followed by RC car attack. Trials were classified as successful escape if the mouse reached the shelter within 5 seconds upon the onset of the RC car attack. Expectedly, control mice made rapid and successful escape to shelter upon RC car attack in both light-off and light-on epochs (Figure 23B, C). However, GFAP-ChR2 mice failed to escape and showed significantly increased latency to reach the shelter during light-on epoch even in the presence of an RC car attack compared to light-off epoch (Figure 23B, C). The mouse instinctive escape behavior to reach the shelter in the presence of an innate threat was disrupted by freezing (Figure 23D), directionless fleeing (Figure 23E), retreat (Figure 23F), and tail rattling (Figure 23G) upon dPAG astrocyte light stimulation.

Therefore, these data suggest that optogenetic stimulation of dPAG astrocyte evoked aberrant defensive-like behaviors that defies the goal of defensive behavior to seek safety.

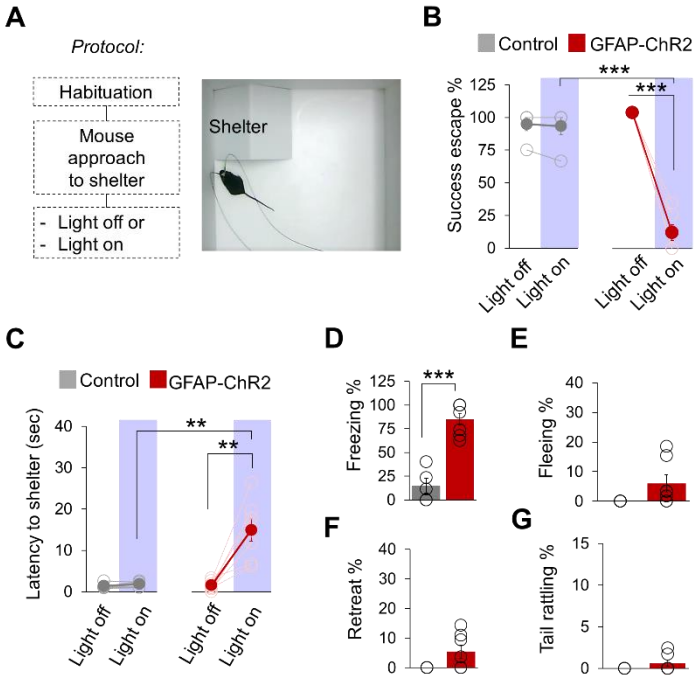

Figure 22. Optogenetic stimulation of dPAG astrocyte altered the safety-directed behavior of mice against an anxiogenic environment

(**A**) Left: Behavioral protocol which starts with habituation with a shelter in an open arena and delivery of light-off or light-on epochs when mouse approach the shelter. Right: an open arena with a shelter. (**B**) Percentage of successful escape (reaching the shelter within 5 sec upon availability of shelter in open space) in light-off and light-on (shaded) epochs between control and GFAP-ChR2 mice (control n = 5 mice, GFAP-ChR2 n = 7 mice; Paired and independent t-Test, ***p<0.001, data are presented as mean ± SEM). (**C**) The time it took the mouse to reach the shelter during light-off and light-on epochs between control and GFAP-ChR2 mice (Paired and Independent t-test, **p < 0.01). (**D**) Percentage of freezing, (**E**) fleeing, (**F**) retreat, (**G**) tail rattling during light stimulation between control and GFAP-ChR2 in shelter-directed behavioral scheme.

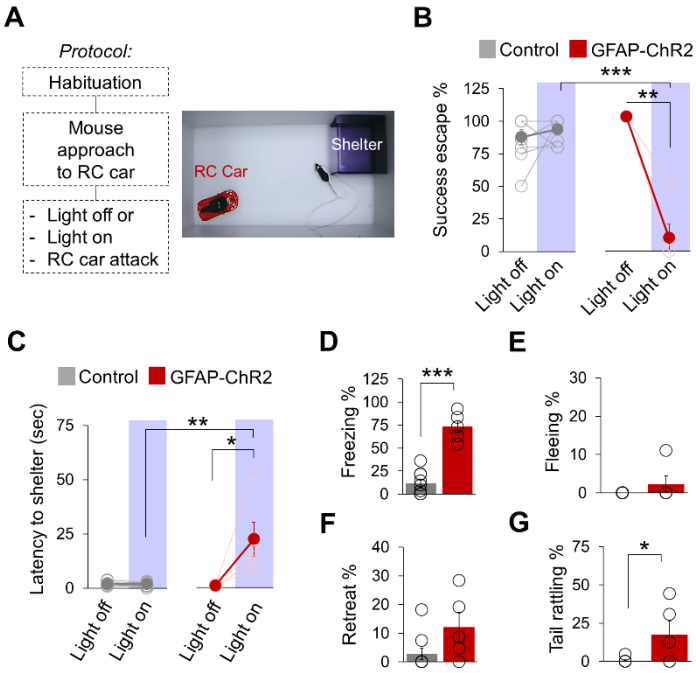

Figure 23. Optogenetic stimulation of dPAG astrocyte altered the safety-directed escape of mice against a threat stimulus

(**A**) Left: behavior protocol which starts with mouse habituation to the arena with only the shelter and on the test day, presented with RC car, a large moving object. Mouse approaching the RC car received light stimulation followed by the RC car attack from the object to evoke escape to shelter. Right: image of the experimental set up of the threat stimulus in an open arena with a shelter opposite to the threat stimulus. (**B**) Percentage of successful escape to shelter upon RC car attack during light-off and light-on epochs between control and GFAP-ChR2 mice (control n = 9 mice, GFAP-ChR2 n = 5 mice; Paired and Independent t-Test, *$p < 0.05$, ***$p < 0.001$, **$p < 0.01$). Successful escape was scored when mouse reach the shelter within 5 sec at the onset of RC car attack while receiving light stimulation. (**C**) The time it took mice to reach the shelter upon RC car attack during light-off or light-on epochs between control and GFAP-ChR2 mice (**D**) Percentage of freezing, (**E**) retreat, (**F**) fleeing, and (**G**) tail rattling behaviors during light stimulation and RC car attack.

Optogenetic stimulation and pharmacologic ablation of dPAG astrocyte dysregulates dPAG neuron-evoked defensive response

Recent studies demonstrated that optogenetic stimulation of dPAG neurons evoked shelter-directed or safety-seeking escape behaviors [3,22]. Thus, author investigated whether the innate safety-seeking defensive escape instigated by dPAG neuron activation is affected by dPAG astrocytes activation. Schematics and timeline of the experiment are demonstrated in Figure 24A and B. To stimulate dPAG neurons, AAV virus encoding hSyn-oChIEF tagged with tdTomato were injected to dPAG of GFAP-ChR2 mice (Figure 24C, similar dPAG slice with Figure 24F). Expression of hSyn-oChIEF-tdTomato was mostly colocalized with $NeuN^+$ neurons but not with $S100\beta^+$ astrocytes as shown in the histology data (Figure 24D), which was further confirmed in the quantification of the $tdTomato^+$ cell percentage (Figure 24E). Seven days after virus injection, optic fibers were implanted and mice were allowed to recover for another 7 days and then applied dPAG neuronal stimulation during an escape experiment (Figure 24B). After acquiring data from dPAG neuron-induced escape behaviors, tamoxifen was injected for 5 days to the same GFAP-ChR2 mice to induce ChR2 expression (Figure 24F, same mouse dPAG area with Figure 24C). It was further confirmed in the histology data that ChR2-eYFP expression was specifically colocalized with $S100\beta^+$ but not with $NeuN^+$ neurons as compared to the percentage of $eYFP^+$ cells (Figure 24H). Then, mice were subjected to an escape experiment delivering simultaneous optogenetic stimulation of dPAG neurons and astrocytes.

Similar to previous report [3], data showed that optogenetic activation of dPAG neurons using 40 Hz (10 ms, 2 mW) light stimulation evoked the optimal and immediate escape to shelter (Figure 25A, left panel) with significantly reduced latency to reach the shelter (Figure 25B, left panel) and a significantly reduced freezing response (Figure 25C) and risk assessment of the stimulation zone with a small novel object (Figure 25D). The constant light stimulation that was previously used for astrocyte stimulation (Figure 18-23) also elicited similar escape behaviors with the 40 Hz stimulation when it was applied for dPAG neuron stimulation (Figure 25A-D, left panels). Meanwhile, when dPAG neuron and astrocyte were simultaneously stimulated, the shelter-seeking and escape behavior evoked by dPAG neuron stimulation was completely abrogated by the dPAG astrocyte stimulation (Figure 25A, right panel). In addition, mice showed a significantly increased latency to reach the shelter (Figure 25B, right panel). The prolonged latency and disrupted escape to shelter was due to the significant increase of freezing (Figure 25C, right panel) and reduced risk assessment behaviors (Figure 25D, right panel) upon light stimulation. The escape and freezing behaviors were not observed in light-off epoch or control mice that were injected with control virus and vehicle (Figure 25E-H). These data indicate that dPAG astrocyte stimulation induces aberrant and dysregulated defensive-like behaviors which disrupts the immediate and instinctive safety-seeking behavior of mice evoked by dPAG neuronal stimulation.

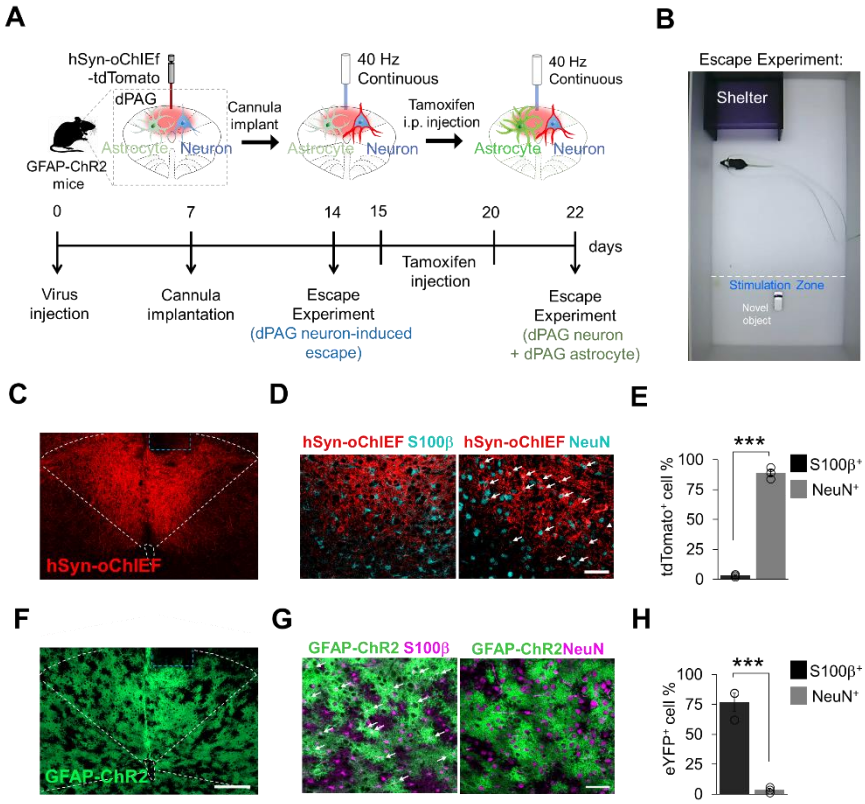

Figure 24. Simultaneous optogenetic manipulation of dPAG neurons and astrocytes

(**A**) Experimental timeline of dPAG neuronal and astrocyte stimulation in an escape experiment. Non-tamoxifen injected GFAP-ChR2 mice were injected with hSyn-oChIEF-tdTomato and implanted with optic fiber 7 days post-surgery. Seven days after implantation recovery, neuronal stimulation experiment (blue, 'hSyn-oChIEF') was done to establish neuron-induced escape response. Then, the same mice were injected with tamoxifen to induce Cre and optogenetically stimulate astrocyte (green, 'hSyn-oChIEF $^{+}$ GFAP-ChR2') with neurons. Escape experiment was done with the same mice receiving simultaneous stimulation of dPAG neuron and astrocyte at ~2mW 40 Hz, 10ms and continuous/constant light stimulations. (**B**) Image of the escape experiment set up consisting of a rectangular arena with a shelter/ safe zone and a stimulation zone with a small novel object to engage mice in exploration opposite to the shelter. (**C**) Representative image of hSyn-oChIEF-tdTomato (red)

virus expression in the injected dPAG, same slice with (F). (**D**) Representative image of hSyn-oChIEF (red) expression colocalized with $NeuN^+$ (right, blue-green) but not with $S100\beta^+$ (left, blue-green) cells. White arrows indicate merge. Scale bar, 50 µm. (**E**) Quantification in percentage of the $S100\beta^+$ and $NeuN^+$ dPAG cells colocalized with hSyn-oChIEF-tdTomato (n = 3 mice per group, 4 slices per mouse, Independent t-Test, ***$p < 0.001$) (**F**) Representative image of ChR2-EYFP (green) expression after tamoxifen injection, same slice with (C). (**G**) Representative images of GFAP-ChR2 (green) expression colocalized with colocalized with $S100\beta^+$ (left, purple) but not with $NeuN^+$ (right, purple) cells. White arrows indicate merge. Scale bar, 50 µm. (**H**) Quantification in percentage of the $S100\beta^+$ and $NeuN^+$ dPAG cells colocalized with GFAP-ChR2-EYFP.

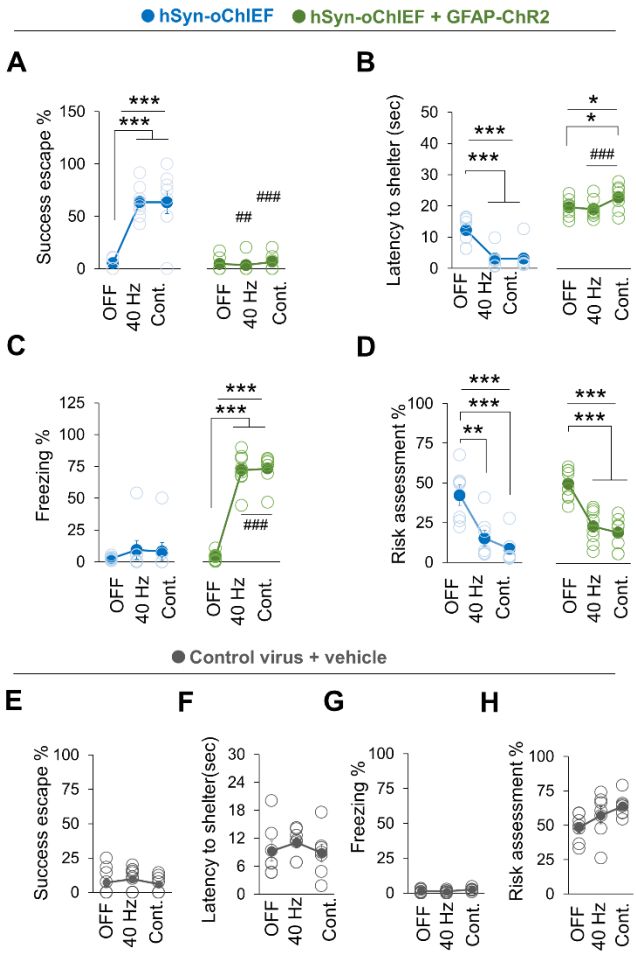

Figure 25. dPAG astrocyte stimulation disrupted dPAG neuron-evoked safety-directed escape behaviors

(**A**) Percentage of successful escape during light-off, 40 Hz, 10ms light-on, and constant light-on stimulation of only dPAG neuron (left, hSyn-oChIEF; blue) and both neuron and astrocytes (right, hSyn-oChIEF + GFAP-ChR2; green). Reaching the shelter within 5 sec from the onset of light stimulation counts as a success escape score. (**B**) Mice latency to reach the shelter upon light stimulation schemes of neuron only (hSyn-oChIEF) and neuron and astrocyte (hSyn-oChIEF + GFAP-ChR2) simultaneous stimulation (**C**) The freezing percentage, and (**D**) risk assessment percentage during light-off, 40 Hz light-on, and constant light-on epochs in hSyn-oChIEF and hSyn-oChIEF + GFAP-ChR2 conditions. (hSyn-oChIEF n = 8, hSyn-

oChIEF + GFAP-ChR2 n = 6, One-way ANOVA followed by LSD post hoc analysis, *$p < 0.05$, ***$p < 0.001$, Paired t-Test to compare hSyn-oChIEF vs hSyn-oChIEF + GFAP-ChR2 in each light conditions, $^{\#}p < 0.05$, $^{\#\#}p < 0.01$ $^{\#\#\#}p < 0.001$) (**E**) Success escape percentage of vehicle injected GFAP-ChR2 mice injected with control virus during light-off, 40 Hz,10 ms, and continuous light-on epochs (control virus + vehicle n = 9) (**F**) Control mice latency to reach the shelter, (**G**) Percentage of freezing, and (**H**) Percentage of risk assessment behaviors during the light-off, 40 Hz,10 ms, and continuous light-on epochs (control virus + vehicle n = 9, One-way ANOVA followed by LSD post hoc analysis).

Furthermore, it was investigated whether the pharmacological ablation of dPAG astrocyte influences the escape and safety-seeking behaviors of mice induced by dPAG neuronal stimulation. To this end, AAV-hSyn-oChIEF-tdTomato was injected to dPAG to manipulate neurons. Two weeks after the virus expression, PBS or L-AAA was injected and optic fiber was implanted unilaterally to dPAG. The schematics and timeline of this experiment were demonstrated in Figure 26A. Two to 3 days after the surgery, mice were subjected to the escape experiment paradigm shown in Figure 25B. The pharmacological ablation of S100β$^+$ astrocytes in dPAG were demonstrated in the histology data (Figure 26B) and was further confirmed with manual quantification showing that the number of S100β$^+$ astrocyte was significantly reduced in L-AAA-injected mice compared to PBS-injected mice (Figure 26C). Author also confirmed that the NeuN$^+$ cell density between PBS and L-AAA -injected mice showed no significant difference (Figure 26D, E). Moreover, the expression of AAV-hSyn-oChIEF-tdTomato injection site was demonstrated in dPAG area of both PBS and L-AAA injected mice (Figure 26F). It was also confirmed that virus expression was primarily colocalized with NeuN$^+$ cells but not in S100β$^+$ astrocytes (Figure 26G).

Furthermore, upon establishing the manipulation of dPAG neurons using AAV-hSyn-oChIEF-tdTomato with pharmacological ablation of dPAG astrocytes, author observed the defensive behaviors by subjecting mice in an escape behavior paradigm. Results showed that PBS-injected mice made successful escape upon receiving 40 Hz and constant light stimulations while L-AAA-injected mice showed a significantly reduced successful escape rate (Figure 27A). The latency to reach the shelter was significantly higher in L-AAA -injected mice compared to PBS-injected

(Figure 27B). L-AAA-injected mice also showed significant increase in bouts of freezing and risk assessment behaviors contributing to the increased latency to reach the shelter (Figure 27C, D). Notably, L-AAA-injected mice did not completely abolish the behavioral effect of dPAG neuronal stimulation as it still imposed threat-evoked defensive responses which enabled mice to seek shelter but in a slower and less effective manner. Taken together, dPAG requires not only neurons but also astrocytes to exert an optimal defensive response to threatening environment, and aberrant dPAG astrocyte activation may lead to dysregulation of it.

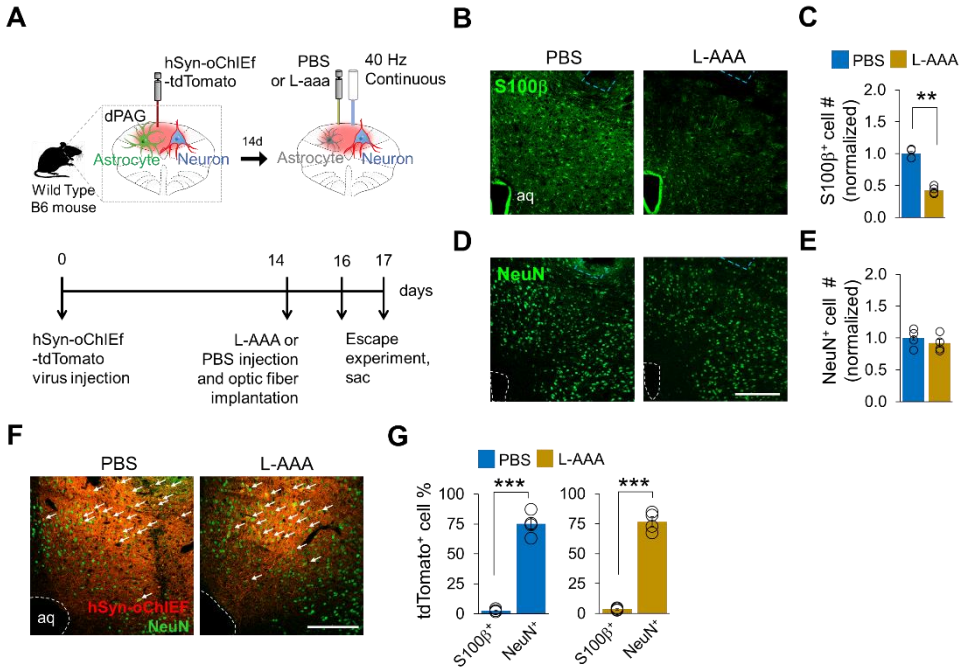

Figure 26. dPAG neuron stimulation while ablating dPAG astrocyte in escape behavior paradigm

(**A**) Experimental timeline of dPAG neuronal stimulation and astrocyte ablation. Wild type mice were injected with hSyn-oChIEF-tdTomato and after 14 days, mice were injected with PBS (blue, 'hSyn-oChIEF + PBS) or L-AAA (hSyn-oChIEF + L-AAA) and implanted with optic fiber. Post recover, mice were subjected to the same escape experiment in Figure 20B. (**B**) Representative images of S100β^{+} astrocyte (green) after PBS- and L-AAA -injection in dPAG, same slice with (D). Blue broken lines indicate optic fiber implant for neuron manipulation (**C**) Quantification of S100β^{+} astrocyte in PBS and L-AAA – injected mice, data are normalized to PBS control (n = 4 mice per group, 3 slices per mouse, Independent t-Test, **$p < 0.01$) (**D**) Representative images of Neun^{+} cells (green) after PBS- and L-AAA -injection in dPAG. Same slice with (B). Blue broken lines indicate optic fiber implant for neuron manipulation. Scale bar, 200µm. (**E**) Quantification of Neun^{+} cells in PBS and L-AAA -injected mice, normalized to PBS control (**F**) Representative image of hSyn-oChIEF-tdTomato (red) expression and colocalization with Neun^{+} cells (green)

in PBS and L-AAA -injected mice. White arrows indicate merge. Scale bar, 200 μm. (**G**) Quantification of the percentage of S100β^{+} astrocyte and NeuN^{+} cells expressing hSyn-oChIEF in PBS- and L-AAA-injected mice (Independent t-Test, ***$p < 0.001$).

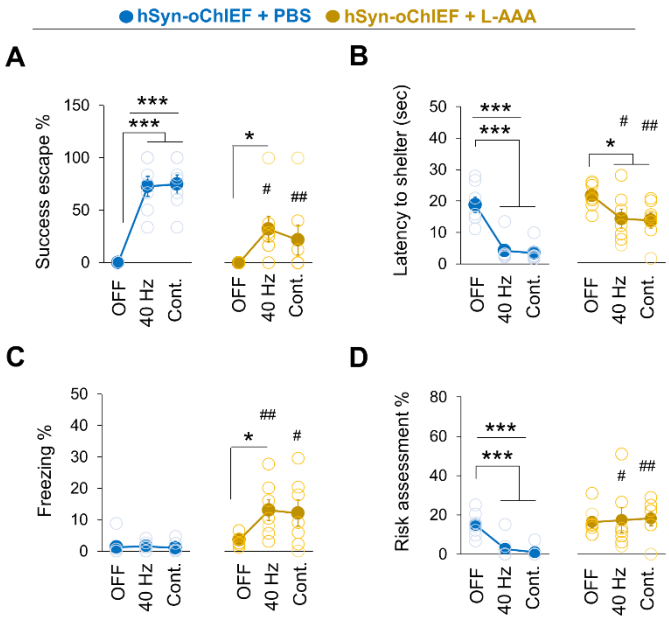

Figure 27. dPAG astrocyte attenuated dPAG neuron-induced safety-directed escape

(**A**) Percentage of successful escape during light-off, 40 Hz, 10ms light-on, and constant light-on stimulation between hSyn-oChIEF + PBS (left, blue) and hSyn-oChIEF + L-AAA (right, yellow). Reaching the shelter within 5 sec from the onset of light stimulation counts as a success escape score. (**B**) Mice latency to reach the shelter upon light stimulation schemes of neuron only (hSyn-oChIEF) and neuron and astrocyte (hSyn-oChIEF + GFAP-ChR2) simultaneous stimulation (**C**) The freezing percentage, and (**D**) risk assessment percentage during light-off, 40 Hz light-on, and constant light-on epochs in hSyn-oChIEF and hSyn-oChIEF + GFAP-ChR2 conditions. (n = 7 mice per group, One-way ANOVA followed by LSD post hoc analysis, $^{*}p < 0.05$, $^{***}p < 0.001$, Paired t-Test to compare hSyn-oChIEF + PBS vs hSyn-oChIEF + L-AAA in each light condition, $^{\#}p < 0.05$, $^{\#\#}p < 0.01$)

dPAG astrocyte evoked a distinct Ca^{2+} activity elevation in response to panicogenic stimulus

Notably, these dPAG astrocyte stimulation-evoked defensive-like behaviors altered the natural and instinctive behavior of mice to seek safety or escape when exposed to an imminent threat and potentially harming environment. The dysregulated behavioral feature observed in the dPAG astrocyte-activated mice is reminiscent of maladaptive fear and panic-related behaviors which were previously described in prior studies [4,53]. Therefore, it was investigated whether dPAG astrocyte is involved in panic-related behaviors by exposing mice to CO_2, a known panicogenic agent used for both humans and animal studies [125,126].

A previous study reported that mouse exposure to CO_2 evoked panic-related jumping, but not escape behavior even with an escape route provided [4]. Whereas mouse exposed to a chamber with hot plate floor successfully escaped using the route provided to avoid the harm [4]. These experiments were replicated in this study by subjecting mice to a chamber with hot plate or a chamber with CO_2 (Figure 28A). Data showed that mice exposed to hot plate escaped the threatening environment through climbing the rope provided as an escape route (Figure 28B). However, mice that were exposed to CO_2 manifested aimless jumping behavior (Figure 28B) even there was a rope provided as an escape route. Therefore, the mice exposed to hot plate were able to escape successfully whereas mice exposed to CO_2 were not (Figure 28C). Also, the latency to escape from the chamber with hot plate was much lower than from the chamber with CO_2 (Figure 28D). To measure panic-related behaviors, the number of jumps was counted and mice behaviors were observed upon exposure to pure CO_2 or air applied in an open-top chamber. Similar to previously reported

[4,126], CO_2-exposed mice showed significant increase in aimless jumping and intermittent freezing (Figure 28E, F). Significantly less exploration was also evident in mice exposed to CO_2 compared to air-exposed mice (Figure 28G).

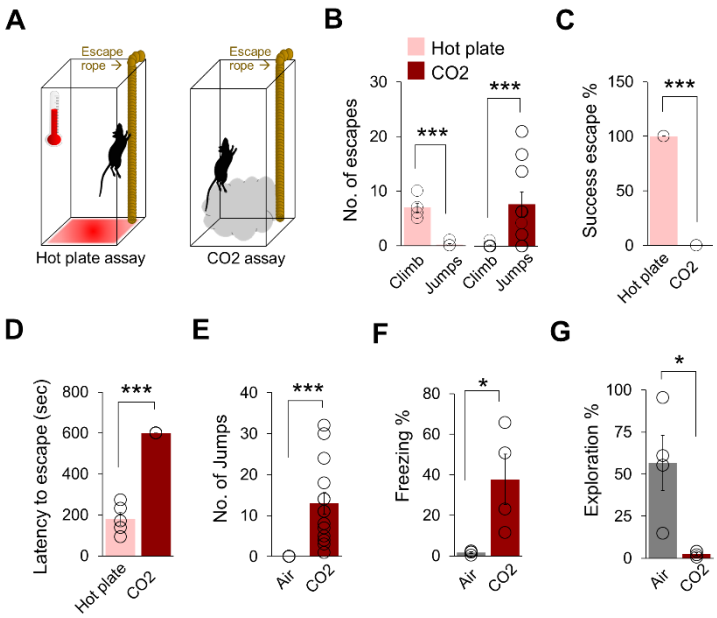

Figure 28. Establishing panic-related behaviors by CO_2 exposure

(**A**) Left: experiment scheme of CO_2 exposure. After habituation in the chamber, mice were exposed to 5 ~7% CO2 and mice behavior were observed for 10 min. Right: image of the CO_2 assay chamber (n = 9, Paired t-Test, *$p < 0.05$, **$p < 0.01$, ***$p < 0.001$) (**B**) Number of jumps between air-exposed and CO2-exposed mice (n = 9, Paired t-Test, *p < 0.05, **p < 0.01, ***p < 0.001). (**C**) Percentage of freezing behaviors observed upon mice exposure to air or CO2. (**D**) Duration of the observed agonal breathing of mice upon exposure to air or CO2. (**E**) Percentage of time mice explored (includes rearing, stretching, risk assessing, and sniffing) in the chamber when exposed to air or CO2.

Upon establishing the panic-like behaviors in mice, the involvement of dPAG astrocyte in panic-related behaviors was further investigated. Therefore, mice were injected with either PBS or L-AAA in dPAG to ablate astrocyte and were subjected to a CO_2 chamber provided with a rope as an escape route (Figure 29A). Interestingly, mice injected with L-AAA showed significantly reduced panic-related jumping behavior upon CO2 exposure compared to PBS-injected group (Figure 29B). However, although the panic-related jumping was reduced in L-AAA injected mice, it did not induce successful escape using the rope provided as an escape route (Figure 29C). Moreover, the latency to escape the panicogenic environment or the freezing response were not significantly different between PBS and L-AAA-injected mice (Figure 29D, E). Whereas exploration behavior was significantly increased in the L-AAA-injected mice compared to PBS-injected group (Figure 29F). Although astrocyte ablation by L-AAA did not completely abolish aberrant behaviors of mice upon CO_2 exposure, these data indicate that mouse panic-related jumping behavior was attenuated by the dPAG astrocyte ablation. These results suggested that dPAG astrocytes are involved in mouse panic-related behaviors.

The involvement of dPAG astrocyte in response to a panicogenic agent was further confirmed by measuring Ca^{2+} activity using TCSPC fiber photometry while exposing mouse to CO_2. In this panicogenic environment, robust increase of Ca^{2+} activity was detected in dPAG astrocytes (Figure 30A). Individual mouse data of Ca^{2+} activity response upon exposure to air and CO_2 were shown in Figure 30C and D. Notably, the CO_2-evoked Ca^{2+} increase in dPAG astrocyte was significantly higher compared to the Ca^{2+} response elicited by other threat stimuli evoking defensive responses in mice (Figure 30B). These results suggest that dPAG

astrocytes are actively engaged in panic-related behaviors by eliciting a distinct Ca^{2+} activity elevation.

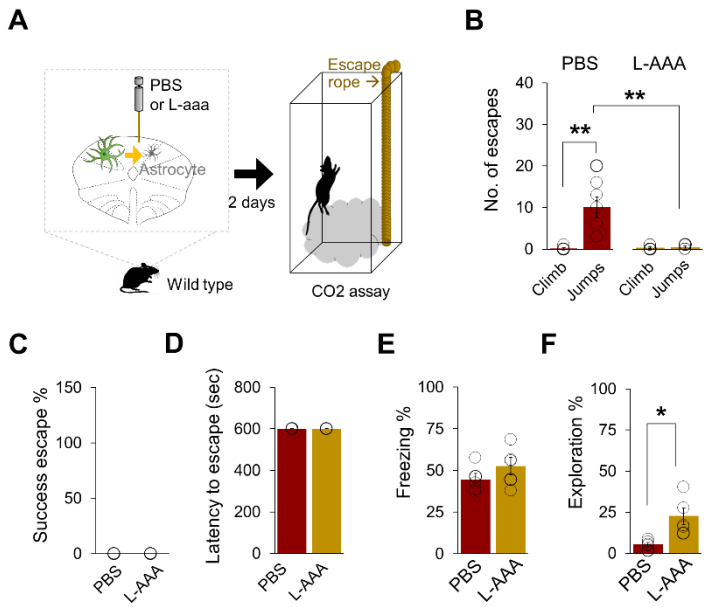

Figure 29. dPAG astrocyte ablation attenuated panic-related jumping in mice

(**A**) Schematic illustration of the wild type mouse dPAG astrocyte ablation by L-AAA injection or PBS for control and subjecting mice in CO_2 assay 2 days post recovery. (**B**) Number of jumps between PBS- and L-AAA -injected mice when exposed to CO_2. (PBS n = 10, L-AAA n = 8, Independent t-Test $^{**}p < 0.01$) (**C**) Percentage of successful escape between PBS and L-AAA injected mice upon exposure to CO_2. (**D**) Latency of PBS and L-AAA-injected mice to escape the panicogenic environment. (**E**) Percentage of freezing behavior between PBS- and L-AAA -injected mice when exposed to CO_2 (**F**) Percentage of exploration time (includes rearing, stretching, risk assessing, and sniffing) between PBS or L-AAA -injected mice in the chamber when exposed to CO2.

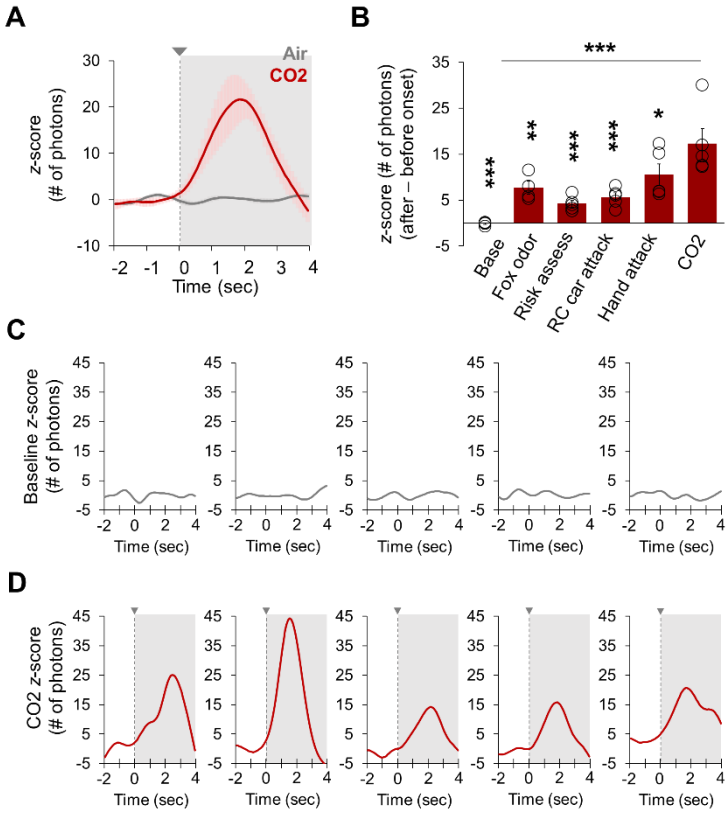

Figure 30. dPAG astrocyte showed distinct Ca^{2+} elevation upon exposure to panicogenic stimulus

(**A**) *In vivo* dPAG astrocyte Ca^{2+} activity mean trace presented as z-score upon air exposure (gray line) and CO2 exposure (red line) indicated with broken gray line at onset 0 sec, n = 5 mice. (**B**) Quantification of changes in z-scored Ca^{2+} activity recorded *in vivo* via TC–PC from all threat assays (1 - 3 sec after minus 0 - 2 sec before on–set of threat stimulus, n = 4 - 5, One-way ANOVA followed by Dunnet's t-Test, comparing groups to CO2, *$p < 0.05$, **$p < 0.01$, ***$p < 0.001$) (**C**) Individual mouse Ca^{2+} activity trace used in the experiment, activity is presented as z-score during air exposure. (**D**) Individual mouse Ca^{2+} activity trace used in the experiment, activity is presented as z-score upon CO2 exposure. Gray shade and broken gray line indicate exposure to CO2 at onset 0 sec.

Optogenetic activation of dPAG astrocyte modulates mouse defensive and panic-like behaviors through ATP release

To investigate possible mechanism underlying the panic-like behaviors involving astrocytes, author employed *in vivo* microdialysis and optogenetics to activate dPAG astrocytes while collecting dialysates in dPAG. Firstly, microdialysis guide cannula and optic fiber were implanted in GFAP-ChR2 mice (Figure 31A) then gliotransmitters released upon optogenetic activation of astrocyte were assessed. Data showed that optogenetic activation of astrocytes from GFAP-ChR2 mouse dPAG induced significant increase of extracellular ATP level (Figure 31B). However, levels of GABA, glutamate, D-serine, and serotonin (5-HT) did not show significant change between light-off and light-on epochs (Figure 31C-F). These data concur with previous studies showing the release of ATP by optogenetic astrocyte activation [78,79,94]

To further confirm exocytotic release of ATP from astrocyte upon optogenetic activation, author injected Opto-vTrap virus under GFAP promoter to dPAG of GFAP-ChR2 mice (Figure 32A). Opto-vTrap is an optogenetic tool employed to inhibit the release of vesicle-containing molecules through light stimulation [110]. Data showed that indeed optogenetic astrocyte activation with control virus evoked a significant increase of ATP levels (Figure 32B, left). However, in Opto-vTrap-injected dPAG slice, the increase of extracellular ATP level evoked by the optogenetic astrocyte activation was abrogated (Figure 32B, right). The extracellular ATP levels measured from control and Opto-vTrap groups during light-on epoch was shown in Figure 32C. These results demonstrate that the increased

extracellular ATP levels upon optogenetic activation were derived from dPAG astrocyte.

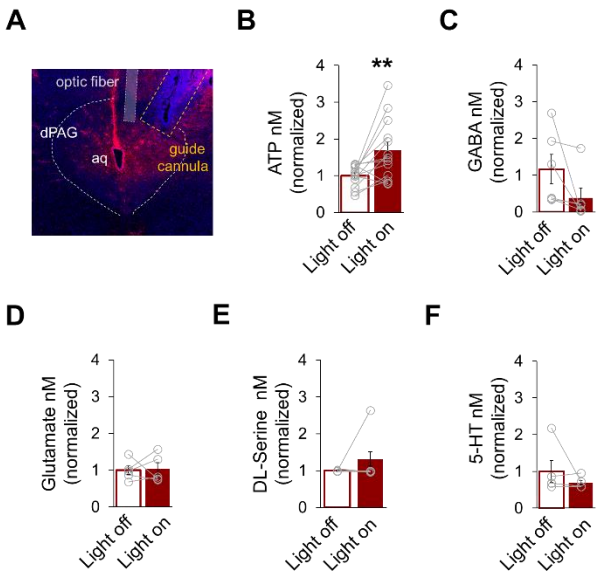

Figure 31. Optogenetic stimulation of dPAG astrocyte increased extracellular ATP level

(**A**) Representative image of the implantation of microdialysis guide cannula and optic fiber in dPAG. (**B**) Extracellular ATP levels during light-off and light-on epochs, data was normalized to light-off controls (n = 13 mice, Paired t-Test, **p < 0.01). (**C**) GABA, (**D**) Glutamate, (**E**) D, L-serine, (**F**) Serotonin (5-HT) levels during light-off and light-on of GFAP-ChR2 dPAG slice (n = 5 mice, Paired t-Test)

It was further investigated whether the ATP gliotransmitter release is involved in the modulation of defensive behaviors. Therefore, GFAP-Opto-vTrap virus was injected to dPAG of wild type mice which were subjected to behavioral test to observe defensive and panic-related behaviors (Figure 33A). Histology data confirmed the expression of Opto-vTrap in midbrain dPAG and its colocalization with $GFAP^+$ and $S100\beta^+$ astrocytes (Figure 33B). In the behavioral assays, both control and opto-vTrap virus-injected mice received 3 mW of constant blue light stimulation during experiment sessions. Interestingly, upon exposure to hand attack assay, mice injected with Opto-vTrap exhibited a significantly reduced flight speed against threat compared to control group (Figure 33C). Also, Opto-vTrap-injected mice demonstrated a significantly reduced total distance travelled compared to control (Figure 33D). These data indicate that the gliotransmitter release derived from astrocyte is required for mouse optimal defensive response from threat stimulus.

Furthermore, to test whether inhibition of gliotransmitter release affects panic-related behavior, mice were injected with GFAP-Opto-vTrap or control virus and were exposed to panicogenic CO_2 during light stimulation. Data showed that the panic-related jumping of GFAP-Opto-vTrap virus-injected mice was significantly reduced compared to control group (Figure 33E) indicating a pivotal role of dPAG astrocyte-derived gliotransmitter release in mouse panic-like behavior.

The effect of dPAG astrocyte gliotransmitter release inhibition using Opto-vTrap on mouse behaviors upon exposure to non-threatening situations were also investigated. Control and Opto-vTrap groups were subjected to a 5-min OFT session where both groups received 2 min light-off epoch followed by 2 min light-on epoch and another 1 min light-off epoch. The percentage of freezing behavior (Figure 34A),

speed (Figure 34B), total distance travelled (Figure 34C), or the percentage of time spent in the center (Figure 34D) did not yield significant differences between control and Opto-vTrap groups, nor between mice responses during light-off and light-on epochs. Also, the number of sniffing behaviors observed when Opto-vTrap-injected mice were exposed to non-threat stimuli, novel object (Figure 34E) or female conspecific (Figure 34F), did not show significant difference during light-off and light-on epochs. These data indicate that astrocyte gliotransmitter release, particularly ATP, is primarily involved in mouse defensive and panic-like behaviors.

Taken together, these results provide evidence that dPAG astrocytes are actively involved in mouse defensive behavior through increasing intracellular Ca^{2+} activity in response to threat, and are required to efficiently avoid danger. Also, it was demonstrated that optogenetic activation and pharmacologic ablation of dPAG astrocyte dysregulated defensive behaviors by disrupting mouse safety-seeking behavior, which are reminiscent of panic-like behavior. The study revealed that dPAG astrocytes, through distinct Ca^{2+} elevation and ATP release, are neurobiological substrates underlying defensive response and its dysregulation may underlie as mechanisms for panic disorders (Figure 35).

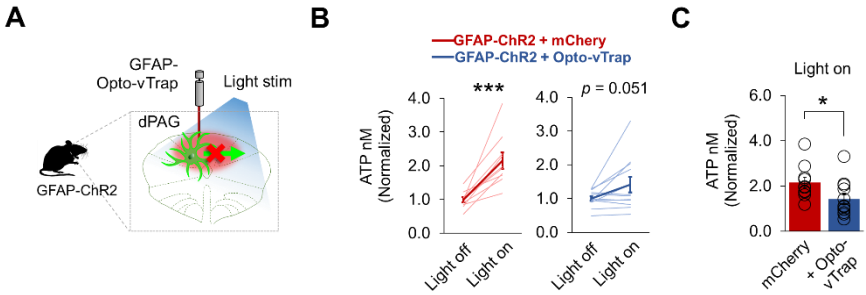

Figure 32. Inhibition of dPAG astrocyte gliotransmitter release via Opto-vTrap abolished extracellular ATP increase induced by astrocyte activation

(**A**) Schematic illustration of dPAG slice astrocyte stimulation using GFAP-ChR2 mice with prior injection of control or GFAP- Opto-vTrap virus used to measure extracellular ATP level. (**B**) Extracellular ATP levels measured from aCSF of GFAP-ChR2 dPAG slice injected with control or Opto-vTrap during light-off and light-on epochs (control n = 10 mice, Opto-vTrap n =12, Paired t-Test, ***$p < 0.001$) (**C**) The same data from (B) emphasizing the comparison between control and Opto-vTrap injected GFAP-ChR2 dPAG slice during light-on epoch (Independent t-Test, * < 0.05)

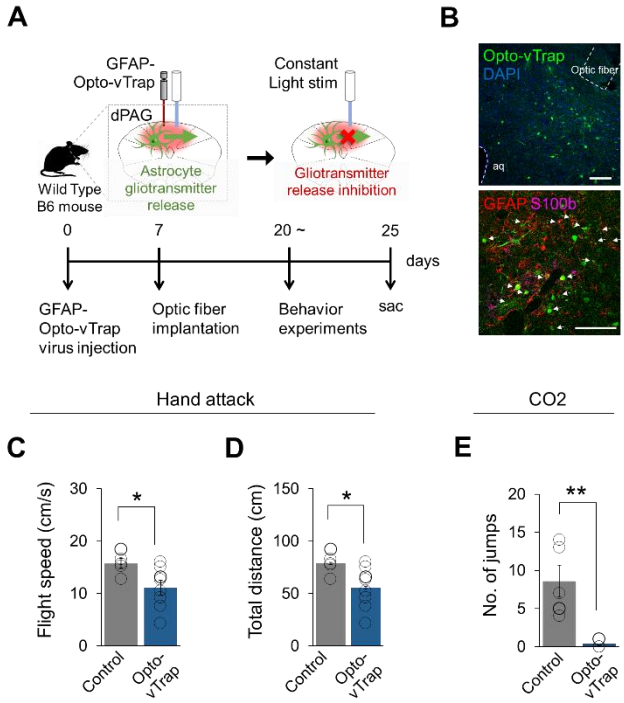

Figure 33. Inhibition of dPAG astrocyte gliotransmitter release via Opto-vTrap attenuated defensive response and panic-related jumping in mice

(**A**) Schematic illustration of the experimental procedure of GFAP-Opto-vTrap virus injection and optic implantation to wild type mouse dPAG which was then subjected to threat exposure experiments. (**B**) Opto-vTrap virus (green) expression in dPAG. Scale bar, 200 μm (top) and its colocalization with $GFAP^{+}$ (red) and S100β+ (purple) astrocytes. Scale bar, 100 μm (bottom) (**C**) Flight speed of mice upon fleeing from hand attack threat stimulus between control and Opto-vTrap injected mice (n = 8 mice per group, Independent t-Test, $*p < 0.05$). (**D**) Total distance travelled between control and Opto-vTrap mice upon exposure to hand attack. (**E**) The number of panic-related jumps between control and Opto-vTrap mice upon exposure to 10% CO2.

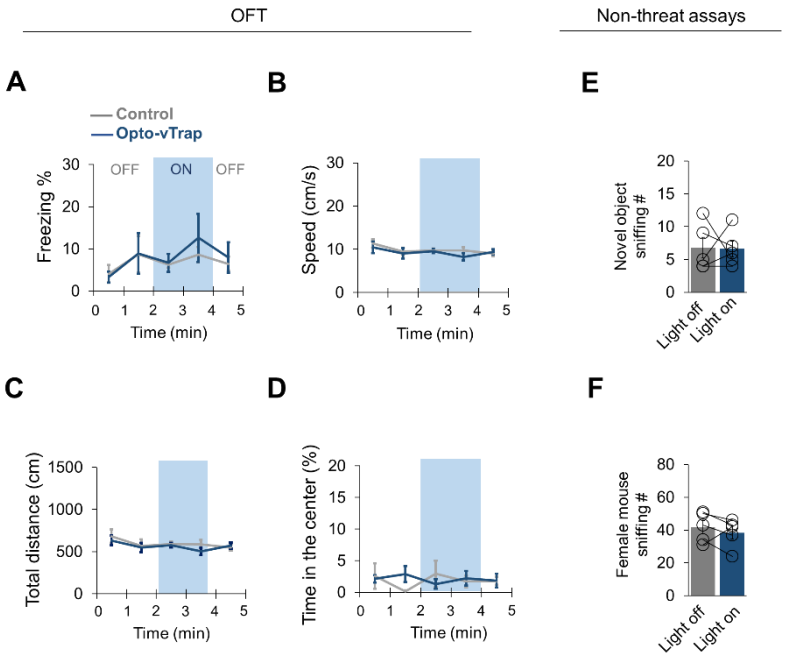

Figure 34. Inhibition of dPAG astrocyte gliotransmitter release via Opto-vTrap did not affect mouse behaviors upon exposure to non-threatening stimuli.

(**A**) Percentage of freezing behavior between control and Opto-vTrap-injected mice along 5 min session of OF with light-off and light-on stimulation (n = 8 mice per group, Independent t-Test) (**B**) Locomotor speed of control and Opto-vTrap mice in an OFT in response to light stimulation epochs. (**C**) The total distance travelled between control and Opto-vTrap in the OFT in response to light stimulation epochs. (**D**) Percentage of time mice spent in the center of the OF upon light stimulation epochs (**E**) The number of sniffing events Opto-vTrap mice interacted with a novel object during light-off and light-on epochs (n = 5 mice, Paired t-Test) (**F**) The number of sniffing events Opto-vTrap mice performed upon exposure to a female conspecific during light-off and light-on stimulations.

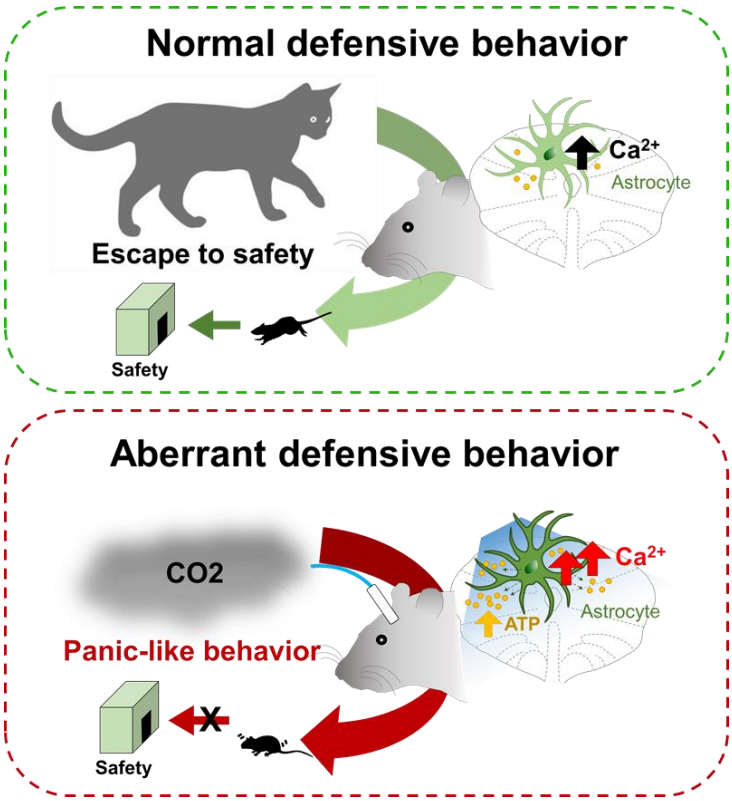

Figure 35. Schematic illustration of the summary

Upon exposure to threat, mouse exhibit defensive behaviors to seek safety to avoid or reduce harm. dPAG astrocyte increases Ca^{2+} activity triggering defensive behaviors. Meanwhile, pharmacologic and optogenetic activation of dPAG astrocyte induced dysregulated defensive behaviors which disrupted mouse safety-seeking and defensive behaviors which resembles panic-like behaviors. The panicogenic agent CO_2 and optogenetic astrocyte activation induced aberrant defensive-like responses through distinct Ca^{2+} elevation in dPAG astrocyte and a subsequent increase of extracellular ATP level.

4. Discussion

In this study, it was revealed that dPAG astrocyte actively participate in the regulation of mouse defensive behaviors and is involved in panic-related behavior. Increasing evidences propose the crucial role of astrocyte in the regulation of fear, avoidance, and anxiety. Previous studies showed that ventral tegmental area (VTA) astrocyte activation drives avoidance behavior in mice by facilitating excitation of VTA GABAergic neurons [93]. Astrocytes in central amygdala affect fear expression in mice via depressed excitatory synapses through purinergic receptors of amygdala neurons [95]. Hippocampal astrocytes regulate fear memory in fear conditioned rodents, anxiety-like behavior, and models of PTSD [91,94,96]. These studies further elucidated astrocyte role in fear and anxiety behaviors. In addition, in light with the canonical divisions of PAG which are known to dictate appropriate defensive responses, it was recently reported that PAG functions do not only depend on its subregions, but also on the diverse array of cell types spanning the PAG subregions [35,36]. However, it remains unexplored whether midbrain dPAG astrocytes are involved in defensive behaviors and its dysregulation. In this regard, this study uncovers, for the first time to our knowledge, that midbrain dPAG astrocyte modulates mouse defensive responses and propose that its dysregulation may underlie panic-related behaviors.

This study demonstrated that midbrain dPAG astrocyte responds with increased Ca^{2+} activity to threatening stimuli by performing fiber photometry using TCSPC. TCSPC has been used in freely moving animals to observe neuron and astrocyte calcium activities. In this study, TCSPC detects bulk Ca^{2+} activity changes in astrocytes of GCaMP6 virus-injected free-moving mice during threat exposure

assays. Although there were technical limitations on the temporal resolution of the calcium activity detection, TCSPC detects Ca^{2+} activity changes with higher sensitivity than the conventional fiber photometry [127]. The threat stimuli used in the experiments such as fox odor (TMT), large moving object like RC car, and experimenter's hand, were previously used in other studies of fear and defensive behaviors [115,116,118]. Similar with the previous reports, these salient objects used in the experiments aimed to stimulate mouse sensory modalities; visual, olfactory, and or mechanosensory. Notably, all the threat stimuli used to stimulate mouse sensory modalities evoked dPAG astrocyte activity through Ca^{2+} elevations along with the appropriate action selection of mice to avoid danger.

The threats used in this work, which are similarly used in a wide variety of studies, stimulate mouse sensory modalities and get integrated and evaluated in brain areas that receive sensory input. Such brain areas include mSC [3], hypothalamus [4,42], amygdala [23], and mPFC [39] which were reported to send inputs to PAG, which, in turn, generate defensive responses. Although this study did not further explore the neural circuits of threat detection, previous works reported that PAG receives information from brain areas that carries sensory information and threat value enabling them to compute appropriate and efficient defensive responses to threat [3]. It is possible that astrocytes increased calcium activities in response to dPAG neurons that are activated upon the incoming sensory threat information to PAG. Previous studies reported that glutamatergic neurons in dPAG elicited calcium activity increase upon exposure to threat stimuli such as a looming object, predator, or exposure to CO_2 [3,4]. Therefore, it is possible that these neuronal activity changes affect astrocyte Ca^{2+} activity in midbrain dPAG. Astrocytes express diverse receptors and transporters to

sense neurotransmitters, neuropeptides and even changes in extracellular pH [79,128], which can trigger intracellular Ca^{2+} elevation. In previous studies, midbrain VTA astrocytes regulate extracellular glutamate level in VTA through GLT-1, glutamate transporter, which was reported to orchestrate approach and avoidance behaviors in mice [93]. It was also reported that ventral midbrain astrocytes exhibited calcium responses to glutamate and dopamine through D2 receptor signaling [129]. Therefore, these mechanisms might also regulate dPAG astrocyte activity.

The activation of dPAG astrocytes using optogenetic stimulation evoked various defensive behaviors such as freezing, fleeing, retreat, and tail-rattling. However, data showed that passive freezing behavior was dominantly expressed by mice receiving astrocyte stimulation and was observed consistently through all the GFAP-ChR2 mice tested. This data showed that the defensive action selection of mice was affected by the manipulations of dPAG astrocyte activity.

Previous studies showed that using neuronal optogenetic manipulations, paraventricular thalamus (PVT) and its projections to central amygdala (CeA) and nucleus accumbens (NAc) biases mouse action selection towards passive freezing and active avoidance or flight defensive responses upon exposure to threat [43,123]. Notably, these brain areas were also reported to send inputs to PAG subregions which then mediate passive and active defensive behaviors [23,42,130]. Interestingly, optogenetic activation of dPAG astrocytes biases mouse defensive responses towards more passive freezing behavior than active defensive responses regardless of the threat present and available shelter. Author speculates that the active defensive responses observed might be due to the nonselective effect of astrocyte stimulation to PAG neural populations and its indirect effect to other brain areas responsible for

active defensive responses. However, these data present evidence that optogenetic stimulation of dPAG astrocyte disrupts the appropriate action selection of mice upon exposure to threat and biases it to passive freezing behavior dominantly.

Meanwhile, pharmacological ablation and gliotransmitter release inhibition of midbrain dPAG astrocyte through L-AAA and Opto-vTrap did not ablate the whole defensive behavior but significantly attenuated mouse defensive behaviors to threat. Author speculates that other brain areas such as the amygdala [123], hypothalamus [4,42] and VTA [38,131], which were also reported to generate defensive behaviors, compensate to respond to threat stimuli presented to mice. However, data showed that dPAG astrocyte is necessary to generate optimal defensive behaviors against threatening situations. In addition, ablation of astrocyte in the panicogenic environment showed reduced panic-related jumping, but mice were still unable to escape from the panicogenic environment. Author speculates that this behavior of navigation and successful safety-directed escape might be contributed by activities of other brain areas in addition to dPAG such as the superior colliculus and retrosplenial cortex [132,133]. Still, my finding that panic-related jumping is reduced by dPAG astrocyte ablation supports my hypothesis that astrocyte is involved in mouse panic-related behaviors.

Furthermore, it was shown in this study that the aberrant activation or ablation of dPAG astrocytes impaired the predicted and physiological defensive behaviors of mice. These data suggest that dPAG astrocyte play a modulatory role in optimizing dPAG neuron-triggered defensive behaviors. Author speculates that changes in dPAG astrocyte activity significantly influence neural conditions and

local circuit within PAG and possibly the neural projections connected to it through gliotransmitter release (Figure 36).

Previous studies indicate that dPAG excitatory neurons exclusively encode escape behaviors towards shelter or safety [3,134], which was disrupted when astrocyte was ablated or optogenetically activated. Astrocytes may influence neuronal activity in dPAG through the release of gliotransmitters. dPAG astrocyte activation evoked a significant increase of extracellular ATP levels that may render changes in neural activity of dPAG thereby producing aberrant responses in mice. A recent study showed that mouse exposure to aversive stimuli induce astrocyte Ca^{2+} elevation and a subsequent release of ATP in prefrontal cortex. [135]. In addition, our recent study also showed the active involvement of ATP release in mouse anxiety-like behavior upon optogenetic stimulation of hippocampal astrocytes [96]. It was also reported that astrocyte-derived ATP modulate phasic and tonic inhibition in neocortex and hippocampal local circuitry through purinergic A1 receptors present in neurons showing activation of the G protein-gated inwardly rectifying potassium channel which hyperpolarizes neurons (Figure 37) [136,137].

Furthermore, the extracellular level of ATP is reduced upon stimulation of Opto-vTrap which inhibits gliotransmitter release via inhibition of synaptic vesicle release. Although Opto-vTrap did not completely abrogate the increasing trend of dPAG ATP levels upon astrocyte activation, a significant reduction was observed in the GFAP-Opto-vTrap group. Author speculates that ATP might be also released through other channels besides astrocytic vesicular release [138]. Whether the extracellular ATP increase is solely due to astrocyte activity or is also partially contributed by neuronal activity still needs to be clarified. However, this study

provides an insight on the mechanism underlying the dysregulated defensive behaviors. Author suggests that the release of ATP from dPAG astrocyte activation may disrupt the normal tonic inhibition in dPAG through A1 receptors. Dr. Tiago Branco and colleagues found that inhibitory neurons in PAG control the glutamatergic neurons responsible for active escape behaviors in mice [3] (Figure 36A). Author proposes that dPAG astrocyte somehow inhibits putative GABAergic neurons that control excitatory neurons in dPAG thereby assisting the activation of glutamatergic neurons that facilitate escape behavior in mouse upon threat exposure (Figure 36B). Meanwhile, author speculates that the ablation of astrocytes impairs the disinhibition of glutamatergic neurons in dPAG (Figure 36C) which then results to inefficient and reduced defensive behaviors as shown in this study, especially escape and induced bouts of freezing and risk assessment or explorative behaviors in mice even in the presence of threat. With these speculations, it is then possible that the optogenetic activation of dPAG astrocyte might be inhibiting the whole circuit output in dPAG (Figure 36D, inhibiting both GABAergic and glutamatergic neurons) which causes the drastic freezing behaviors and disruption of active escape to shelter behavior regardless of the threatening environment and available safe zone through ATP release. ATP released might act on the A1 receptors associated with GIRK channels that hyperpolarizes neurons.

Also, these speculations are supported by previous studies showing that optogenetic inhibition of glutamatergic neurons and non-selective muscimol inactivation of dPAG disrupted and halted escape behaviors and produced freezing behaviors in response to looming stimulus instead [3]. Similar findings were reported by Tovote and colleague on the local circuitry of defensive freezing and escape being

Figure 36. Hypothetical schematic diagram of the influence of astrocyte activity and its manipulations on dPAG local neuronal circuit.

(**A**) dPAG inhibitory neurons control dPAG activity at baseline or exploratory behaviors in mice [132]. (**B**) A possible Dpag neuronal circuit-dependent astrocyte activity on the disinhibition of glutamatergic neuron-evoked escape behavior during threat exposure. (**C**) L-AAA ablation of astrocyte might dysregulate the efficient disinhibition of dPAG glutamatergic neurons during threat exposure thereby demonstrating reduced and inefficient defensive response (Figure 29) (**D**) A possible inhibition of the whole circuit output by optogenetic activation of dPAG astrocyte dominantly evoking freezing and panic-like behaviors. GABA, γ-aminobutyric acid neuron; Glu, glutamatergic neuron

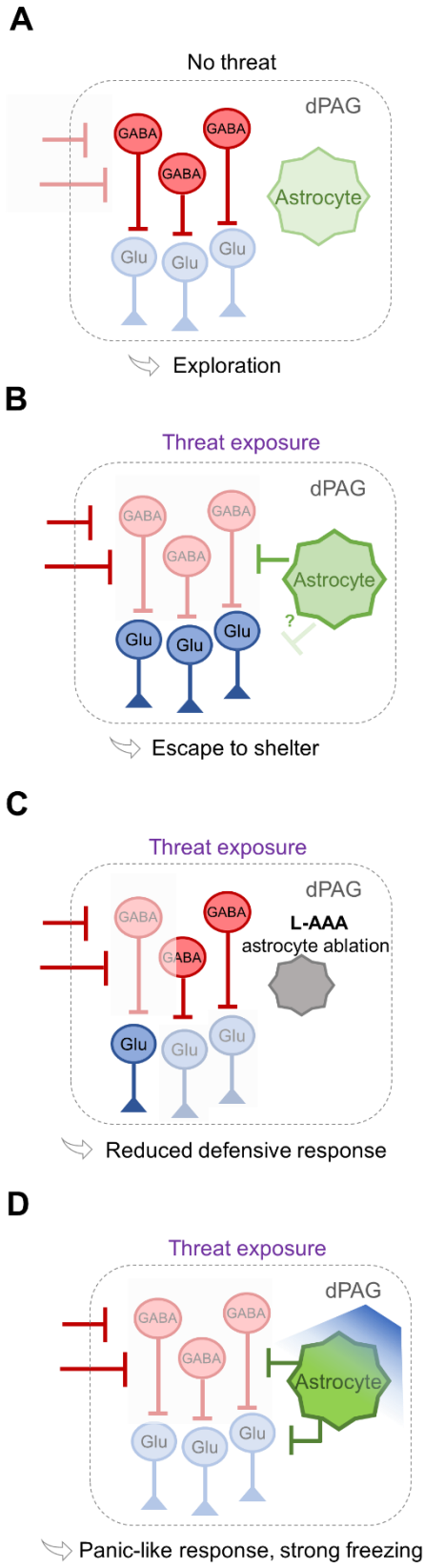

control by GABAergic interneurons in the lateral and ventral subregions of PAG [23]. Furthermore, earlier studies showed that disruption of the tonic inhibition in dPAG using microinjection of

semicarbadize and bicuculine, known GABA blockers, evoked jumping and freezing behaviors in mice mimicking panic-like behaviors [139]. It is also possible that the strong freezing behaviors were produced by lateral and ventrolateral PAG given the speculated whole circuit inhibition induced by the activation of astrocytes in the dorsal part [23]. This notion is further supported by previous studies suggesting the lateral and ventrolateral subregions of PAG are primarily responsible for mouse freezing [23,35]. With these, author speculates that astrocytes might inhibit the whole circuit output of dPAG through a possible decrease of neuronal excitability or the inhibitory effect of ATP via A1 receptors and GIRK channels [136,137], thereby producing aberrant passive freezing behavior and failure to efficiently escape a threatening situation reminiscent of panic-like behaviors.

ATP might be also involved in the mouse panic-related response [140,141]. PAG is an integrated area that connects the midbrain and the brainstem. Therefore, there is a possibility that the activity of PAG might also affect the brainstem activity and its acid-base homeostasis which was reportedly regulated by astrocytes through ATP release [142]. There is also a possibility that astrocytes in PAG are responsible for panic-related behaviors induced by CO2 through astrocytic regulation of brain pH [140-143]. It was reported that CO2 reduced brain pH and evoked fear and panic-like behaviors in animals [144-146]. Moreover, this changes in the brain pH is primarily regulated by astrocytes and its communications with pH-sensing neurons in the brain [79,142,143].

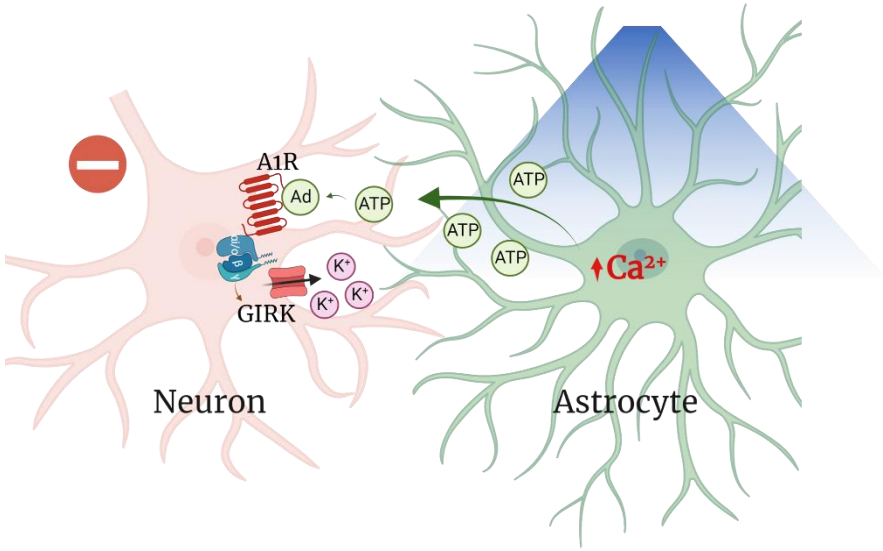

Figure 37. Hypothetical schematic diagram of the inhibitory effect of the astrocyte-derived ATP on dPAG neurons.

Optogenetic activation of dPAG astrocyte (right) releases ATP that can be degraded into Adenosine (Ad) which may inhibit or decreases the excitability of neighboring neurons (left) through A1receptors (A1R) which activates G protein-gated inwardly rectifying potassium (GIRK) channel.

Meanwhile, it should also be noted the limitations of this study especially the use of optogenetics in astrocytes and the use of a transgenic mouse line expressing ChR2 across the whole midbrain PAG region. It is important to note that this exogenous stimulation of astrocytes in dPAG might affect proximal brain areas and unselectively affect neural populations that yield unspecific defensive-like responses. In addition, it should be noted that this study uses human Synaptophysin promoter to target and optogenetically manipulate dPAG neurons therefore, it is possible that not only glutamatergic neurons but also non-glutamatergic neurons

were stimulated during the experiments and might affect results with the simultaneous stimulations with astrocytes.

To date, the neurobiological mechanism of the intense fear with increased autonomic nervous symptoms which describe panic-related behaviors are still unknown. This study only covered the disruption of safety-seeking and the heightened defensive-like behaviors mimicking panic-related behaviors in mice. It will be interesting to further investigate animals' physiological changes and or autonomic responses to panicogenic stimulus such as CO2 together with astrocyte activities. Nonetheless, it is also fascinating to further assess the electrophysiological properties of specific neural populations in PAG with astrocyte and the possibility of astrocytes regulating pH homeostasis in PAG which mediate the appropriate defensive behaviors in animals.

Most notably, the aberrant dPAG astrocyte activation induced abnormal defensive responses and uncontrollable panic-like behaviors characterized with intense and heightened fear-like response. These panic-like behaviors disrupted the physiological and goal-directed defensive response to seek safety to avoid threat and maximize the chance survival. Furthermore, dPAG astrocyte manifest distinct Ca^{2+} activity elevation upon exposure to a panicogenic stimulus. dPAG is putatively known to be involved in panic-related behaviors in both human and animal studies [49,56,125,147,148]. The findings of this work suggest that aberrant dPAG astrocyte activity, observed through distinct Ca^{2+} elevation and increased ATP release may underlie mechanisms for the panic-like behaviors.

5. Conclusion

Survival in the face of threatening situations depends on animals' optimal defensive behaviors, yet dysregulated and maladaptive defensive behaviors leads to panic-like behavior, failure to seek safety and avoid harm. Defensive behaviors are also used as read-out of psychiatric disorders such as maladaptive anxiety, panic-related behaviors, and PTSD. Human and rodent studies revealed that the midbrain PAG responds and generates fear and defensive responses and is also involved in panic-related behaviors. Previous studies on the mouse defensive behavior mainly focus on neuronal activity underlying defensive responses. However, increasing number of evidences showed that not only neurons but also astrocytes regulate animal behaviors particularly fear and anxiety. Therefore, in this study, the role of astrocytes in mouse defensive behavior and the possible underlying mechanism were investigated.

This study showed that dPAG astrocytes respond to various threatening and panicogenic stimuli with distinct calcium activities, and participate in the regulation of mouse defensive behaviors against threat. Through in vivo fiber photometry, the study provides evidence that dPAG astrocytes primarily responds to threatening situations by increased Ca^{2+} activity which was not observed when mouse was exposed to non-threatening stimuli such as a novel object or a female conspecific. Pharmacologic ablation of dPAG astrocyte revealed that dPAG astrocytes are required for the manifestation of optimal defensive behavior against threatening situations.

Also, aberrant activation of dPAG astrocytes leads to maladaptive defensive behavior exemplified by disruption of safety-seeking escape behaviors. This was further confirmed by dPAG neuronal manipulation to evoke escape responses in mice which were shown disrupted by the aberrant activity of dPAG astrocytes producing passive freezing behaviors dominantly. Notably, dPAG astrocyte manifested a distinct Ca^{2+} elevation upon exposure to CO2, a panicogenic agent used for both humans and animals to study panic-related behaviors.

Given the distinct calcium elevation of dPAG astrocyte upon exposure to panicogenic agent, optogenetics was employed to induce calcium activity elevation in astrocytes. Extracellular ATP level was significantly increased upon optogenetic activation of dPAG astrocyte. Furthermore, defensive behavior and panic-related jumping behavior were significantly attenuated by the inhibition of astrocytic gliotransmitter release. These data indicate that dPAG astrocyte-derived ATP release is involved in modulating mouse defensive and panic-like behaviors.

Although the mechanism of astrocytic calcium response upon exposure to threat and panicogenic stimuli were not fully elucidated, optogenetic manipulations allowed the investigation of the putative in vivo role of dPAG astrocyte calcium activity and subsequent gliotransmitter release such as ATP. These findings suggest a possibility that aberrant dPAG astrocyte activity underlie as a mechanism for the panic-like behaviors in the threatening environment.

In conclusion, this study discovered that, upon exposure to threatening situations, the midbrain dPAG astrocyte is actively involved and is required for optimal defensive behaviors. Through distinct Ca^{2+} activity and ATP release, dPAG astrocyte modulates mouse defensive behaviors. Furthermore, this study suggests

that dysregulation of dPAG astrocyte activity may result in panic-like behaviors. These findings may open new avenue elucidating pathogenic mechanisms of debilitating maladaptive defensive behavior or panic-like disorder in light of dPAG astrocytes activity.

Bibliography

1 Blanchard, R. J. & Blanchard, D. C. Crouching as an index of fear. *Journal of comparative and physiological psychology* **67**, 370 (1969).

2 Fanselow, M. S. & Bolles, R. C. Naloxone and shock-elicited freezing in the rat. *Journal of comparative and physiological psychology* **93**, 736 (1979).

3 Evans, D. A. *et al.* A synaptic threshold mechanism for computing escape decisions. *Nature* **558**, 590-594 (2018).

4 Wang, W. *et al.* Coordination of escape and spatial navigation circuits orchestrates versatile flight from threats. *Neuron* **109**, 1848-1860. e1848 (2021).

5 Xie, Z. *et al.* Mechanically evoked defensive attack is controlled by GABAergic neurons in the anterior hypothalamic nucleus. *Nature Neuroscience* **25**, 72-85 (2022).

6 Blanchard, D. C., Griebel, G., Pobbe, R. & Blanchard, R. J. Risk assessment as an evolved threat detection and analysis process. *Neuroscience & Biobehavioral Reviews* **35**, 991-998 (2011).

7 Blanchard, D. C., Griebel, G. & Blanchard, R. J. Mouse defensive behaviors: pharmacological and behavioral assays for anxiety and panic. *Neuroscience & Biobehavioral Reviews* **25**, 205-218 (2001).

8 Gross, C. T. & Canteras, N. S. The many paths to fear. *Nature Reviews Neuroscience* **13**, 651-658 (2012).

9 Yilmaz, M. & Meister, M. Rapid innate defensive responses of mice to looming visual stimuli. *Current Biology* **23**, 2011-2015 (2013).

10 Fanselow, M. S. & Lester, L. S. A functional behavioristic approach to aversively motivated behavior: predatory imminence as a determinant of the topography of defensive behavior. (1988).

11 Blanchard, D. C., Litvin, Y., Pentkowski, N. S. & Blanchard, R. J. Defense and aggression. (2009).

12 Berntson, G. G. & Cacioppo, J. T. *Handbook of Neuroscience for the Behavioral Sciences, Volume 2*. Vol. 2 (John Wiley & Sons, 2009).

13 Busch, F. N., Milrod, B. L., Singer, M. B. & Aronson, A. C. *Manual of panic focused psychodynamic psychotherapy-extended range*. (Routledge, 2012).

14 Deisseroth, K. Circuit dynamics of adaptive and maladaptive behaviour. *Nature* **505**, 309-317 (2014).

15 Tovote, P., Fadok, J. P. & Lüthi, A. Neuronal circuits for fear and anxiety. *Nature Reviews Neuroscience* **16**, 317-331 (2015).

16 Rosen, J. B. & Schulkin, J. From normal fear to pathological anxiety. *Psychological review* **105**, 325 (1998).

17 O'Connell, L. A. & Hofmann, H. A. Evolution of a vertebrate social decision-making network. *Science* **336**, 1154-1157 (2012).

18 Silva, C. & McNaughton, N. Are periaqueductal gray and dorsal raphe the foundation of appetitive and aversive control? A comprehensive review. *Progress in neurobiology* **177**, 33-72 (2019).

19 Behbehani, M. M. Functional characteristics of the midbrain periaqueductal gray. *Progress in neurobiology* **46**, 575-605 (1995).

20 Motta, S. C., Carobrez, A. P. & Canteras, N. S. The periaqueductal gray and primal emotional processing critical to influence complex defensive

responses, fear learning and reward seeking. *Neuroscience & Biobehavioral Reviews* **76**, 39-47 (2017).

21 Graeff, F. G. Neuroanatomy and neurotransmitter regulation of defensive behaviors and related emotions in mammals. *Brazilian journal of medical and biological research= Revista brasileira de pesquisas medicas e biologicas* **27**, 811-829 (1994).

22 Deng, H., Xiao, X. & Wang, Z. Periaqueductal gray neuronal activities underlie different aspects of defensive behaviors. *Journal of Neuroscience* **36**, 7580-7588 (2016).

23 Tovote, P. *et al.* Midbrain circuits for defensive behaviour. *Nature* **534**, 206-212 (2016).

24 Hashemi, M. M. *et al.* Neural dynamics of shooting decisions and the switch from freeze to fight. *Scientific reports* **9**, 1-10 (2019).

25 Mobbs, D. *et al.* When fear is near: threat imminence elicits prefrontal-periaqueductal gray shifts in humans. *Science* **317**, 1079-1083 (2007).

26 Mobbs, D. *et al.* Neural activity associated with monitoring the oscillating threat value of a tarantula. *Proceedings of the National Academy of Sciences* **107**, 20582-20586 (2010).

27 Linnman, C., Moulton, E. A., Barmettler, G., Becerra, L. & Borsook, D. Neuroimaging of the periaqueductal gray: state of the field. *Neuroimage* **60**, 505-522 (2012).

28 Wang, S. *et al.* Distinct networks of periaqueductal gray columns in pain and threat processing. *NeuroImage* **250**, 118936 (2022).

29 Faull, O. K., Subramanian, H. H., Ezra, M. & Pattinson, K. T. The midbrain periaqueductal gray as an integrative and interoceptive neural structure for breathing. *Neuroscience & Biobehavioral Reviews* **98**, 135-144 (2019).

30 Yeh, L.-F., Ozawa, T. & Johansen, J. P. Functional organization of the midbrain periaqueductal gray for regulating aversive memory formation. *Molecular brain* **14**, 1-9 (2021).

31 Assareh, N., Sarrami, M., Carrive, P. & McNally, G. P. The organization of defensive behavior elicited by optogenetic excitation of rat lateral or ventrolateral periaqueductal gray. *Behavioral neuroscience* **130**, 406 (2016).

32 Bittencourt, A., Nakamura-Palacios, E., Mauad, H., Tufik, S. & Schenberg, L. Organization of electrically and chemically evoked defensive behaviors within the deeper collicular layers as compared to the periaqueductal gray matter of the rat. *Neuroscience* **133**, 873-892 (2005).

33 Reis, F. M. *et al.* Shared dorsal periaqueductal gray activation patterns during exposure to innate and conditioned threats. *Journal of Neuroscience* **41**, 5399-5420 (2021).

34 Reis, F. M. *et al.* Dorsal periaqueductal gray ensembles represent approach and avoidance states. *Elife* **10**, e64934 (2021).

35 La-Vu, M. Q. *et al.* Sparse genetically defined neurons refine the canonical role of periaqueductal gray columnar organization. *Elife* **11**, e77115 (2022).

36 Vaughn, E., Eichhorn, S., Jung, W., Zhuang, X. & Dulac, C. Three-dimensional Interrogation of Cell Types and Instinctive Behavior in the Periaqueductal Gray. *bioRxiv* (2022).

37 Shang, C. *et al.* A parvalbumin-positive excitatory visual pathway to trigger fear responses in mice. *Science* **348**, 1472-1477 (2015).

38 Zhou, Z. *et al.* A VTA GABAergic neural circuit mediates visually evoked innate defensive responses. *Neuron* **103**, 473-488. e476 (2019).

39 Rozeske, R. R. *et al.* Prefrontal-periaqueductal gray-projecting neurons mediate context fear discrimination. *Neuron* **97**, 898-910. e896 (2018).

40 Ciocchi, S. *et al.* Encoding of conditioned fear in central amygdala inhibitory circuits. *Nature* **468**, 277-282 (2010).

41 Amorapanth, P., LeDoux, J. E. & Nader, K. Different lateral amygdala outputs mediate reactions and actions elicited by a fear-arousing stimulus. *Nature neuroscience* **3**, 74-79 (2000).

42 Wang, L., Chen, I. Z. & Lin, D. Collateral pathways from the ventromedial hypothalamus mediate defensive behaviors. *Neuron* **85**, 1344-1358 (2015).

43 Ma, J. *et al.* Divergent projections of the paraventricular nucleus of the thalamus mediate the selection of passive and active defensive behaviors. *Nature Neuroscience* **24**, 1429-1440 (2021).

44 Association, A. P. *Diagnostic and Statistical Manual of Mental Disorders*. 5th edn, (2013).

45 Lueken, U. *et al.* Altered top-down and bottom-up processing of fear conditioning in panic disorder with agoraphobia. *Psychological medicine* **44**, 381-394 (2014).

46 Cryan, J. F. & Sweeney, F. F. The age of anxiety: role of animal models of anxiolytic action in drug discovery. *British journal of pharmacology* **164**, 1129-1161 (2011).

47 Deakin, J. W. & Graeff, F. G. 5-HT and mechanisms of defence. *Journal of psychopharmacology* **5**, 305-315 (1991).

48 Ashcroft, G., Walker, L. & Lyle, A. A psychobiological model for panic: including models for the mechanisms involved in the regulation of mood and anxiety and implications for behavioural and pharmacological therapies. *Psychopharmacology of panic* **12**, 131-143 (1993).

49 Nashold, B. S., Wilson, W. P. & Slaughter, D. G. Sensations evoked by stimulation in the midbrain of man. *Journal of neurosurgery* **30**, 14-24 (1969).

50 Ribeiro, S. *et al.* Functional and ultrastructural neuroanatomy of interactive intratectal/tectonigral mesencephalic opioid inhibitory links and nigrotectal GABAergic pathways: involvement of GABAA and μ1-opioid receptors in the modulation of panic-like reactions elicited by electrical stimulation of the dorsal midbrain. *Journal of Chemical Neuroanatomy* **30**, 184-200 (2005).

51 Jenck, F., Moreau, J.-L. & Martin, J. R. Dorsal periaqueductal gray-induced aversion as a simulation of panic anxiety: elements of face and predictive validity. *Psychiatry research* **57**, 181-191 (1995).

52 Coimbra, N. & Brandão, M. Effects of 5-HT2 receptors blockade on fear-induced analgesia elicited by electrical stimulation of the deep layers of the superior colliculus and dorsal periaqueductal gray. *Behavioural brain research* **87**, 97-103 (1997).

53 Johnson, P. L. *et al.* Induction of c-Fos in 'panic/defence'-related brain circuits following brief hypercarbic gas exposure. *Journal of Psychopharmacology* **25**, 26-36 (2011).

54 Graeff, F. G., Silveira, M. C. L., Nogueira, R. L., Audi, E. A. & Oliveira, R. M. W. Role of the amygdala and periaqueductal gray in anxiety and panic. *Behavioural brain research* **58**, 123-131 (1993).

55 Griebel, G., Blanchard, D. C. & Blanchard, R. J. Predator-elicited plight responses in Swiss-Webster Mice: An experimental model of panic attacks. *Progress in Neuro-Psychopharmacology and Biological Psychiatry* **20**, 185-205 (1996).

56 Lovick, T. Panic disorder-a malfunction of multiple transmitter control systems within the midbrain periaqueductal gray matter? *The Neuroscientist* **6**, 48-59 (2000).

57 Chawla, N. *et al.* Drug treatment for panic disorder with or without agoraphobia: systematic review and network meta-analysis of randomised controlled trials. *bmj* **376** (2022).

58 Baldwin, D. S. *et al.* Evidence-based pharmacological treatment of anxiety disorders, post-traumatic stress disorder and obsessive-compulsive disorder: a revision of the 2005 guidelines from the British Association for Psychopharmacology. *Journal of Psychopharmacology* **28**, 403-439 (2014).

59 Bighelli, I. *et al.* Antidepressants and benzodiazepines for panic disorder in adults. *Cochrane Database of Systematic Reviews* (2016).

60 Breilmann, J. *et al.* Benzodiazepines versus placebo for panic disorder in adults. *Cochrane database of systematic reviews* (2019).

61 Volterra, A. & Meldolesi, J. Astrocytes, from brain glue to communication elements: the revolution continues. *Nature Reviews Neuroscience* **6**, 626-640 (2005).

62 Araque, A., Parpura, V., Sanzgiri, R. P. & Haydon, P. G. Tripartite synapses: glia, the unacknowledged partner. *Trends in neurosciences* **22**, 208-215 (1999).

63 Haydon, P. G. GLIA: listening and talking to the synapse. *Nature Reviews Neuroscience* **2**, 185-193 (2001).

64 Bernardinelli, Y. *et al.* Activity-dependent structural plasticity of perisynaptic astrocytic domains promotes excitatory synapse stability. *Current Biology* **24**, 1679-1688 (2014).

65 Papouin, T., Dunphy, J., Tolman, M., Foley, J. C. & Haydon, P. G. Astrocytic control of synaptic function. *Philosophical Transactions of the Royal Society B: Biological Sciences* **372**, 20160154 (2017).

66 Palygin, O., Lalo, U., Verkhratsky, A. & Pankratov, Y. Ionotropic NMDA and P2X1/5 receptors mediate synaptically induced Ca2+ signalling in cortical astrocytes. *Cell calcium* **48**, 225-231 (2010).

67 Hamilton, N. *et al.* Mechanisms of ATP-and glutamate-mediated calcium signaling in white matter astrocytes. *Glia* **56**, 734-749 (2008).

68 Toth, A. B. *et al.* CRAC channels regulate astrocyte Ca2+ signaling and gliotransmitter release to modulate hippocampal GABAergic transmission. *Science signaling* **12**, eaaw5450 (2019).

69 Wang, X. *et al.* Astrocytic Ca2+ signaling evoked by sensory stimulation in vivo. *Nature neuroscience* **9**, 816-823 (2006).

70 Di Castro, M. A. *et al.* Local Ca2+ detection and modulation of synaptic release by astrocytes. *Nature neuroscience* **14**, 1276-1284 (2011).

71 Bootman, M. D., Lipp, P. & Berridge, M. J. The organisation and functions of local Ca2+ signals. *Journal of cell science* **114**, 2213-2222 (2001).

72 Agulhon, C., Fiacco, T. A. & McCarthy, K. D. Hippocampal short-and long-term plasticity are not modulated by astrocyte Ca2+ signaling. *Science* **327**, 1250-1254 (2010).

73 Bazargani, N. & Attwell, D. Astrocyte calcium signaling: the third wave. *Nature neuroscience* **19**, 182-189 (2016).

74 Mulligan, S. J. & MacVicar, B. A. Calcium transients in astrocyte endfeet cause cerebrovascular constrictions. *Nature* **431**, 195-199 (2004).

75 Guček, A., Vardjan, N. & Zorec, R. Exocytosis in astrocytes: transmitter release and membrane signal regulation. *Neurochemical research* **37**, 2351-2363 (2012).

76 Halassa, M. M., Fellin, T. & Haydon, P. G. The tripartite synapse: roles for gliotransmission in health and disease. *Trends in molecular medicine* **13**, 54-63 (2007).

77 Hamilton, N. B. & Attwell, D. Do astrocytes really exocytose neurotransmitters? *Nature Reviews Neuroscience* **11**, 227-238 (2010).

78 Cao, X. *et al.* Astrocyte-derived ATP modulates depressive-like behaviors. *Nature medicine* **19**, 773-777 (2013).

79 Gourine, A. V. *et al.* Astrocytes control breathing through pH-dependent release of ATP. *Science* **329**, 571-575 (2010).

80 Kimelberg, H., Goderie, S., Higman, S., Pang, S. & Waniewski, R. Swelling-induced release of glutamate, aspartate, and taurine from astrocyte cultures. *Journal of Neuroscience* **10**, 1583-1591 (1990).

81 Parpura, V. *et al.* Glutamate-mediated astrocyte–neuron signalling. *Nature* **369**, 744-747 (1994).

82 Lee, S. *et al.* Channel-mediated tonic GABA release from glia. *Science* **330**, 790-796 (2010).

83 Kozlov, A., Angulo, M., Audinat, E. & Charpak, S. Target cell-specific modulation of neuronal activity by astrocytes. *Proceedings of the National Academy of Sciences* **103**, 10058-10063 (2006).

84 Henneberger, C., Papouin, T., Oliet, S. H. & Rusakov, D. A. Long-term potentiation depends on release of D-serine from astrocytes. *Nature* **463**, 232-236 (2010).

85 Khakh, B. S. & Sofroniew, M. V. Diversity of astrocyte functions and phenotypes in neural circuits. *Nature neuroscience* **18**, 942-952 (2015).

86 Li, B., Parpura, V., Verkhratskiĭ, A. N. & Scuderi, C. *Astrocytes in Psychiatric Disorders*. (Springer, 2021).

87 Zhou, X. *et al.* Astrocyte, a promising target for mood disorder interventions. *Frontiers in molecular neuroscience*, 136 (2019).

88 Adamsky, A. *et al.* Astrocytic activation generates de novo neuronal potentiation and memory enhancement. *Cell* **174**, 59-71. e14 (2018).

89 Jo, S. *et al.* GABA from reactive astrocytes impairs memory in mouse models of Alzheimer's disease. *Nature medicine* **20**, 886-896 (2014).

90 Sheikhbahaei, S. *et al.* Astrocytes modulate brainstem respiratory rhythm-generating circuits and determine exercise capacity. *Nature communications* **9**, 1-10 (2018).

91 Xia, L. *et al.* FGF2 blocks PTSD symptoms via an astrocyte-based mechanism. *Behavioural brain research* **256**, 472-480 (2013).

92 Wahis, J. *et al.* Astrocytes mediate the effect of oxytocin in the central amygdala on neuronal activity and affective states in rodents. *Nature neuroscience* **24**, 529-541 (2021).

93 Gomez, J. A. *et al.* Ventral tegmental area astrocytes orchestrate avoidance and approach behavior. *Nature communications* **10**, 1-13 (2019).

94 Li, Y. *et al.* Activation of astrocytes in hippocampus decreases fear memory through adenosine A1 receptors. *Elife* **9** (2020).

95 Martin-Fernandez, M. *et al.* Synapse-specific astrocyte gating of amygdala-related behavior. *Nature neuroscience* **20**, 1540-1548 (2017).

96 Cho, W.-H. *et al.* Hippocampal astrocytes modulate anxiety-like behavior. *Nature Communications* **13**, 1-14 (2022).

97 Gill, T. *et al.* Imaging of astrocytes in posttraumatic stress disorder: A PET study with the monoamine oxidase B radioligand [11C] SL25. 1188. *European Neuropsychopharmacology* **54**, 54-61 (2022).

98 Yu, X., Nagai, J. & Khakh, B. S. Improved tools to study astrocytes. *Nature Reviews Neuroscience* **21**, 121-138 (2020).

99 Fenno, L., Yizhar, O. & Deisseroth, K. The development and application of optogenetics. *Annual review of neuroscience* **34**, 389 (2011).

100 Boyden, E. S., Zhang, F., Bamberg, E., Nagel, G. & Deisseroth, K. Millisecond-timescale, genetically targeted optical control of neural activity. *Nature neuroscience* **8**, 1263-1268 (2005).

101 Perea, G., Yang, A., Boyden, E. S. & Sur, M. Optogenetic astrocyte activation modulates response selectivity of visual cortex neurons in vivo. *Nature communications* **5**, 1-12 (2014).

102 Cho, W.-H., Barcelon, E. & Lee, S. J. Optogenetic glia manipulation: possibilities and future prospects. *Experimental neurobiology* **25**, 197-204 (2016).

103 Sasaki, T. *et al.* Application of an optogenetic byway for perturbing neuronal activity via glial photostimulation. *Proceedings of the National Academy of Sciences* **109**, 20720-20725 (2012).

104 Kyung, T. *et al.* Optogenetic control of endogenous Ca2+ channels in vivo. *Nature biotechnology* **33**, 1092-1096 (2015).

105 Mederos, S. *et al.* Melanopsin for precise optogenetic activation of astrocyte-neuron networks. *Glia* **67**, 915-934 (2019).

106 Kol, A. *et al.* Astrocytes contribute to remote memory formation by modulating hippocampal–cortical communication during learning. *Nature neuroscience* **23**, 1229-1239 (2020).

107 Nagai, J. *et al.* Hyperactivity with disrupted attention by activation of an astrocyte synaptogenic cue. *Cell* **177**, 1280-1292. e1220 (2019).

108 Tsai, M. J., Chang, Y.-F., Schwarcz, R. & Brookes, N. Characterization ofl-α-aminoadipic acid transport in cultured rat astrocytes. *Brain research* **741**, 166-173 (1996).

109 Sun, C., Fukushi, Y., Wang, Y. & Yamamoto, S. Astrocytes protect neurons in the hippocampal CA3 against ischemia by suppressing the intracellular Ca2+ overload. *Frontiers in cellular neuroscience* **12**, 280 (2018).

110 Won, J. *et al.* Opto-vTrap, an optogenetic trap for reversible inhibition of vesicular release, synaptic transmission, and behavior. *Neuron* **110**, 423-435. e424 (2022).

111 Hunskaar, S. & Hole, K. The formalin test in mice: dissociation between inflammatory and non-inflammatory pain. *Pain* **30**, 103-114 (1987).

112 Nam, Y. *et al.* Reversible induction of pain hypersensitivity following optogenetic stimulation of spinal astrocytes. *Cell reports* **17**, 3049-3061 (2016).

113 Lee, S. J., Zhou, T., Choi, C., Wang, Z. & Benveniste, E. N. Differential regulation and function of Fas expression on glial cells. *The Journal of Immunology* **164**, 1277-1285 (2000).

114 Canteras, N. S. & Goto, M. Fos-like immunoreactivity in the periaqueductal gray of rats exposed to a natural predator. *Neuroreport* **10**, 413-418 (1999).

115 Rosen, J. B., Asok, A. & Chakraborty, T. The smell of fear: innate threat of 2, 5-dihydro-2, 4, 5-trimethylthiazoline, a single molecule component of a predator odor. *Frontiers in neuroscience* **9**, 292 (2015).

116 Choi, J.-S. & Kim, J. J. Amygdala regulates risk of predation in rats foraging in a dynamic fear environment. *Proceedings of the National Academy of Sciences* **107**, 21773-21777 (2010).

117 Kim, E. J. *et al.* Dynamic coding of predatory information between the prelimbic cortex and lateral amygdala in foraging rats. *Science advances* **4**, eaar7328 (2018).

118 Boillat, M. *et al.* Neuroinflammation-associated aspecific manipulation of mouse predator fear by Toxoplasma gondii. *Cell reports* **30**, 320-334. e326 (2020).

119 Haga, S. *et al.* The male mouse pheromone ESP1 enhances female sexual receptive behaviour through a specific vomeronasal receptor. *Nature* **466**, 118-122 (2010).

120 Ishii, K. K. *et al.* A labeled-line neural circuit for pheromone-mediated sexual behaviors in mice. *Neuron* **95**, 123-137. e128 (2017).

121 Jäkel, S. & Dimou, L. Glial cells and their function in the adult brain: a journey through the history of their ablation. *Frontiers in cellular neuroscience* **11**, 24 (2017).

122 JOHN, R. D. S. Genetic analysis of tail rattling in the mouse. *Nature* **241**, 549-551 (1973).

123 Fadok, J. P. *et al.* A competitive inhibitory circuit for selection of active and passive fear responses. *Nature* **542**, 96-100 (2017).

124 Vale, R., Evans, D. A. & Branco, T. Rapid spatial learning controls instinctive defensive behavior in mice. *Current Biology* **27**, 1342-1349 (2017).

125 Leibold, N. *et al.* CO2 exposure as translational cross-species experimental model for panic. *Translational psychiatry* **6**, e885-e885 (2016).

126 Spiacci Jr, A. *et al.* Panic-like escape response elicited in mice by exposure to CO2, but not hypoxia. *Progress in Neuro-Psychopharmacology and Biological Psychiatry* **81**, 178-186 (2018).

127 Cui, G. *et al.* Deep brain optical measurements of cell type–specific neural activity in behaving mice. *Nature protocols* **9**, 1213 (2014).

128 Corkrum, M. & Araque, A. Astrocyte-neuron signaling in the mesolimbic dopamine system: The hidden stars of dopamine signaling. *Neuropsychopharmacology* **46**, 1864-1872 (2021).

129 Xin, W. *et al.* Ventral midbrain astrocytes display unique physiological features and sensitivity to dopamine D2 receptor signaling. *Neuropsychopharmacology* **44**, 344-355 (2019).

130 Johnson, S. B. *et al.* Activity in a prefrontal-periaqueductal gray circuit overcomes behavioral and endocrine features of the passive coping stress response. *Proceedings of the National Academy of Sciences* **119**, e2210783119 (2022).

131 Barbano, M. F. *et al.* VTA glutamatergic neurons mediate innate defensive behaviors. *Neuron* **107**, 368-382. e368 (2020).

132 Branco, T. in *Society for Neuroscience Annual Meeting Presidential Lecture.* (Society for Neuroscience, 2022).

133 Keshavarzi, S. *et al.* The retrosplenial cortex combines internal and external cues to encode head velocity during navigation. *BioRxiv* (2021).

134 Masferrer, M. E., Silva, B. A., Nomoto, K., Lima, S. Q. & Gross, C. T. Differential encoding of predator fear in the ventromedial hypothalamus and periaqueductal grey. *Journal of Neuroscience* **40**, 9283-9292 (2020).

135 Pittolo, S. *et al.* Dopamine activates astrocytes in prefrontal cortex via α1-adrenergic receptors. *Cell reports* **40**, 111426 (2022).

136 Lalo, U. *et al.* Exocytosis of ATP from astrocytes modulates phasic and tonic inhibition in the neocortex. *PLoS biology* **12**, e1001747 (2014).

137 Tan, Z. *et al.* Glia-derived ATP inversely regulates excitability of pyramidal and CCK-positive neurons. *Nature communications* **8**, 1-14 (2017).

138 Xiong, Y., Sun, S., Teng, S., Jin, M. & Zhou, Z. Ca2+-dependent and Ca2+-independent ATP release in astrocytes. *Frontiers in Molecular Neuroscience* **11**, 224 (2018).

139 Borelli, K. G., Ferreira-Netto, C., Coimbra, N. C. & Brandão, M. L. Fos-like immunoreactivity in the brain associated with freezing or escape induced by inhibition of either glutamic acid decarboxylase or GABAA receptors in the dorsal periaqueductal gray. *Brain research* **1051**, 100-111 (2005).

140 Esquivel, G., Schruers, K., Maddock, R. J., Colasanti, A. & Griez, E. Acids in the brain: a factor in panic? *Journal of psychopharmacology* **24**, 639-647 (2010).

141 Vollmer, L., Strawn, J. & Sah, R. Acid–base dysregulation and chemosensory mechanisms in panic disorder: a translational update. *Translational psychiatry* **5**, e572-e572 (2015).

142 Theparambil, S. M. *et al.* Astrocytes regulate brain extracellular pH via a neuronal activity-dependent bicarbonate shuttle. *Nature communications* **11**, 1-15 (2020).

143 Turovsky, E. *et al.* Mechanisms of CO2/H+ sensitivity of astrocytes. *Journal of Neuroscience* **36**, 10750-10758 (2016).

144 Ziemann, A. E. *et al.* The amygdala is a chemosensor that detects carbon dioxide and acidosis to elicit fear behavior. *Cell* **139**, 1012-1021 (2009).

145 Magnotta, V. A. *et al.* Detecting activity-evoked pH changes in human brain. *Proceedings of the National Academy of Sciences* **109**, 8270-8273 (2012).

146 Friedman, S. D., Mathis, C. M., Hayes, C., Renshaw, P. & Dager, S. R. Brain pH response to hyperventilation in panic disorder: preliminary evidence for altered acid-base regulation. *American Journal of Psychiatry* **163**, 710-715 (2006).

147 Tuescher, O. *et al.* Differential activity of subgenual cingulate and brainstem in panic disorder and PTSD. *Journal of anxiety disorders* **25**, 251-257 (2011).

148 Graeff, F. G. & Del-Ben, C. M. Neurobiology of panic disorder: from animal models to brain neuroimaging. *Neuroscience & Biobehavioral Reviews* **32**, 1326-1335 (2008).

Abstract in Korean

방어 및 공황관련 행동에서 중뇌 수도관주위의 회색질 성상교세포의 역할

서울대학교 대학원

자연과학대학 협동과정 뇌과학전공

엘레인

위협적 상황에 노출될 때 정상적 방어 행동은 생존 확률을 높이지만, 부적응적 방어는 공황 행동을 초래하여 생존을 보장 받을 수 없게 된다. 그러므로 동물이 효율적으로 위험을 피하고 생존 가능성을 극대화 하기 위해서는 방어 행동의 최적화가 이루어 져야 한다. 동물과 임상 연구에 의하면 중뇌의 배측 수도관 주의 회색질영역은 전뇌와 뇌간 사이의 정보를 통합하고 방어 행동과 공황 관련 행동을 조절 하는 영역으로 알려져 있다. 정상적 공포 반응과 부적응적 불안상태는 다양한 형태의 방어적 행동을 통해 해석 할 수 있지만 그 와 관련된 메커니즘은 거의 연구 되어있지 않다. 또한 기존에 알려진 방어 행동에 관련된 생쥐 연구들은 대부분 신경세포의 활성에 만 초점이 맞춰져 있다. 그러나 최근 연구들에 의하면 신경세포 뿐 만 아니라 성상교세포 또한 동물의 공포와 불안 행동을 조절할 수 있다는 증거들이 많아지고 있다. 이러한 증거들로 미루어 볼 때 배측 수도관 주의 회색질

영역의 성상교세포가 방어 행동 조절에 관여할 수 있는 가능성은 충분하지만, 전혀 연구되지 않았다. 따라서 이 연구를 통해 배측 수도관 주의 회색질 영역 성상교세포의 방어 및 공황 관련 행동 조절 관여 여부와 관련된 메커니즘을 알아보고자 한다.

이 연구에서는 생쥐의 생체 내 칼슘 기록으로 방어적 행동을 유발 할 수 있는 위협적인 상황에 노출 되었을 때 배측 수도관 주의 회색질 영역 성상교세포가 활성화 되는 것을 밝혔다. 또한 성상교세포의 광유전학적 활성화 및 약리학적 비활성화를 통해 배측 수도관 주의 회색질 영역 성상교세포의 ATP 방출이 최적의 방어 행동에 중요하다는 것을 증명하였고, 배측 수도관 주의 회색질 영역 성상교세포의 비정상적 활성화가 부적응 방어 행동을 이끌어 낸다는 증거를 제시했다. 따라서 이 연구는 배측 수도관 주의 회색질 영역 성상교세포가 공포 반응과 방어 행동 조절 장애의 중요한 세포이며 칼슘 활성 증가와 ATP 방출이 공황 관련 행동의 중요한 요소가 될 수 있음을 시사한다.

주요어:방어행동, 성상교세포, 배측 수도관 주의 회색질, 위협, 공황관련행동

학 번: 2016-2207

Soli Deo Gloria